

PART - III

MICROHARDNESS OF CRYSTALS
(GENERAL)

VARIATION OF LOAD WITH DIAGONAL
LENGTH OF INDENTATION MARK

VARIATION OF HARDNESS WITH LOAD

GRAPHICAL ANALYSES OF EXPERIMENTAL
OBSERVATIONS

CHAPTER - 9

MICROHARDNESS OF CRYSTALS (GENERAL)

	<u>PAGE</u>
9.1 Introduction	173
9.2.1 Definitions and measurements	173
9.2.2 Hardness measurements	176
9.3 General information on hardness	179
9.4 Variation of Hardness with load	185

References



9.1 INTRODUCTION

Of all the mechanical properties of materials, hardness is least understood. It may be broadly defined as the ability of one body to resist penetration by another. It is by definition a relative property of a material and depends on the elastic and plastic properties of both the penetrated body and the penetrator. In addition, the comparative hardness of different materials is strongly dependent upon the method of measurement. All hardness tests measure some combination of various material properties, namely elastic modulus, yield stress (which denotes the onset of plastic behaviour or permanent distortion), physical imperfection, impurities and workhardening capacity. The latter is a measure of the increase in stress to continue plastic flow as strain increases. Since each hardness test measures a different combination of these properties, hardness itself is not an absolute quantity and, to be meaningful, any statement of hardness of a body must include the method used for measurements.

9.2 DEFINITIONS AND MEASUREMENTS

From time to time many definitions have been

given for hardness but none has been found to be satisfactory for quantitative interpretation of the processes taking place in indented materials. Tuckerman (1929)¹ explained hardness as a hazily conceived aggregate or conglomeration of properties of a material more or less related to each other. The best general definition is given by Ashby (1951).² "Hardness is a measure of the resistance to permanent deformation or damage". The general definition of indentation hardness which is related to the various forms of the indenters is the ratio of load applied to the surface area of the indentation. Mayer (1908)³ proposed that hardness should be defined as the ratio of load to the projected area of the indentation. Hence the hardness has the dimensions of stress. Spaeth (1940)⁴ suggested that hardness should not be defined as stress but as the resistance to indentation in the form of the ratio of the specific surface load to the unrecovered deformation. In short, the hardness of a solid is defined by the resistance against lattice destruction and is considered to be a function of inner atomic forces⁵⁻⁷ (Tertsch, 1948 ; Tertsch, 1951 ; Tertsch, 1952). Attempts towards a physical definition of hardness were made by Friedrich (1926)⁸ Goldsmith (1926)⁹ and Chatterjee (1954).¹⁰

Chatterjee (1954)¹⁰ defined indentation hardness as the work done per unit volume of the indentation in a static indentation test for a definite angle of indentation. On the basis of this definition and Mayer's law $P = ad^n$ for spherical indenters, he derived a formula for measurement of hardness. According to Plendlí and Gielisse (1962)¹¹ hardness can be defined as pressure or force per square centimeter, and thus it can be conceived as an energy per unit volume, e.g. the ratio between the input energy and volume of indentation. They have concluded that resistance is a function of the lattice energy per unit volume and called it volumetric lattice energy (U/V) having the dimension ergs/c.c. U is the total cohesive energy of the lattice per mole and V is the molecular volume defined as M/S , where M is molecular weight and S is specific heat. The hardness was thus considered to be the absolute overall hardness. Matkin and Caffyn (1963)¹² from their studied on hardness of sodium chloride single crystals containing divalent impurities, correlated hardness with the dislocation theory. They redefined hardness in terms of generation and/or movement of dislocations associated with indentation. It is the measure of the rate at

which the dislocations dissipate energy when moving through a crystal lattice. It is now realized¹³ (Westbrook and Conard, 1973) that hardness is not a single property but rather a whole complex of mechanical properties and at the same time a measure of the intrinsic bonding of the material.

9.2.2 Hardness measurements

There are basically four methods to determine hardness of materials. They are as follows :

- (i) Scratch hardness tester
- (ii) Abrasive method
- (iii) Dynamic method and
- (iv) Static indentation method.

They are briefly reviewed here.

- (i) Scratch hardness

An early method of measuring scratch hardness still in wide use today by mineralogists was developed by Friedrich Mohs in 1822. This gives a relative ranking of minerals based simply on their

ability to scratch one another. The Mohs method is not suitable for a general use with materials of hardness greater than 4, since in this range the intervals are rather closely and unevenly spaced. The modifications of this method were overshadowed by other sensitive methods and experiments.

(ii) Abrasive hardness

Abrasive hardness is defined as the resistance to mechanical wear, a measure of which is the amount of material removed from the surface under specific conditions. The hardness may be found by the depth of penetration.

(iii) Dynamic hardness

The hardness measurement in this method involves the dynamic deformation of specimen under study and is determined by following different considerations :

(a) Here a steel sphere or a diamond-tipped hammer is dropped from a given height, and the height to which the ball or hammer rebounds is read on a scale. This is taken to be measure of hardness. The kinetic energy of a ball or hammer is used up partly in plastically deforming the specimen surface by creating

a slight impression and partly in rebound. This test is sometimes referred to as 'dynamic rebound test'. (b) Here a steel sphere or diamond-tipped hammer is dropped from a given height, the depth and size of the impression produced and the energy of impact gives the hardness of the substance, i.e. hardness is given as ratio of the energy of impact to the volume of indentation mark. (c) Chalmers (1941)¹⁴ assessed the surface hardness in terms of the reduction in optical reflectivity when a known amount of sand was allowed to impinge on the surface under standard conditions.

(iv) Static indentation hardness

The most widely used method of hardness testing is the indentation method. This is the simplest, and a very sensitive, method in which a hard indenter (e.g. diamond, sapphire, quartz or hardened steel) of a particular geometry is applied slowly, and after a certain time of application, is carefully removed, leaving behind a permanent indentation mark on the surface of specimen. Measurement is made either of the size of the indentation resulting from a fixed load on the indenter or the load necessary to

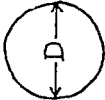
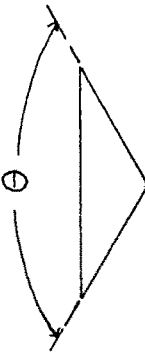
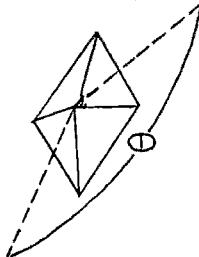
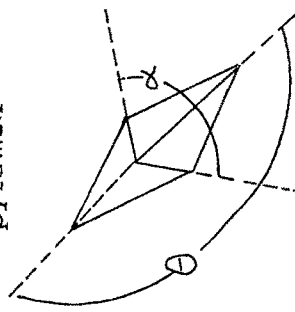
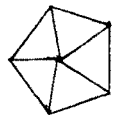
force the indenter down to a predetermined depth and the hardness of material is then defined as the ratio of the load to the area of the indentation mark. The hardness values so obtained vary with the indenter geometry and with the method of calculations.

Many combinations of indenter, load, loading procedure, and means of indentation measurement are used among the various tests in order to accommodate various shapes, sizes and hardnesses of specimens, and this has resulted in a proliferation of hardness scales. The most commonly used indenters are described in table 9.1. Diamond indenters must be used for hard materials in order to minimize errors due to elastic distortion of the indenter. In case ball indenters are used, the hardness number will be independent of load only when the ratio of load to indenter diameter is held constant. For cone and pyramidal indenters, hardness number will be independent of load for all loads above a certain minimum value depending upon specimen material.

9.3 GENERAL INFORMATION ON HARDNESS

The hardness study undertaken, so far for studying

Table 9.1

	Brinell	Rockwell	Vickers	Knoop	Broker & Moxley
Material of which indenter is made	Hardened steel or tungsten carbide	Diamond	Diamond	Diamond	Diamond
Shape of indenter	Sphere	Cone	Square based pyramid	Rhomb based pyramid	Pentagonal
Material of specimen	Hardened Steel				
Shape of indenter	Sphere	Sphere	Square based pyramid	Rhomb based pyramid	Pentagonal
Dimensions of indenter	 D	 $\theta = 120^\circ$	 $\theta = 136^\circ$	 $\alpha = 130^\circ$ $\theta = 172^\circ 36'$	
Dimensions of indenter		$D = 10\text{mm}$			
Dimensions of indenter		$D = \begin{cases} 1/16 \text{ in} \\ 1/8 \text{ in} \\ 1/4 \text{ in} \\ 1/2 \text{ in} \end{cases}$			
Characteristics	1. Geometrically similar impressions are not obtained	1. Prepares the surface upon which the further penetration due to major load is based. 2. Hardness is read directly on the dial gauge 3. Hardness value may be appreciable in error due to large amount of recovery along depth	1. Geometrically similar impressions are obtained	1. Hardness of upper most surface layers can be found 2. Sensitive to anisotropy of crystals 3. Shorter diagonal under goes recovery	1. Eliminates the anisotropy normally observed in hardness with all other indenters

the strength of solids and the effect of various treatments on the hardness of a solid, have proved somewhat useful. Most of the work has been reported on alkali halides and metals. Previously, hardness studies were made only from the view of materials research but as the expansion in the field of scientific research increased, the study on hardness helped in understanding various other mechanical properties of solids. Gilman and Roberts (1961)¹⁵ correlated indentation hardness with the elastic modulus by gathering the data for various materials. Their empirical linear relation shows that elastic modulus is an important factor which determines plastic resistivity against the dislocation motion. The behaviour of the indented region during the propagation of stresses which initiate dislocations and their motion is not understood clearly. When an indenter is pressed on a solid surface, the stresses which initiate the dislocations and their motion are not yet understood clearly. When an indenter is pressed on a crystalline surface, the stresses are not simply tensile or compressive in nature. Stresses in various directions are set up and the one should treat the resultant plastic flow as a result of these combined stresses. It is also

observed that the fundamental mechanisms of deformation can be either slip or twin or both or at times a fracture.

- (i) Slip is the most common mode of plastic deformation, which is characterised by the displacement of one part of crystal relative to another along certain definite crystallographic planes. The slip planes are usually of low indices and the slip directions are those of closely packed ones in a crystal structure.

- (ii) Certain crystals may also deform by twinning, a mechanism by means of which a portion of a crystal may change lattice orientation with respect to the other in a definite symmetrical fashion. Schmidt and Boas (1955)¹⁶ described the twinning as the simple sliding of one plane of atoms over the next, the extent of the movement of each plane being proportional to its distance from the twinning plane. Partridge (1964)¹⁷ studied the microhardness anisotropy of magnesium and zinc crystals. He observed twin in these crystals and concluded resolved shear stress criterion to be insufficient

to account for the observed distribution of twins. Any analysis which attempts to relate deformation twinning with hardness anisotropy must take into account the dimensional changes which occur during twin deformation. Indenting diamond flats with diamond indenter Phaal (1964)¹⁸ reported the slip and twinning of diamonds. Vahldick (1966)¹⁹ studied the slip systems and twinning in molybdenum carbide single crystals with the help of knoop and vickers indenters. When the indented crystal is etched by a dislocation etchant, rosettes are formed on some crystals casually alkali halides indicating the dislocation distribution around an indentation. Dislocation loops are also formed around the indentation mark in cesium iodide and sodium chloride. (Urusovskaya, 1965²⁰ and Kubo, 1970²¹).

Many workers have proposed some or other explanation for the microcrack formation during indentation of a crystal surface. Smakula and Klein (1951)²² from their punching experiments on sodium chloride explained the crack formation on the basis of shear on slip planes. Gilman (1958)²³

attributed these microracks which have a definite crystallographic direction to the piling up of dislocations on the slip plane. Breidth et al. (1957)²⁴ observed crack formation to be less at higher temperatures (375°C) than at lower temperatures (25°C). The cracks are usually observed to propagate from the corners of the impression.

The interferometric studies of indented surface have revealed the nature of the deformation and the history of the sample under test. Votava et al. (1953)²⁵ were the first to study the deformed region on the cleavage faces of mica and sodium chloride. Tolansky and Nickols (1949, 1952)^{26,27} studied the indented surfaces of steel, tin and bismuth. They observed maximum distortion along the median's bisecting sides of the square and minimum along diagonals, showing thereby that no distortion projects beyond the diagonal. They could easily show that difference between ' piling-up ' and the ' sinking-in ' with the help of FICO fringes. They established interferometrically the asymmetry in the fringe pattern to be purely crystallographic and dependent on the previous history of samples. It

has nothing to do with the orientation of the square of indentation mark. Further they concluded that the convex sides, corresponding to extended wings in the interference pattern were 'piled-up' regions and the concave sides were 'sunked-in' regions. Satyanarayan (1956)²⁸ observed barrel or pin-cushion shape of indentation marks interferometrically and gave idea about 'Sinking-in' occurring mostly at faces with very little along the diagonals of the indentation mark. Detailed study of dislocation rosette structure on various crystallographic planes and determination of microhardness at high temperature (1200°C, 1600°C and 1800°C) of $Y_3Al_5O_{12}$ revealed local plastic deformation around the indentation mark²⁹ (Voinova and Berezhkova, 1985). They observed that (112) plane of $Y_3Al_5O_{12}$ exhibited highest value of microhardness at 1800°C.

In crystalline materials plastic deformation or slip occurs through the movement of the imperfections called dislocations. As dislocations are multiplied (by one of several mechanisms) during deformation, their spacing decreases and they interact and impede each other's motion, thus leading to work-hardening. The strength of dislocation

interference depends on the nature of the crystal and on the ratio of temperature of deformation of the melting point of the crystal.

In general, hardening of crystals can be accomplished by the introduction of any barrier to dislocation motion. This can occur by (a) Work hardening (b) impurity hardening, (impurities tend to aggregate to dislocations and pin them) (c) decreasing grain size in a polycrystal (grain boundaries are barriers to dislocation motion) (d) dispersion of fine particles of second phase in the crystal and (e) phase transformations (by quenching).

It can be seen from this brief review that the amount of plastic deformation induced in a material by an indenter under load depends in complicated way on a variety of factors which defy simple analysis.

9.4 VARIATION OF HARDNESS WITH LOAD

For geometrically similar shapes of the indent marks for all loads, it can be shown that the hardness is independent of load. However this is not completely true. It is clear that during a hardness test the

formation of indentation mark leads to an increase in effective hardness of the material and so the hardness number obtained is not the actual hardness of the material in the initial stage. This is mainly due to work hardening of the substance during the process of indentation which will be varying with the load. Attempts have been made to determine the absolute hardness by eliminating work hardening. This can be done only, if the method does not appreciably deform the substance plastically. Absolute hardness was found to be one third of the normal hardness³⁰ (Harrise, 1922).

A large number of workers have studied the variation of hardness with load and the result given are quite confusing. Their findings are summarised below : Knoop (1937)³¹, Bernhardt (1941)³² etc. observed an increase in hardness with decrease in the load whereas Campbell et al. (1948)³³, Mott (1956)³⁴ etc. observed a decrease in hardness with decrease in load. Some authors e.g. Taylor (1948)³⁵, Bergsman (1948)³⁶ reported no significant change of hardness with load. In view of these different observations it has become rather difficult to establish any definite relationship of general validity between

microhardness values and applied load.

There are two ways of studying relation between hardness (H) and applied load (P) or relation between load (p) and diagonal (d) of the indentation mark.

Mayer³ (1908) gave an empirical formula

$$P = ad^n \quad \dots (9.1)$$

where 'a' and 'n' are constants of the material under test. The hardness number is given by

$$H = \frac{rp}{d^2} \quad \dots (9.2)$$

where r is a constant and depends upon the geometry of the indenter. The combination of the above two equations yields

$$H = a_1 d^{n-2} \quad \dots (9.3)$$

$$H = a_2 p^{\frac{n-2}{n}} \quad \dots (9.4)$$

where $a_1 = ra \quad \dots (9.5)$

and $a_2 = ra^{2/n} \quad \dots (9.6)$

It has been shown that in case of vickers microhardness the value of the exponent n is equal to 2 for all indenters that give geometrically similar impressions. This implies a constant hardness value for all loads.

Hanemann and Schulz (1941)³⁷ from their observations concluded that in the low load region ' n ' generally had a value less than two. Onitsch (1947)³⁸ found such low values of n (1 to 2) by observing variation of hardness with load while Grodzinski (1952)³⁹ found variation of n values from 1.3 to 4.9 ; the value of n was nearly found to be 1.8. The standard hardness values thus obtained were expected to yield constant result, but actual results obtained by different workers revealed disparities amounting to 30-50%. Due to this variation in the results, a high load region was selected which led to definition of an independent region of microhardness. The hardness values so obtained for this region again showed scattered results even though the apparatus had a good mechanical precision. The scattered observations may be attributed to the following reasons :

- (1) Equation i.e. $P = ad^n$ is not valid.
- (2) Microstructures exercise a considerable influence on measurements involving very small indentations.
- (3) The experimental errors due to mechanical polishing, preparation of specimen, vibrations loading rate, shape of indenter, measurement of impression, affect the hardness measurements considerably.

The term connected with the above test, microhardness means the microindentation hardness, as it actually refers to the hardness measurement on the microscopic scale. Some authors prefer the term low load hardness for the above. This confusion has arisen because these ranges have not been sharply defined. However, three possible regions can be defined as follows :

- (1) Microhardness : From lowest possible loads upto maximum of 200 gms.
- (2) Low load hardness : Loads from 200 gms to 3 kg. The most characteristic region comprises of loads from 200 gms to 1 Kg.

(3) Standard hardness : Loads over 3 kg.

Since the present study is made in the region of microhardness as defined in (1) above ; the following presents a brief review of the work reported on microhardness of various crystals.

In the recent work reported by many workers (1960 onwards) the hardness has been found to be increasing at low loads, then remaining constant for a range of higher loads. Murphy (1969)⁴⁰ studied hardness anisotropy in copper crystal ; the variation in hardness by plastic deformation is shown to be in part due to the escape of primary edge dislocations.

Sugita (1963)⁴¹ while studying the indentation hardness of crystals found occurrence of ring cracks and radial cracks. Further load required to produce the observable cracks increased with temperature. The temperature at which the microscopic slip lines became observable was higher in heavily doped crystals than in high purity crystals, indicating that dislocation multiplication was strongly affected by impurities.

Koserich and Bashmakov (1960)⁴² studied the formation of twins produced in Bi, Sb, Bi-Sb, Bi-Sn

and Bi-Pb single crystals under action of concentrated load by diamond pyramid microhardness tester. They showed that the length (l) of twins was proportional to the diagonal (d), of the indentation (and the intensity of the twinning thus given by the coefficient α in the equation $l = a + \alpha d$). The value of α was more for homogeneous alloys and increased with Sb content and remained constant for higher concentration of Sn and Pb in alloy crystals of bismuth.

The variation of hardness with load was also studied by Shah and Mathai (1969)⁴³ who explained hardness in terms of slip taking place due to deformation in tellurium crystal. Edelman (1964)⁴⁴ showed that microhardness of InSb and GaSb single crystals decreased exponentially with temperature. The presence of deflection points on the curves at $0.45 - 0.50 T_m$ indicate the deformation by slip. The activation energy for plastic flow in InSb and GaSb was estimated to be 0.6 eV.

Samsonov et al. (1969)⁴⁵ studied temperature dependence of microhardness of titanium carbide in the homogeneity range and found that the hardness

decreased with decrease in carbon content in carbide. They also determined the activation energies of dislocation movement by plastic deformation.

Hardness variation was also studied with respect to the impurity content, dislocation density and the change in mobility of dislocation by various workers. Mil'vidski et al. (1965)⁴⁶ observed decrease in hardness with increase in concentration of impurity and dislocation density in silicon single crystals, Kuz'menko et al. (1963)⁴⁷ showed decrease in hardness due to change in mobility of dislocations as a result of excitation of electrons during lighting and their transition to higher energetic zone in titanium iodide and termed this a 'Photomechanical effect'. Beilin and Vekilov (1963)⁴⁸ observed decrease in the hardness of Ge & Si upto 60% by illumination. Decrease in the hardness was attributed to the induced photoconductivity, which altered the widths of the dislocation cores at the sample surface and in turn altered the plasticity.

Westbrook and Gilman (1963)⁴⁹ studied electro-chemical effect in a number of semiconductors. They observed decrease in resistance of semiconducting

crystals to mechanical indentations in the presence of a small electric potential (0.05 to 1.0V) between the indenter and the crystal surface. This was found to be due to significant enhancement of the surface photovoltage by a longitudinal electric field.

Many workers studied variation of hardness in a number of semiconductors in terms of concentration of charge carriers, mobility and their interaction. Osvenskii et al. (1968)⁵⁰ observed decrease in microhardness due to increase in carrier concentration for different contents of donor and acceptor impurities for GaAs and InSb semiconductors. In addition to this they also showed that decrease in hardness was independent of the type of carrier. Semirnov et al. (1969)⁵¹ studied the temperature-dependence of carrier density and mobility in Ge crystals after irradiation with electrons and during various stages of annealing. They observed that the microhardness of such crystals did not recover fully and this was attributed to the interaction between radiation, defects and dislocations, which could act as sinks or condensations for components of Frankel pairs. Sellzer (1966)⁵² who studied the influence

of charged defects on mechanical properties of lead sulphide found that the rosettee wing length and hardness were nearly independent of concentration of free electrons in n-type ; while they had marked dependence on concentration of holes in p-type. For a hole concentration about $8 \times 10^{-7} \text{ cm}^{-3}$, rapid hardening was observed with an attendant decrease in rosettee size. It was suggested that the behaviour resulted from an e.s. interaction between charged dislocations and acceptor point defects.

Perinova and Urusovskaya (1966)⁵³ studied the hardening of NaCl single crystals by x-rays and found the increase in microhardness by irradiation due to pinning of dislocations in irradiated samples and that the pinning was not destroyed by illumination. The effect of irradiation was also studied by Berzina, et al. (1965)⁵⁴ who gave a relationship between the length of rays of etch figure star and proton irradiation dose in LiF, NaCl and KCl single crystals.

Because of substantial effect of surface layers on the microhardness, the increase in the microhardness was observed when applied load was reduced⁵⁵ (Upit et al. 1969). They showed the ratio P/l^2 (where l is

the length of rays in dislocation rosette around the indentation mark) was not constant at low loads due to retarding influence of the surface on the motion of dislocations. Further they (1970) estimated the change of the mechanical properties of the crystal as the indentation depth decreased on the basis of correlation between the size of an indentation mark and the length of dislocation beam.

The distribution of dislocations around an indentation mark was studied using chemical etch pit technique by Urusovskaya and Tyagaradzhyan (1965).⁵⁶ They found large number of prismatic loops. They examined the process of interaction of dislocations in crystals having CsCl lattice. Shukla and Murthy (1968)⁵⁷ also studied the distribution of dislocations in NaCl single crystals. They found increase in the distance travelled by leading dislocation with increase in load. They further observed that impurity had little effect on the dimensions of the indentation but had a pronounced effect on length of the edge rays of the 'star pattern' and the ratio of the mean diagonal length to mean length of edge rays was nearly constant. Matkin and Caffyn (1963)⁵⁸ observed increase in the hardness with increase in Ca^{++} concentration in

NaCl, while the distance travelled by leading dislocations was observed to decrease.

The effect of impurity on hardness was also studied by various workers. Dryden et al. (1965)⁵⁹ studied the hardness of alkali halides having low concentration of divalent cations on the basis of dielectric measurement of a doped alkali halide crystals. They observed following effects of the state of aggregation of the the divalent impurities on critical resolved shear stress (1) the increase in critical shear stress was proportional to $C^{2/3}$, where C is the concentration of divalent ion-vacancy pairs, (2) there was no increase in hardness as these divalent ion-vacancy pairs aggregate into groups of three (trimers), (3) in NaCl : Mn^{++} , KCl : Sr^{++} and KCl : Ba^{++} there was no increase in hardness as these trimers grow into large aggregates, (4) in LiF : Mg^{++} there was a large increase in hardness as the trimers grow into larger aggregates and (5) in NaCl : Ca^{++} the hardness increases as a second region of dielectric adsorption appears. They have also concluded that the structure of the trimer was same in all these crystals and the trimer can grow in two ways, one of which produces an increase in the resistance to movement of dislocations.

Urusovskaya et al. (1969)⁶⁰ investigated the influence of impurity on the strength of crystals, microhardness, length of dislocation rosettee rays and velocity of dislocation movement in CsI crystals. Takeuchi and Kitano (1971)⁶¹ reported the softening of NaCl crystal due to introduction of water molecules. The plastic resistance was almost independent of dislocation velocity except at very high velocities. It was, however, strongly influenced by temperature, impurities, radiation damage and structure of core of dislocation. Gilman (1960)⁶² observed a sharp drop in plastic resistance of covalent crystal at roughly about two-third of the melting temperature and suggested that the drop was because the cores of dislocation in covalent crystal 'melt' at this temperature.

Temperature-dependence of microhardness was also studied by Sarkozi and Vannay (1971).⁶³ They concluded that besides thermal stress the observed hardening might be due to dislocations piled-up at various impurities, to complexes in solid solution and vacancy clusters which were developed at high temperature. By quenching the clusters become distributed in crystals as fine dispersions.

Quench-hardness of single crystals of different materials was studied by a number of workers in the laboratory. Shah (1976)⁶⁴ found increase of hardness of calcite cleavage faces with quenching temperature. Acharya (1978)⁶⁵ found that the hardness of Zn and KBr decreased with quenching temperature while converse was the case for hardness of TGS & InSb.

Many workers reported microhardness studies on piezoelectric and ferroelectric crystals Anbukumar (1986)⁶⁷ worked on ADP type crystals. Work on ferroelectric crystals such as TGS, TGSe (Martin et al. 1985)⁶⁸ Rochell salt (Pastor et al. 1981)⁶⁹ gadolinium (Nabutovskaya, 1969)⁷⁰ etc. was also reported. Variation of hardness number was marked at curie temperature.

Comparative study of vickers and knoop hardness number was investigated in detail by Mohrnheim (1973)⁷¹ on metallic materials. An analysis of knoop microhardness led Hays and Kendall (1973)⁷² to modify law correlating applied load to the long knoop diagonal by a term which accounted for resistance offered by the test specimens. Results were also discussed for usage of modified law to obtain knoop

hardness numbers independent of applied load. Comparative study of knoop and vickers hardness numbers is also reported by Tietz and Troger (1976)⁷³. In continuation of the problem on the study of various important, interesting and useful facets of hardness of crystalline materials in this laboratory. Bhagia (1982)⁷⁴ and Shah (1984)⁷⁵ carried out the comparative study of vickers hardness number and knoop hardness number on the cleavages of natural calcite crystals and synthetic sodium nitrate crystals.

The variation of hardness on different faces of the same crystal is very well-known if the indentations are made along different directions on the same face, values of hardness are not usually found to be identical. The shape of the indentation mark also changes in many cases. Different values of hardness on the same face are attributed to the anisotropic nature of the crystal surface.

The dependence of the shape of indentations on the crystallographic direction was first reported by O'Neill (1923)⁷⁶ for Brinell impressions in aluminium crystals and later by Pfeidl (1927)⁷⁷ for Brinell

indentations in single crystals of iron. Pfeil described the impressions as 'square' on a cubic face, slightly oval on a rhombododecahedral face and circular with a tendency to be hexagonal on an octahedral face. Roth. Meyer (1950)⁷⁸ reported the slip marks on lead and aluminium. He found two sets of slip lines at right angles on a (100) face and three sets at 60° intervals on both (110) and (111) faces. Variations in appearance of the indentation marks with orientation of the grain were also noted by Roth. Meyer for lead, aluminium and zinc.

Bergman (1945)⁷⁹ observed a little variation in hardness values with respect to change in orientation of indenter for single crystals having high symmetry. However, Hendriques (1957)⁸⁰ reported the dependence of hardness with the crystallographic directions for sphalerite. Mokievskii (1960)⁸¹ and others related the nonsquare shape of the indentation mark to the anisotropy of elastic properties of the crystals, while Boyarskaya (1962)⁸² and his group related it to the anisotropy of the plastic property. The hardness anisotropy was studied on super pure and polycrystalline aluminium crystal with the help

three different indenters by Petty (1962).⁸³ He observed peaks for the regular interval of 90° . The variation was attributed to the pressure resolved in the surface. Partridge (1964)⁸⁴ and Roberts (1963)⁸⁵ reported the asymmetrical shape of diamond-impression on magnesium and zinc crystals and attributed this to the basal slip, pyramidal slip and twinning produced due to indentation. For beryllium and wurtzite compounds hardness variation with orientation were reported by Kahn and Cline (1963).⁸⁶ Hardness maxima have a relation with the symmetry of the particular face. This was shown for various faces of silicon ferrite and basal plane of ~~zinc~~ zinc by Dunn and Daniels (1949).⁸⁷ The curves obtained by plotting hardness (Knoop) number against orientation of the indenter for the (001), (110) and (111) faces of the ferrite crystal show that the number of hardness maxima per complete rotation is consistent with the crystallographic symmetry of the plane indented i.e., four for (001), two for (110) and six for (111). Dunn and Daniels related the variation of hardness to the effective resolved shear stress which was considered to be an inverse function of the ease of slip and is dependent on orientation. Vacher (1949)⁸⁸ reported results on single crystals of copper comparable to

those of Dunn and Daniels on ferrite. Lendvay (1969)⁸⁹ observed microhardness anisotropy in cubic and hexagonal zinc sulphide crystals. Brookes et al. (1971)⁹⁰ confirm that the nature of anisotropy in hardness is essentially determined by the crystal structure and primary slip systems which accommodate dislocation motion during indentation from the Knoop indentation measurements on single crystals.

Various synthetic crystals of corundum were examined under polarised light by Attinger (1952)⁹¹ to identify the optic axis and Knoop hardness tests were made on various faces and in different directions. These tests showed that faces normal to the optic axis gave the lowest hardness numbers, but no marked variation was found when the indenter was rotated about the optic axis. For faces parallel to the optic axis the hardness was greatest when the long diagonal was also parallel to it. These conclusions were confirmed by Stern (1951),⁹² using both a double cone indenter and a micro-abrasion test.

The anisotropic nature of microhardness of semiconductor was studied by Tsinzërling et al.

(1969).⁹³ They observed that the anisotropy was connected with anisotropic bonding and with the position of the cleavage planes relative to the movement of the indenter. Hardness anisotropy of commercially pure beryllium due to low temperature thermocycling was also reported (Lavrentev et al. 1985).⁹⁴ Chakraborty and Mukerji (1982)⁹⁵ studied variation of vickers microhardness in plane parallel [VMH(IIC)] and \perp to the Z-axis [VMH(\perp C)] of hexagonal β -Si₃N₄, α -Si₃N₄, α -SiO₂ (α -quartz) and α -SiC (6H) single crystals and correlated the ratio of VMH(IIC) and VMH(\perp C) with their unit cell parameters (along a and c directions) of the single crystals.

The above represents a brief review of the work done on hardness of various crystals. The present work is centred on the study of the variation of load with diagonal length of the indentation mark and of variation of hardness with load of gel-grown single crystals of ammonium-hydrogen-d-tartrate (d-AHT) at various quenching temperatures by using Knoop and Vickers diamond pyramidal indenters.

REFERENCES

1. TUCKERMAN, L.B. 1925 Mech. Eng. 47, 53
2. ASHBY, A.N. 1951 N.Z. Engng. 6, 33.
3. MAYER, E.Z. 1908 Verdtach Ing., 52, 645.
4. SPAETH, W. 1940 Physik and
Technique der
haetre and Weiche,
Berlin.
5. TERTSCH, H. 1935 Z. Krist. 92, 39.
6. TERTSCH, H. 1951 Neus Jahrb.
Mineral. Monatsch,
73.
7. TERTSCH, H. 1952 Neus Jahrb.
Mineral., Monatsh,
136.
8. FRIEDRICH, F. 1926 Fortschritt
Chem. Physik, 18,
5.
9. GOLDSCHMIDT, V.M. 1926 Norske Vod Akad i
Oslo Skr Mat Nat
KI # 8, p. 102.

10. CHATTERJEE, G.P. 1956 Ind. J. Phys.,
28, 9.
11. Phendl, J.N. and 1962 Phys. Revi., 125,
GIELISSE, P.J. 828.
12. MATKIN, D.I. and 1963 Trans. Britt.
CAFFYN, J.E. Ceram. Soc. 62,
753.
13. WESTBROCK, J.H. 1973 ' The Science of
and CONRAD, H. hardness and its
Research Applications"
American Soc. For
Metals, Ohio.
14. CHAIMERS, B. 1941 J. Inst. Metals,
67, 295.
15. GILMAN, J.J. and 1961 J. Appl. Phys.,
ROBERTS, B.W. 32, 1405.
16. SCHMIDT, E. and 1955 Naturwise, 20,
BOAS, W. 416
17. PARTRIDGE, P.W. 1964 Nature, 203, 634.

18. PHAAL, C. 1964 Phil. Mag., 10, 887.
19. VAHDICK, F.W. 1966 Japan, J. Appl. Phys., 5, 663.
20. URUSOVSKAYA, A.A. 1965 Sov. Phys. Cryst., 10, 437.
21. KUBO, K. 1970 J. Phys. Soc. Japan, 28, 117
22. SMAKULA, A. and KLEIN, M.W. 1951 Phys. Rev., 84, 1056
23. GILMAN, J.J. 1958 Trans, AIME, 212, 783.
24. BREIDTH, P. ; GREIMER, E.S. and EILISE, W.C. 1957 Acta, Met., 5, 60
25. VOTAVA, B. ; AMELINCKX, S. and DEKEYSOR, W. 1953 Physica, 19, 1163.
26. TOLANSKY, S. and NICKOLS, D.K. 1949 Nature, 164, 840

27. TOLANSKY, S. and NICKOLS, D.K. 1952 Phil-Mag., 43, 410
28. SATYANARAYAN, B.S. 1956 Can. J. Teck, 3, 375.
29. VOINOVA, N.M. and BEREZHKOVA, G.V. 1985 Kristallografiya, 30, 825.
30. HARRISE, P.W. 1922 J. Inst. Metals, 27.
31. KNOOP, F. 1937 Tech. Blatter, 27, 472.
32. Bernhardt, E.O. 1941 Z. Metalkunde, 33, 135.
33. CAMPBELL, R.F. ; HENDERSON, O. and DONLEAVY, M.R. 1948 Trans. Amer. Soc. Metals, 40, 954.
34. MOTT, B.W. 1956 "Microindentation hardness testing", Butterworths Scientific Publications, London, Ch. 1.

35. TAYLOR, E.W. 1948 J. Inst. Metals,
74, 493.
36. BERGSMAN, E.W. 1948 Metal Progress,
54, 183.
37. HANEMANN, H. 1941 Z. Metalkunde,
and SCHULTZ, F. 33, 124.
38. ONITSCHÉ, E.M. 1947 Microscopic, 2,
131.
39. GRODZINSKI, P. 1952 Ind. diamond Rev.,
12, 209.
40. MURPHY, R.J. 1969 Scripta Metallurgica,
(USA), 3, 905.
41. SUGITA, Y. 1963 Japan, J. Appl.
Phys., 10, 951.
42. KOSERICH, V.M. 1960 Fiz. Metallovi,
BASHMAKOV, V.I. Metallevendenic, 2,
288.
43. SHAH, B.S. and 1969 Current Sci.
MATHAI, M.B. (India), 38, 4780.

44. EDELMAN, F.L. 1964 Phys. Statussolidi
(Germany), 7, k 65.
45. SAMSONOV, G.V. ; 1969 Fiz. Tekh.,
KOVALCHENKO, V.V. ; Palypravachikav,
DZEMEDINSKII and 3, 1760.
UPADHYAY, G.S.
46. MIL'VIDSKI, M.G. ; 1965 Fiz. Metallov,
OSVENSKII, V.B. ; Metallovidenie,
STOLYAROV, O.G. 20, 150
and SHYLAKOV, D.B.
47. KUZ'MENKO, P.P. 1963 UKVEYIN, FIZ-Zn.
NOVYKOV, N.N. 'USSR), 8, 116
and Ya. HORYDKO, N.
48. BEILIN, V.M. and 1963 Fiz. Tverdogo,
VEKILOV, Yu. Kh. Tela, 5, 2372.
49. WESTBROOK, J.J. 1963 J. Phys. Soc.
and GILMAN, J.J. Japan, 18, 15.
50. OSVENSKII, V.B ; 1968 Fiz. Tuerdo, Tela,
MILVIDSKII, M.G. ; 10(9), 2809
STOLYAROV, O.G.
and IVIEVA, V.S.

- | | | | |
|-----|---|------|---|
| 51. | SMIRNOV, L.S. ;
STAS, V.F. and
KHAINOVSKAYA,
V.V. | 1969 | Fiz. Tekh.
Paluprevachikov,
<u>3</u> , 1760. |
| 52. | SETTZER, M.S. | 1966 | J. Appl. Phys.,
<u>37</u> , 4780. |
| 53. | PERINOVA, M. and
URUSOVSKAYA, A.A. | 1966 | Czech. J. Phys.
<u>B-6</u> , 791, 1966. |
| 54. | BERZINA, I.G. ;
BERMAN, I.B. and
SAVINTSEV, P.A. | 1965 | Sovt. Phys. Crst.,
<u>9</u> , 483. |
| 55. | UPIT, G.P. ;
VARCHOMIYA, S.A.
and MUKTEPAVEL,
F.O. | 1969 | Fiz. Tverdo, Tela,
<u>11</u> , 2841. |
| 56. | VRUSOVSKAYA, A.A.
and TYAGARADZHAN,
R. | 1965 | Kristallographiya,
<u>9</u> , 531. |
| 57. | SHUKLA, S.K. and
MURTHY, T.S. | 1968 | Nucl. Phys. and
Solid State Phys.
Symp., Digest,
Powai, Bombay
(India) 28-31 Dec. |

65. ACHARYA, C.T. 1978 Ph.D. Thesis, M.S.
Univ. of Baroda,
Baroda.
66. PANCHAL, P.J. 1981 M.Sc. Appl. Physics
Desertation, M.S.
University, Baroda,
67. ANBUKUMAR, S.; 1986 J. Mater Sci.
VASUDEVAN, S. Lett. 5, 223.
and RAMASWAMY, P.
68. MARTIN, B. ; 1985 Phys. Status Solidi
PASTOR, J.M. b, 131, pK5.
and de SaJA, J.A.
69. PASTOR, J.M. ; 1981 Ferroelectrics, 34,
RULL, F. ; 227.
MARTIN, B. and
de SAJA, J.A.
70. NABUTOVSKAYA, O.A. 1969 Fiz. Tverdogo
Tela, 11, 1434.
71. MOHRNHEIM, A.F. 1973 Prakt. Metallogr.
(Germany), 10, 2,
94.

- | | | | |
|-----|-------------------------------|------|---|
| 72. | HAYS, C. and
KENDALL, E.G. | 1973 | Metallography
(USA), <u>6</u> , 4, 275 |
| 73. | TIETZ, H.D. and
TROGER, A. | 1975 | Feingeraete,
Tech. (Germany),
<u>24</u> , 8, 355. |
| 74. | BHAGIA, L.J. | 1982 | Ph.D. Thesis, M.S.
Univ. of Baroda,
Baroda. |
| 75. | SHAH, A.J. | 1984 | Ph.D. Thesis, M.S.
Univ. of Baroda,
Baroda. |
| 76. | O'NEILL, H.J. | 1923 | J. Inst. Met. <u>30</u> ,
299 |
| 77. | PFEIL, L.B. | 1927 | Carnegie School.
Mem., <u>16</u> , 153 |
| 78. | ROTH-MEYER, H. | 1950 | C.R. Acad. Sci.,
Paris, <u>231</u> , 906. |
| 79. | BERGSMAN, E.B. | 1945 | Jern. Knotrovets,
Ann., <u>129</u> , 577 |

80. HENDRIQUES, A. 1957 Askiv. Mineral Geol., 2, 283.
81. MOKIEVSKII, V.A. 1960 Sovt. Phys. Cryst., 4, 381.
82. BOYARSKAYA, Yu. S. 1962 Sovt. Phys. Cryst., 7, 202
83. PETTY, E.R. 1962 J. Inst. Metals, 91, 54.
84. PARTRIDGE, P.W. 1964 Nature, 203, 634.
85. ROBERTS, E. and 1963 J. Inst. Metals, 92, 250.
86. KAHN, J.S. and 1963 J. of Electrochem. Soc., 110, 773
CLINE, L F
87. DUNN, C.G. and 1949 Trans. Amer. Soc.,
DANIELS, F.W. Metals, 41, 419
88. VACHER, H.C. 1949 Trans. Amer. Soc.
Metals, 41, 438.
89. LENDVAY, E. 1969 J. Materials Sci.,
4, 747.

90. BROOKES, C.A. ; 1971 Proc. Roy. Soc.
O'NEIL, J.B. and 3222A, 73
REDFERN, B.A.
91. ATTINGER, C. 1952 Industr. Diam.
Rev., 12, 136
92. STERN, W. 1951 Industr. Diam.
Rev., 11, 237
93. TSINZERLING, L.G.; 1969 Kristallografiya
BERKOVICH, E.S. (USSR), 14, 1037
and SHASKAL'SKAYA,
M.P.
94. LAVRENTEV, F.F. ; 1985 Cryst. Res. &
Technol. 20, 1117
95. SHAYAEVA, Ch. Yu. 1982 Mater Res. Bull.
CHAKRABORTHY, D. (USA), 17, 843
MUKERJI, J.

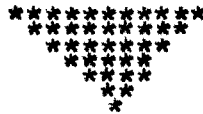
List of Tables

- 9.1 Information of different indenters used for hardness studies of materials.

CHAPTER - 10

VARIATION OF LOAD WITH DIAGONAL
LENGTH OF INDENTATION MARK

	<u>PAGE</u>
10.1 Introduction 	204
10.2 Experimental 	205
10.3 Observations 	207
10.4 Results and discussion 	210
10.4.1 Characteristics of two straight line regions in the graph 	214
10.5 Conclusions 	218
References	



10.1 INTRODUCTION

A variety of useful tests have been devised wherein some kind of mechanical operation is performed on the surface of the specimen. Quantities measured by these surface tests are generally associated with the term 'hardness'. Hardness as applied to amorphous and crystalline materials has long been the subject of discussion amongst engineers, physicists, metallurgists and mineralogists and there are all sorts of conceptions as to what constitutes hardness. The overwhelming difficulty of defining hardness is that it does not appear to be a fundamental property of material. There is no universally accepted single test for hardness, applicable to all materials. Thus there is hardness as measured by resistance to cutting, by scratching, by penetration, by electrical and magnetic properties¹ (Mott, 1956). The fundamental physics of hardness is not yet clearly understood. The present work is taken up with the express purpose of critically reexamining the various formulae connected with hardness by systematically studying 'microhardness' of d-AHT crystals. It is an extension of the work reported earlier on rhombohedral crystals (calcite and sodium nitrate)^{2,3} (Bhagia, 1982, Shah, 1984),

ferroelectric crystal (TGS), metallic crystal (Zn)⁴ (Acharya, 1978) and cubic crystals (alkali halides)^{4,5} (Acharya, 1978 and Shah, 1976). As far as, author is aware, systematic work on synthetic piezoelectric crystal (d-AHT) is not reported so far. In what follows the terms 'hardness' and 'microhardness' of crystals are used to indicate the same meaning.

10.2 EXPERIMENTAL

Single crystal of d-AHT grown in a gel medium (cf Chapter 5) were used in the present investigation. The work was carried out on natural faces $m(11\bar{0})$ and $z(111)$ and cleavage faces of d-AHT crystal for different quenching temperatures. Cleaved crystals of approximately equal sizes were used so that a comparison of thermally treated and untreated samples could be easily made. Freshly cleaved blocks having 2 mm thickness were fixed on glass plates with an adhesive. The levelling of the specimens was tested by using a CZ VERTICAL incident light microscope. The hardness tester described in Chapter-2, was used to produce indentations on cleaved surface by using pyramidal indenters, viz., square-based vickers and rhomb-based knoop indenters. The filar micrometer

eyepiece was used to measure surface dimensions of indentation marks. In order to avoid the influence of one indentation mark on the other, the distance between two consecutive indentations was maintained at a minimum of ~~four~~ four times the diagonal length of the mark and the indentation time for all specimens was kept 15 seconds. The load was varied from 2.5 gm to 140 gm for all quenching temperatures. Care was taken to see that errors introduced during the work of indentation and measurements of the dimensions of the indentation marks are avoided or minimized. The indentation marks were produced by diamond indenters on the surface in such a way that one of their diagonals of vickers diamond indenter and in case of knoop indenter longer diagonal was always parallel to [001] direction on the crystal cleavage and $m(110)$ surface and in case of $z(111)$ face along one of the edges. It should be mentioned here that the indentations were produced by knoop and vickers indenters on the same sample to facilitate comparison. Due to non-availability of a hot stage and optical components of microscope to be used with this stage in hardness tester, the indentation work was carried out at room temperature for annealed and/or

quenched crystals for studying the variation of load with diagonal length of indentations and variation of hardness with quenching temperature. For quenching experiments, crystals of approximately equal sizes and of identical habits were used. They were gradually raised to a desired temperature and kept at that temperature for identical periods running into a few hours (24 hours in the present case). They were then quenched to room temperature. The quenching rates were made as high as possible and were adjusted so that the quenched crystals maintained their shapes. In the present case the rate of quenching varied from $0.25^{\circ}\text{C}/\text{sec.}$ to $0.5^{\circ}\text{C}/\text{sec.}$ These experiments were conducted upto a temperature of 110°C , because beyond this temperature d-AHT begins to decompose into NH_3 and CO_2 .

10.3 OBSERVATIONS

The diagonals of the indentation marks produced by various loads were measured. Several sets consisting of a large number of observations on natural faces $m(110)$, $z(111)$ and freshly cleaved surfaces of d-AHT indented by various loads at room temperature and at different quenching temperatures were taken and

a typical set of observations, recorded in Table 10.1 to 10.6, were graphically studied by plotting $\log P$ versus $\log d$. P is the applied load in grammes and d is the length of a diagonal of indentation mark in microns for vickers indenter and the length of longer diagonal in case of knoop indenter.

Ideally the impression of vickers indentation on a surface is a square with equal lengths of both diagonals. However this is not always true for surfaces of real crystals. This is indeed the case for d-AHT crystal which is non-centrosymmetric. Hence in the present work, measurements were made for both diagonals in the directions $[001]$ and $[100]$. Out of these, the corners of a diagonal along $[001]$ are quite sharp and clear when observed under high magnification and resolution. For diagonal along $[100]$ one corner is quite sharp, whereas the other is not. Hence while locating the relatively less sharp and feebly visible corner, method of focussing and defocussing the same spot was used. The separate observations were therefore recorded for each one of them and also average of the two were taken and recorded. For each one, graph of $\log p$ vs. $\log d$ was plotted. Table 10.1 and 10.2 record variations of diagonal lengths for

Table 10.1

For Vickers indenter diagonals along $[001]$ direction
on d-AlH plane (010)

log P	log d_{Vx} at different quenching temperature				
	308 ^o K	323 ^o K	343 ^o K	363 ^o K	383 ^o K
0.3979	1.1578	1.1292	1.0878	1.1789	1.1484
0.5740	1.2017	1.1827	1.1670	1.2198	1.2256
0.6989	1.2441	1.1942	1.2017	1.2574	1.2828
0.8750	1.3096	1.2541	1.2703	1.2702	1.2670
1.0000	1.2919	1.2937	1.3267	1.3096	1.3370
1.1761	1.3510	1.3510	1.3954	1.3431	1.3888
1.3010	1.4235	1.3741	1.4151	1.4168	1.4367
1.3979	1.4679	1.4100	1.4619	1.4236	1.4659
1.4771	1.5138	1.4789	1.4915	1.4720	1.5064
1.6021	1.5744	1.5452	1.5401	1.5028	1.5452
1.6990	1.6234	1.5884	1.5974	1.5780	1.5914
1.7782	1.6533	1.6359	1.6372	1.6077	1.6368
1.8451	1.7023	1.6599	1.6871	1.6339	1.6637
1.9031	1.7080	1.6788	1.7196	1.6688	1.6825
2.0000	1.7750	1.7474	1.7568	1.7547	1.7250
2.0792	1.8381	1.7441	1.7868	1.7720	1.7568
2.1461	1.8610	1.8411	1.8296	1.8121	1.7963

Table 10.2

For Vickers indenter diagonals along $[100]$
direction on $\alpha\text{-AlF}$ plane (010)

log P	log dV_y at different quenching temperature				
	308 ^o K	323 ^o K	343 ^o K	363 ^o K	383 ^o K
0.3979	1.1225	1.1904	1.1292	1.2127	1.1904
0.5740	1.2127	1.2491	1.2127	1.2541	1.2639
0.6989	1.2491	1.2639	1.2339	1.3182	1.2828
0.8750	1.3267	1.3238	1.3096	1.3308	1.3096
1.0000	1.3225	1.3588	1.3665	1.4168	1.3588
1.1761	1.3349	1.4129	1.4236	1.3741	1.4335
1.3010	1.4389	1.4495	1.4367	1.4302	1.4595
1.3979	1.5028	1.4740	1.4875	1.4972	1.4972
1.4771	1.5315	1.5576	1.5099	1.5791	1.5245
1.6021	1.5773	1.6150	1.5591	1.6400	1.5711
1.6990	1.6400	1.7006	1.6256	1.6788	1.6063
1.7782	1.6676	1.7145	1.6521	1.7212	1.6560
1.8451	1.7279	1.7345	1.7041	1.7614	1.7110
1.9031	1.7246	1.7537	1.7668	1.7809	1.7246
2.0000	1.7705	1.7720	1.8024	1.8487	1.8148
2.0792	1.8255	1.7868	1.8281	1.8707	1.8295
2.1461	1.8537	1.8255	1.7868	1.8281	1.8707
		1.8537	1.8547	1.9014	1.8659

Table 10.3

For Knoop indenter d-AHF plane [010]

log P	$\log d_k$ at different quenching temperature				
	308°K	323°K	343°K	363°K	383°K
0.3979	1.7720	1.7495	1.7552	1.7680	1.7537
0.5740	1.7868	1.8166	1.7982	1.8368	1.7809
0.6989	1.8249	1.8148	1.7925	1.8334	1.8228
0.8750	1.8725	1.8902	1.8490	1.8917	1.8495
1.0000	1.9117	1.9355	1.8574	1.8940	1.8487
1.1761	1.9229	1.9686	1.9287	1.9521	1.8802
1.3010	1.9724	2.0055	1.9695	1.9974	1.9266
1.3978	2.0030	2.0256	1.9901	2.0314	1.9686
1.4771	2.0400	2.0347	2.0488	2.0494	2.0155
1.6021	2.0865	2.0834	2.0654	2.0839	2.0678
1.6990	2.1401	2.1344	2.1108	2.1076	2.1076
1.7782	2.1850	2.1967	2.1656	2.1535	2.1564
1.8451	2.2166	2.2298	2.2149	2.1882	2.1777
1.9031	2.2541	2.2548	2.2448	2.2308	2.1899
2.0000	2.3010	2.3009	2.2775	2.2804	2.2411
2.0792	2.3436	2.3353	2.3411	2.3239	2.2668
2.1461	2.3741	2.3650	2.3637	2.3595	2.3148

Table 10.4

For Vickers indenter d-AMT plane [010]

log P	log d_{va} at different quenching temperature				
	308 ^o K	323 ^o K	343 ^o K	363 ^o K	383 ^o K
0.3979	1.1405	1.1609	1.1089	1.1961	1.1700
0.5740	1.2073	1.2172	1.1905	1.2373	1.2451
0.6989	1.2467	1.2304	1.2181	1.2889	1.2828
0.8750	1.3183	1.2904	1.2904	1.3016	1.2889
1.0000	1.3074	1.3275	1.3471	1.3665	1.3481
1.1761	1.3430	1.3647	1.4097	1.3588	1.4117
1.3010	1.4313	1.4134	1.4261	1.4236	1.4483
1.3979	1.4857	1.4432	1.4749	1.4619	1.4818
1.4771	1.5227	1.5205	1.5008	1.5256	1.5155
1.6021	1.5747	1.5815	1.5501	1.5768	1.5583
1.6990	1.6319	1.6481	1.6118	1.6313	1.5989
1.7782	1.6605	1.6770	1.6447	1.6682	1.6464
1.8451	1.7153	1.6988	1.6957	1.7023	1.6880
1.9031	1.7166	1.7179	1.7386	1.7285	1.7041
2.0000	1.7728	1.7599	1.7802	1.8042	1.7722
2.0792	1.8318	1.7736	1.8079	1.8242	1.7946
2.1461	1.8574	1.8338	1.8423	1.8590	1.8325

Table 10.5

log P	Cleavage plane (010)		m-face (110)		z-face (111)	
	log d_{Vx}	log d_{Vy}	log d_{Vx}	log d_{Vy}	log d_{Vx}	log d_{Vy}
0.3979	1.1578	1.1225	1.2658	1.3573	1.2234	1.2828
0.6989	1.2441	1.2491	1.2339	1.3283	1.2017	1.2441
0.8750	1.3096	1.3267	1.3225	1.4065	1.2441	1.2639
1.0000	1.2919	1.3225	1.4141	1.5083	1.3009	1.3267
1.1761	1.3510	1.3349	1.3665	1.4680	1.3741	1.4065
1.3010	1.4235	1.4389	1.4058	1.5383	1.4558	1.4857
1.4771	1.5138	1.5315	1.4710	1.6409	1.4972	1.5155
1.6021	1.5744	1.5773	1.5639	1.6818	1.5349	1.5591
1.6990	1.6234	1.6400	1.6360	1.7023	1.5601	1.6048
1.7782	1.6533	1.6676	1.6608	1.7434	1.6332	1.6441
1.8451	1.7023	1.7279	1.6963	1.7762	1.6277	1.6427
1.9031	1.7080	1.7246	1.7226	1.8272	1.6751	1.6970
2.0000	1.7750	1.7705	1.7568	1.8360	1.7378	1.7442
2.0792	1.8381	1.8255	1.7831	1.8683	1.7750	1.7846
2.1461	1.8610	1.8537	1.8141	1.8992	1.8134	1.8188

d_{Vx} = diagonals of vickers indenter measured along [001] direction for (010) & (110) planes
 and [101] for (111) plane
 d_{Vy} = diagonals of vickers indenter measured along ^{normal to} [001] direction for (010) & (110) planes
 and [101] for (111) plane

Table 10.6

log P	Cleavage plane (010)		m-face (110)		z-face (111)	
	log d_{Va}	log d_k	log d_{Va}	log d_k	log d_{Va}	log d_k
0.3979	1.1405	1.7720	1.3140	1.7690	1.2541	1.6004
0.6989	1.2467	1.8249	1.2837	1.8188	1.2234	1.6150
0.8750	1.3183	1.8725	1.3665	1.8778	1.2541	1.6657
1.0000	1.3074	1.9117	1.4637	1.8360	1.3140	1.6982
1.1761	1.3430	1.9329	1.4203	1.9084	1.3906	1.7190
1.3010	1.4313	1.9724	1.4771	1.9974	1.4710	1.8188
1.4771	1.5227	2.0400	1.5642	2.0539	1.5064	1.9080
1.6021	1.5747	2.0865	1.6269	2.0942	1.5472	1.9336
1.6990	1.6319	2.1401	1.6704	2.1613	1.5830	1.9478
1.7782	1.6605	2.1850	1.7041	2.1843	1.6387	2.0290
1.8451	1.7153	2.2116	1.7381	2.2318	1.6353	2.0907
1.9031	1.7166	2.2541	1.7781	2.2605	1.6862	2.1252
2.0000	1.7728	2.3010	1.7982	2.2928	1.7410	2.1730
2.0792	1.8318	2.3436	1.8278	2.3308	1.7798	2.2186
2.1461	1.8574	2.3741	1.8587	2.3733	1.8161	2.2511

where log d_{Va} -- logarithm of average of two diagonals of Vickers indenter mark

log d_k -- logarithm of longer diagonal of Knoop indenter mark.

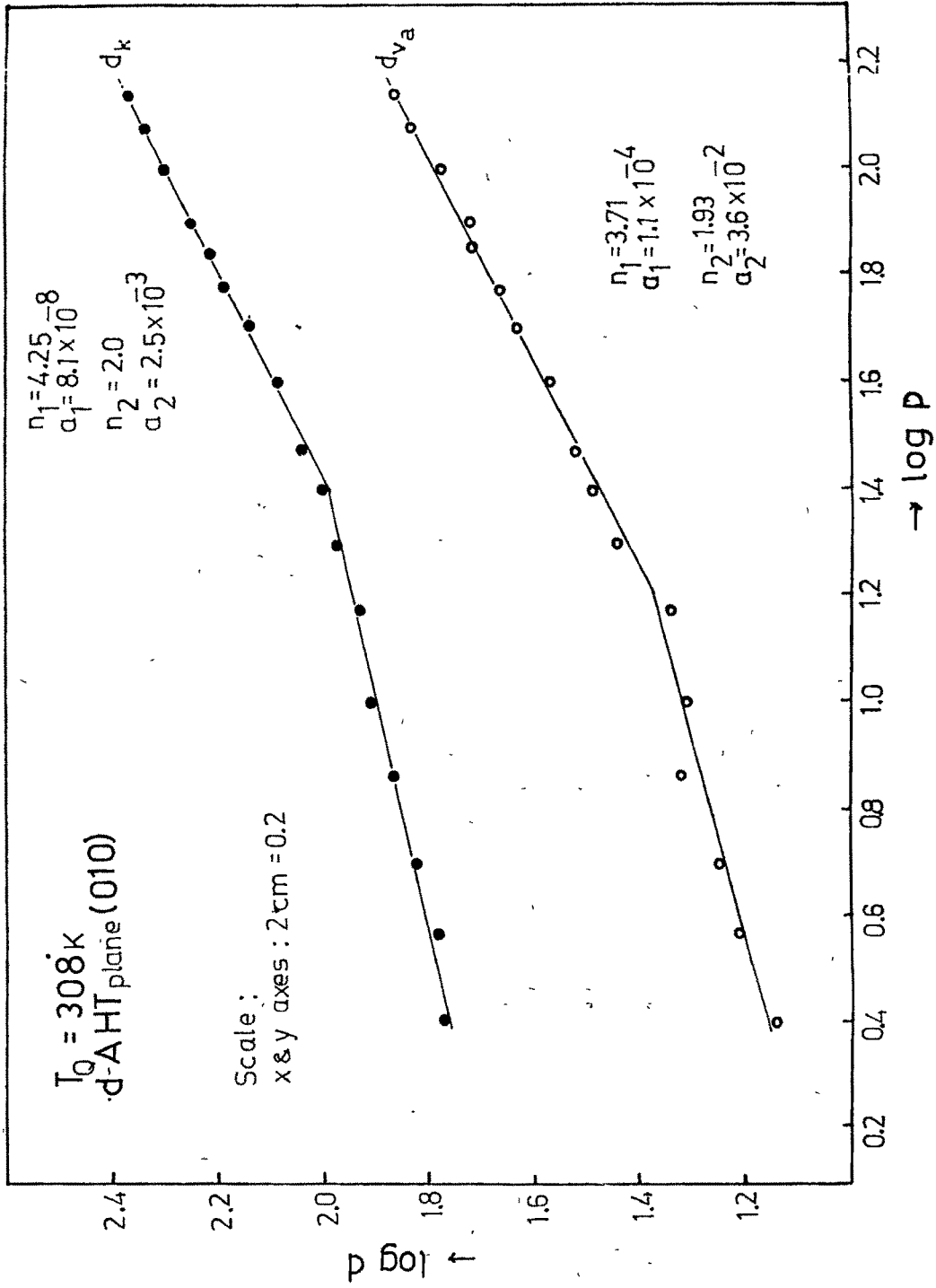


Fig. 10.1

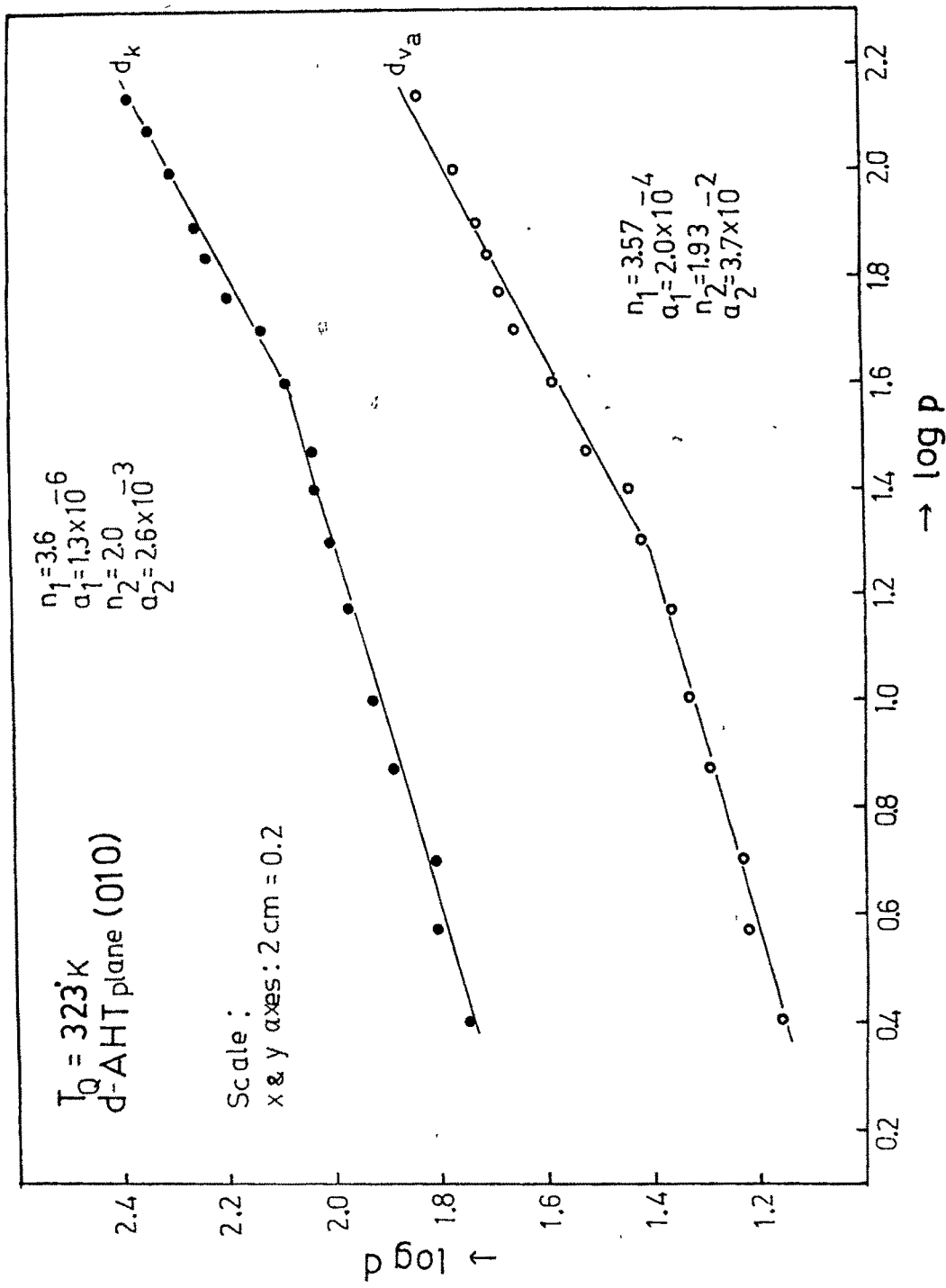


Fig 10.2

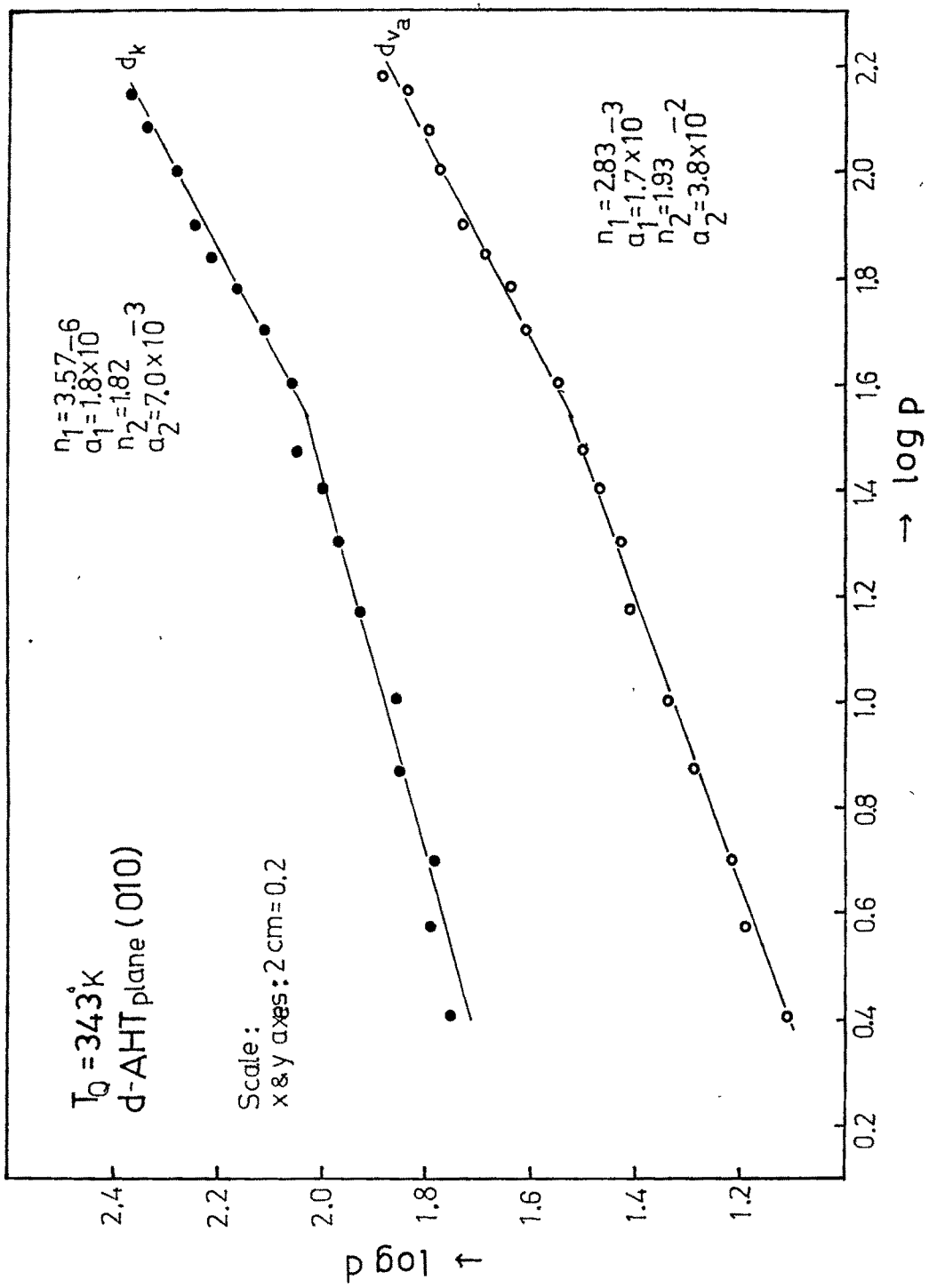


Fig 10.3

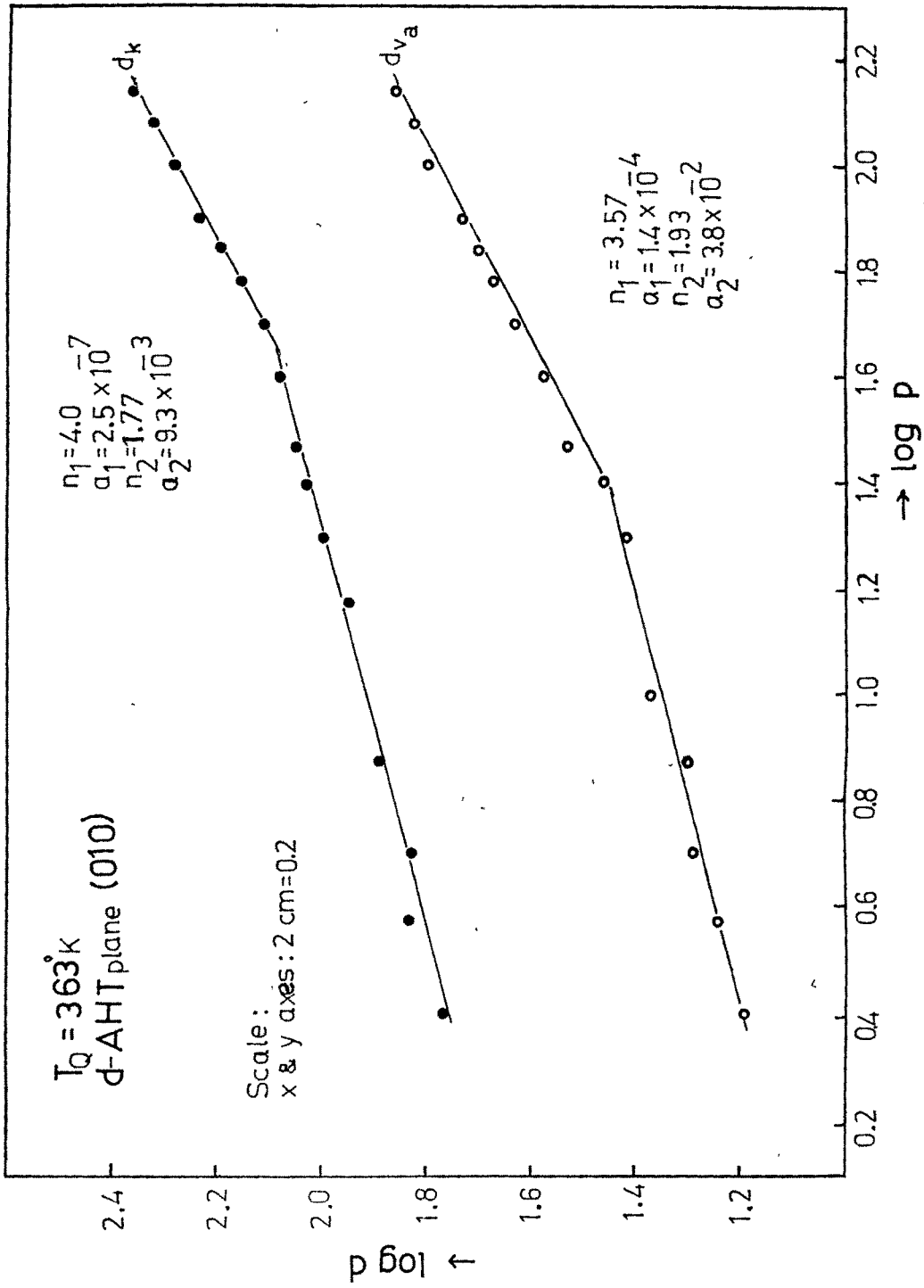


Fig. 10.4

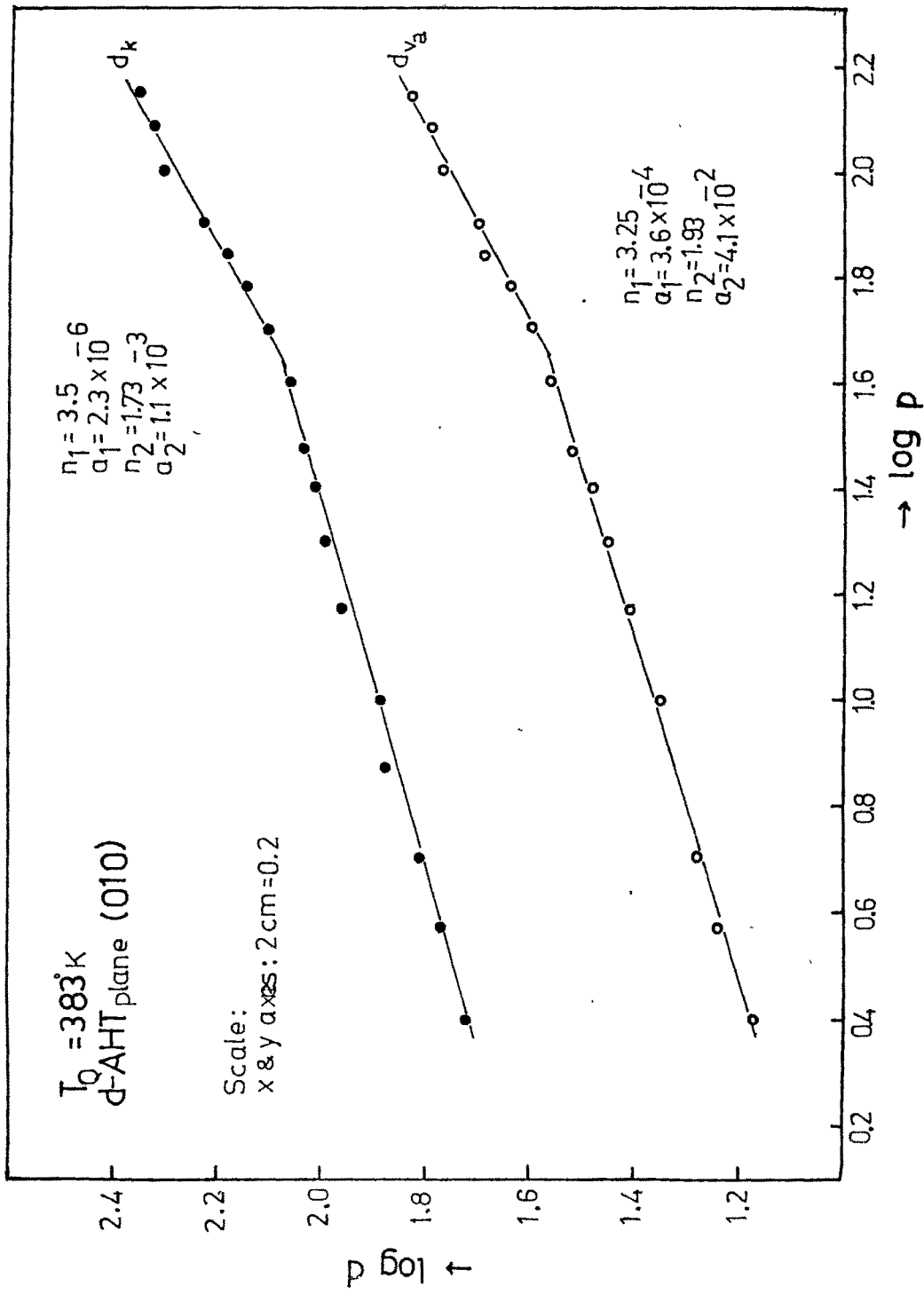


Fig. 10.5

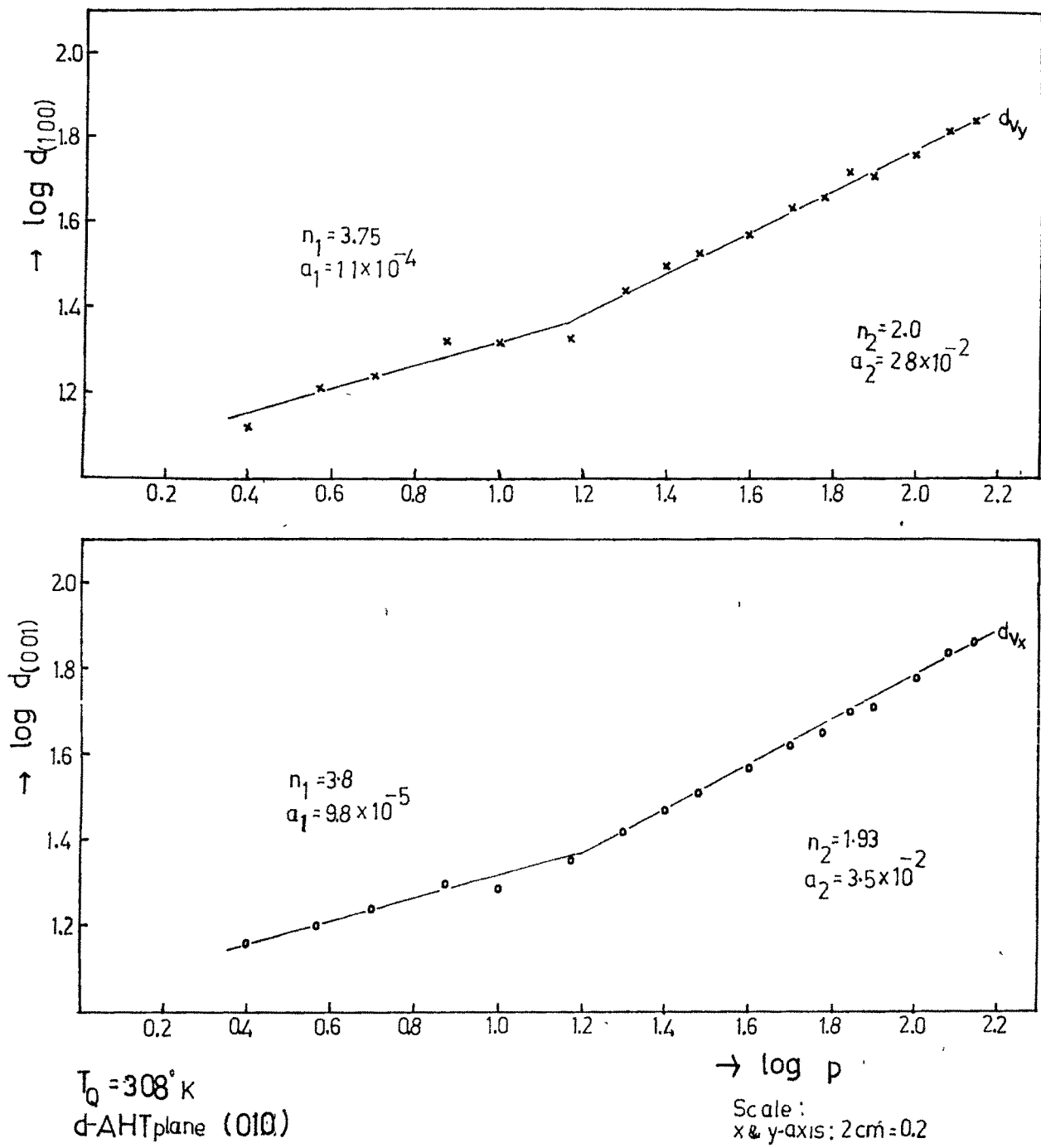
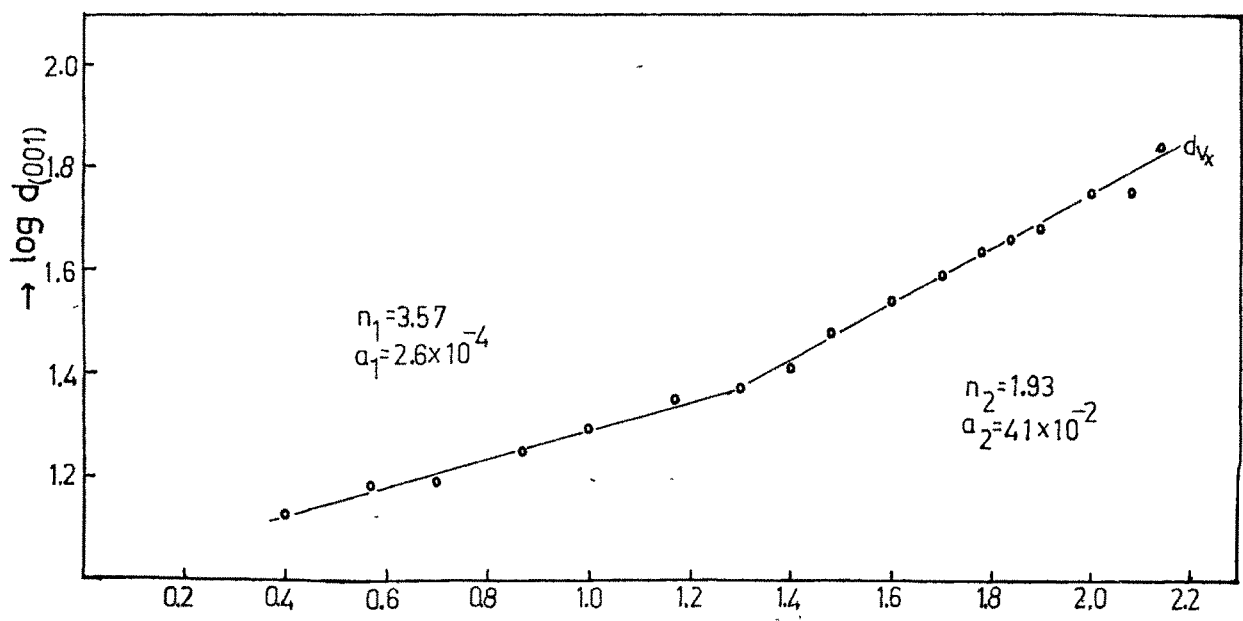
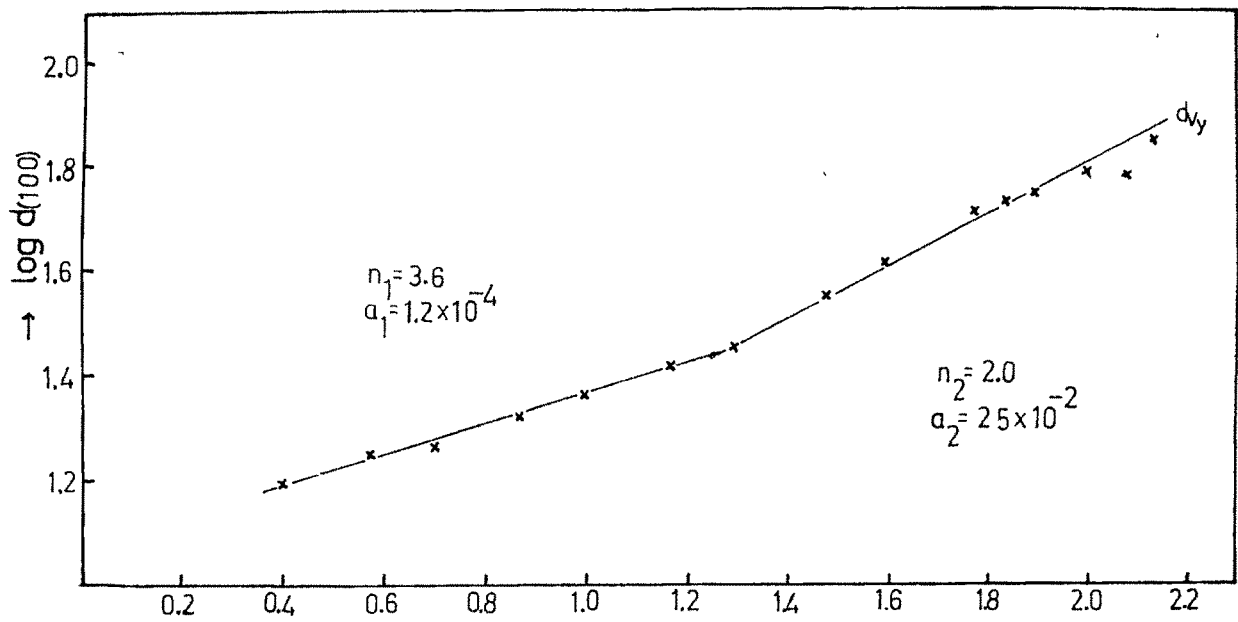


Fig.10.6

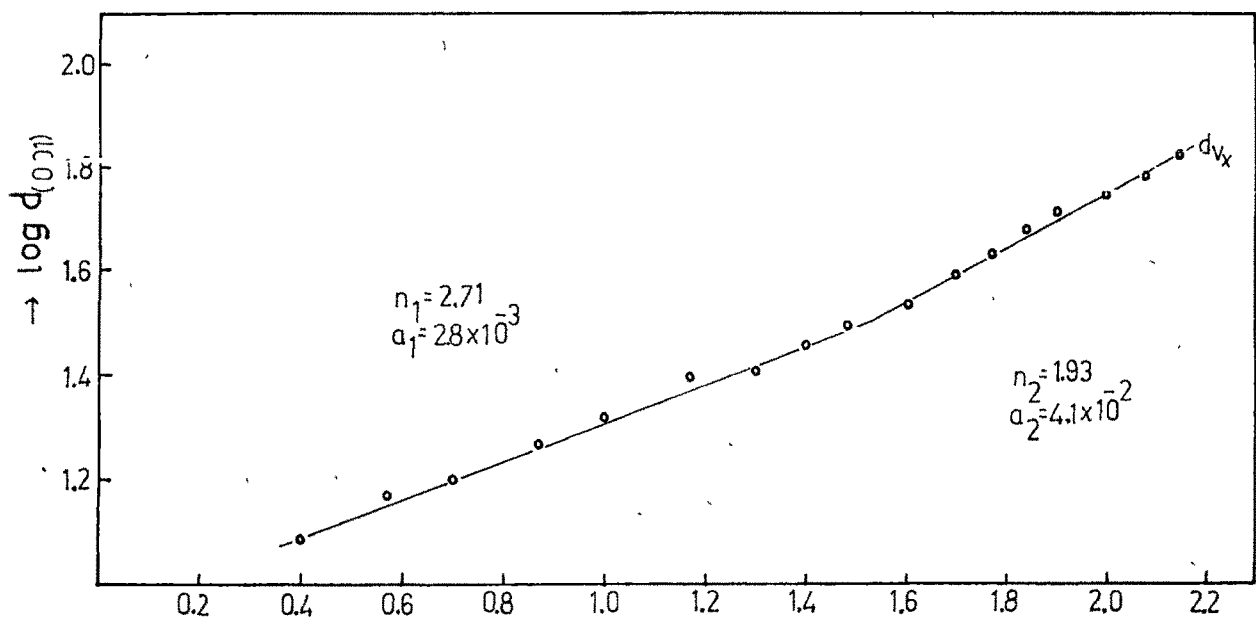
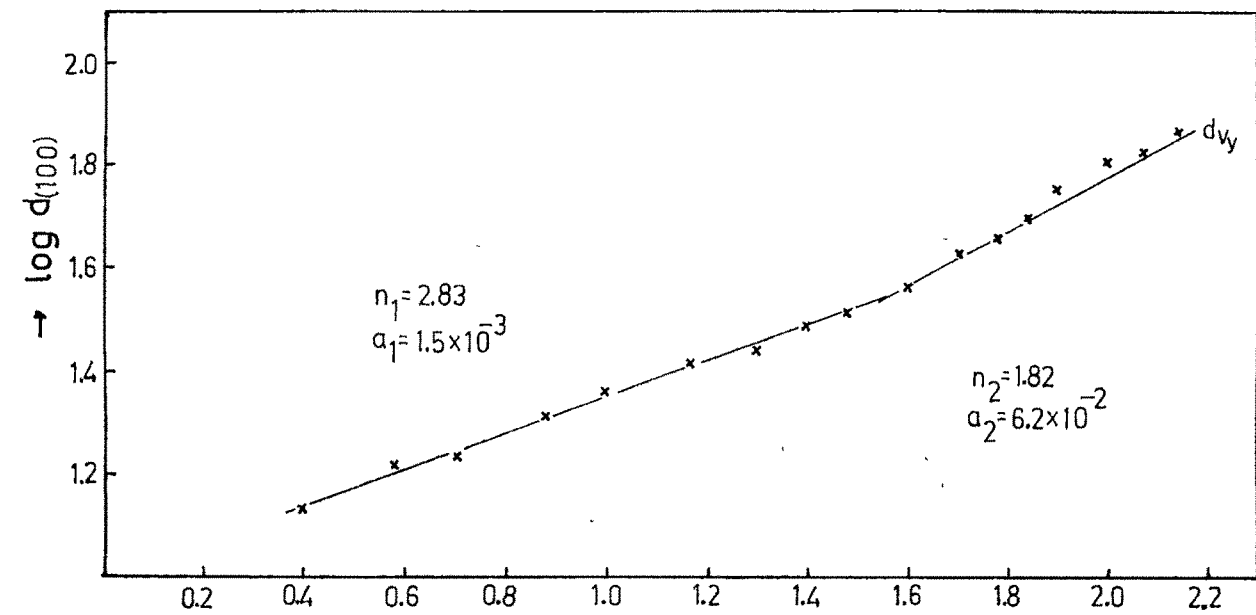


$T_Q = 323\text{K}$
d-AHT plane (010)

$\rightarrow \log p$

Scale:
x & y-axis : 2cm=0.2

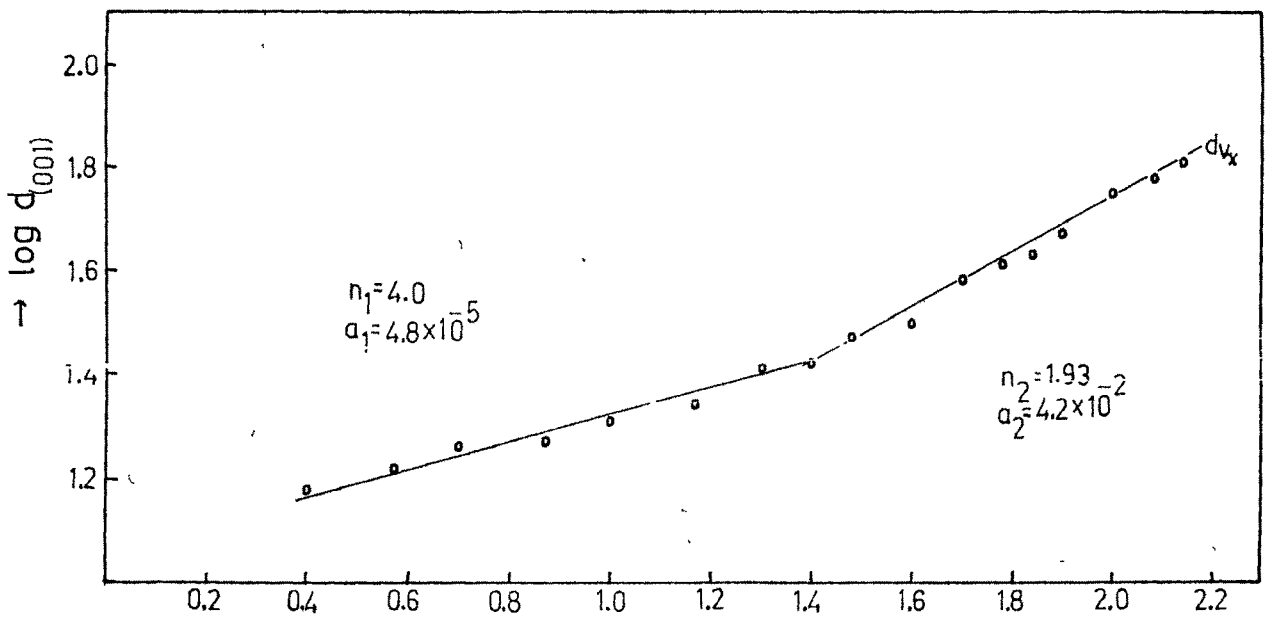
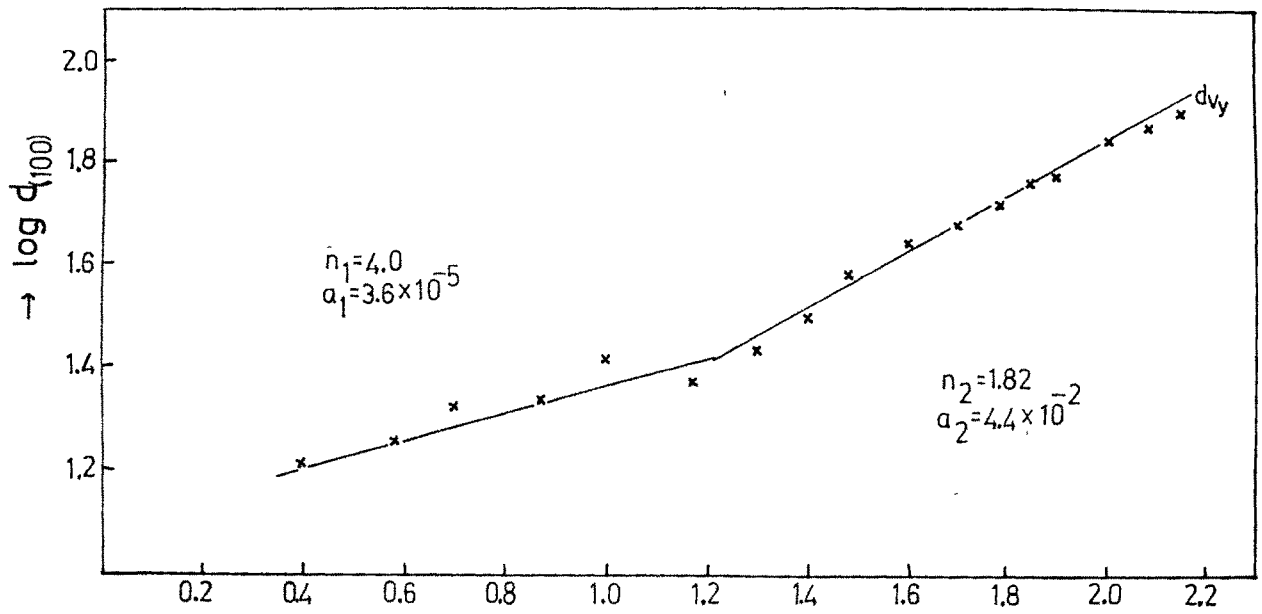
Fig. 10-7



$T_Q = 343 \text{ K}$
 $d\text{-AHT}_{\text{plane (010)}}$

$\rightarrow \log p$ Scale
 $x \ \& \ y\text{-axis} : 2 \text{ cm} = 0.2$

Fig 10.8

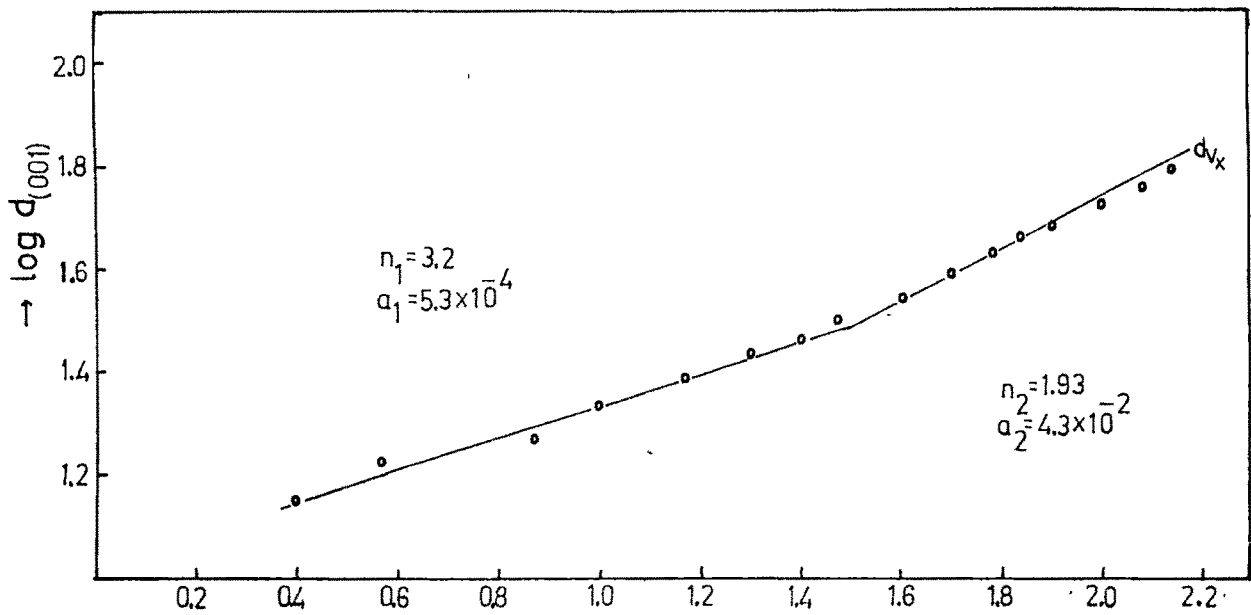
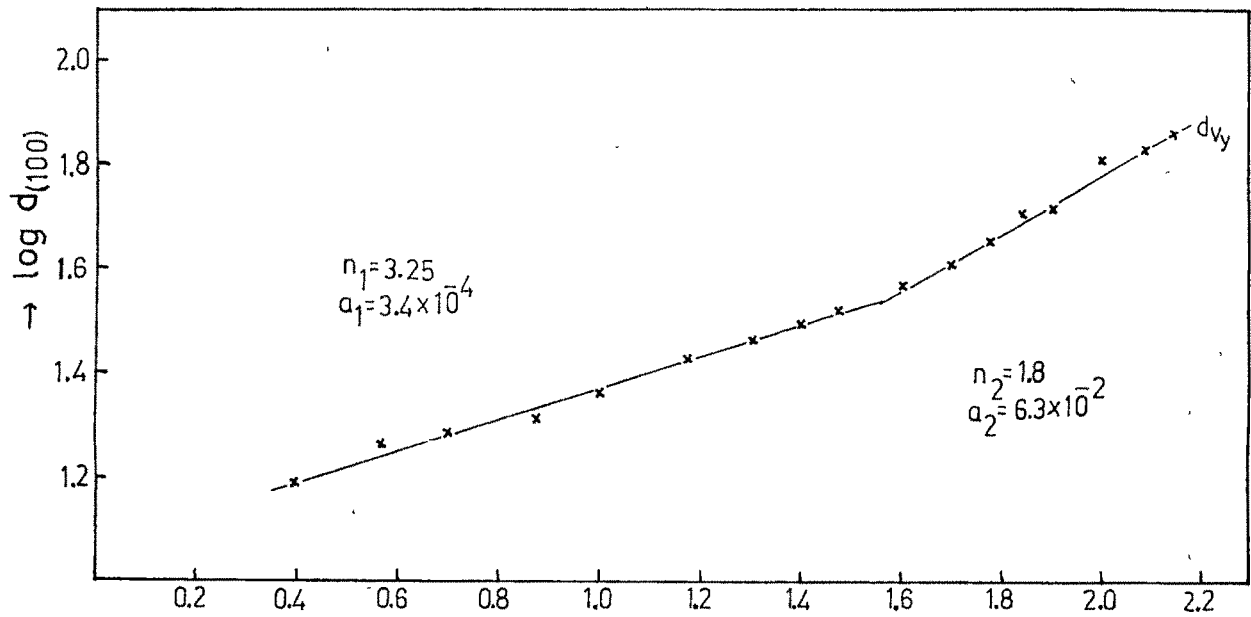


$T_0 = 363\text{K}$
 d -AHT plane (010)

→ log p

Scale:
 x & y-axis: 2cm = 0.2

Fig. 10.9

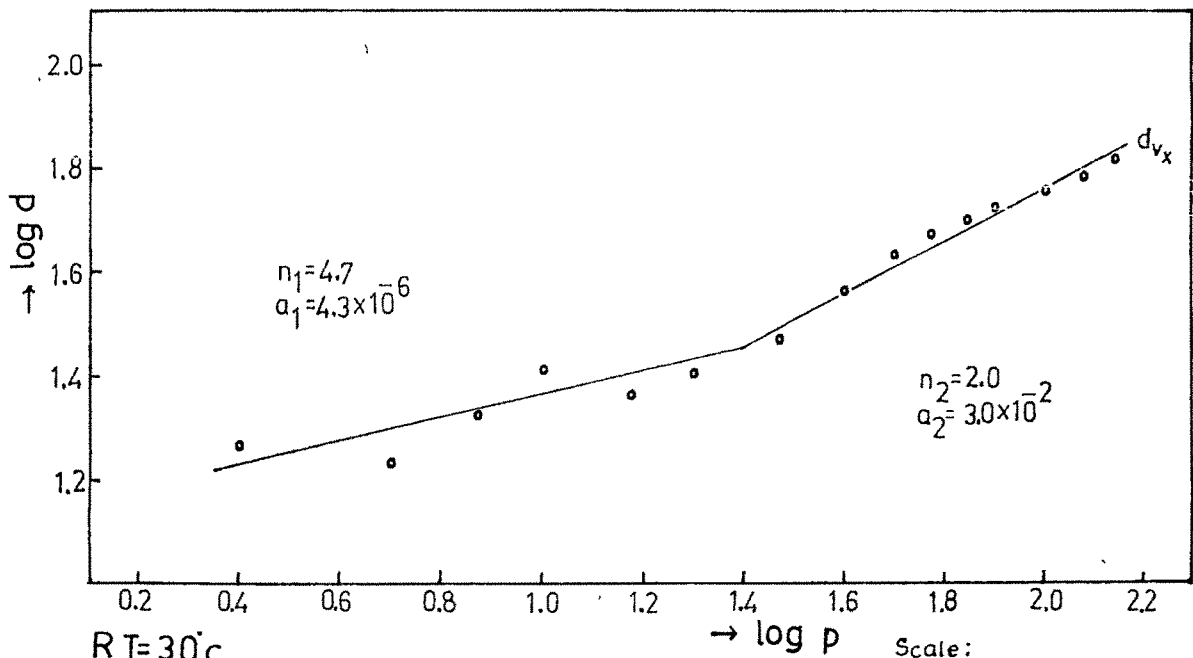
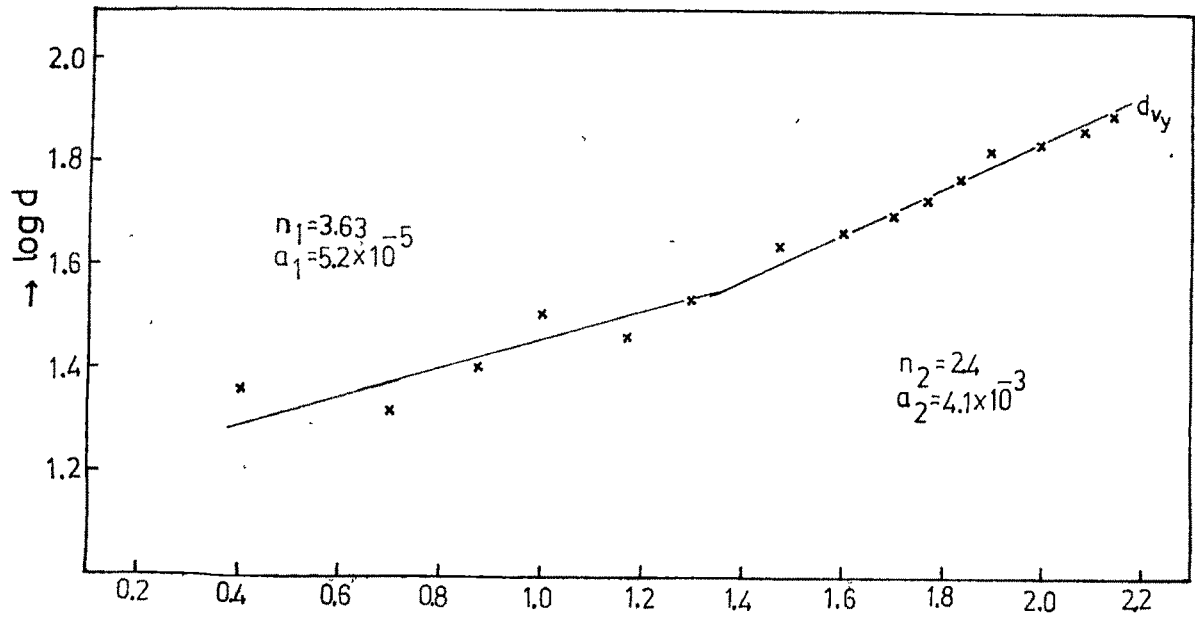


$T_Q = 383\text{K}$
 $d\text{-AHT plane (010)}$

$\rightarrow \log p$

Scale :
 x-axis : 2cm = 0.2
 y-axis : 2cm = 0.2

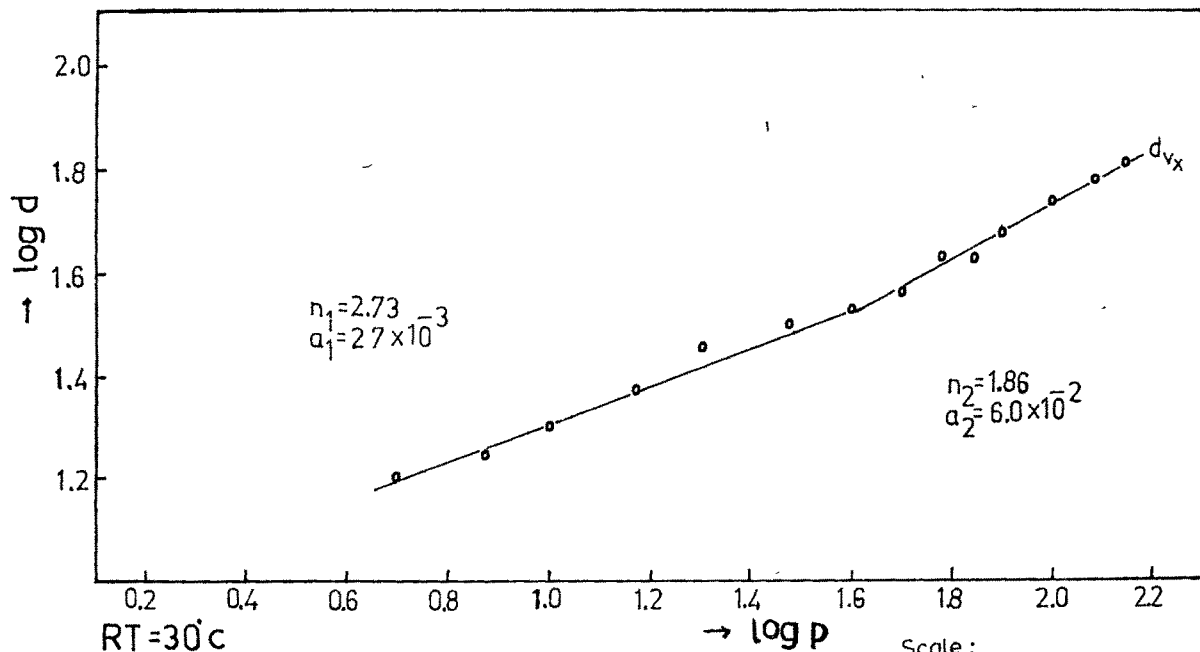
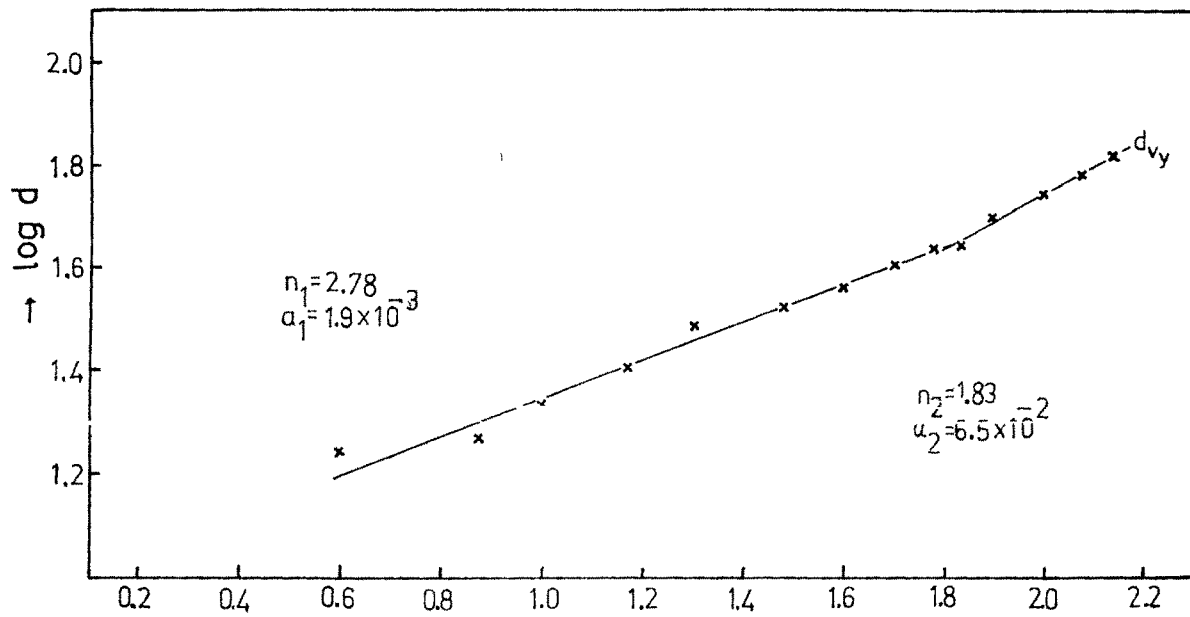
Fig. 10.10



RT=30°C
 m(110) plane
 d_{v_x} = along [001]
 d_{v_y} = normal to [001]

Scale:
 x & y axes: 2cm=0.2

Fig 10.11



RT = 30°C
 z (111) plane
 d_{v_x} = along [101]
 d_{v_y} = normal to [101]

Fig. 10.12

Scale:
 x & y axes: 2 cm = 0.2

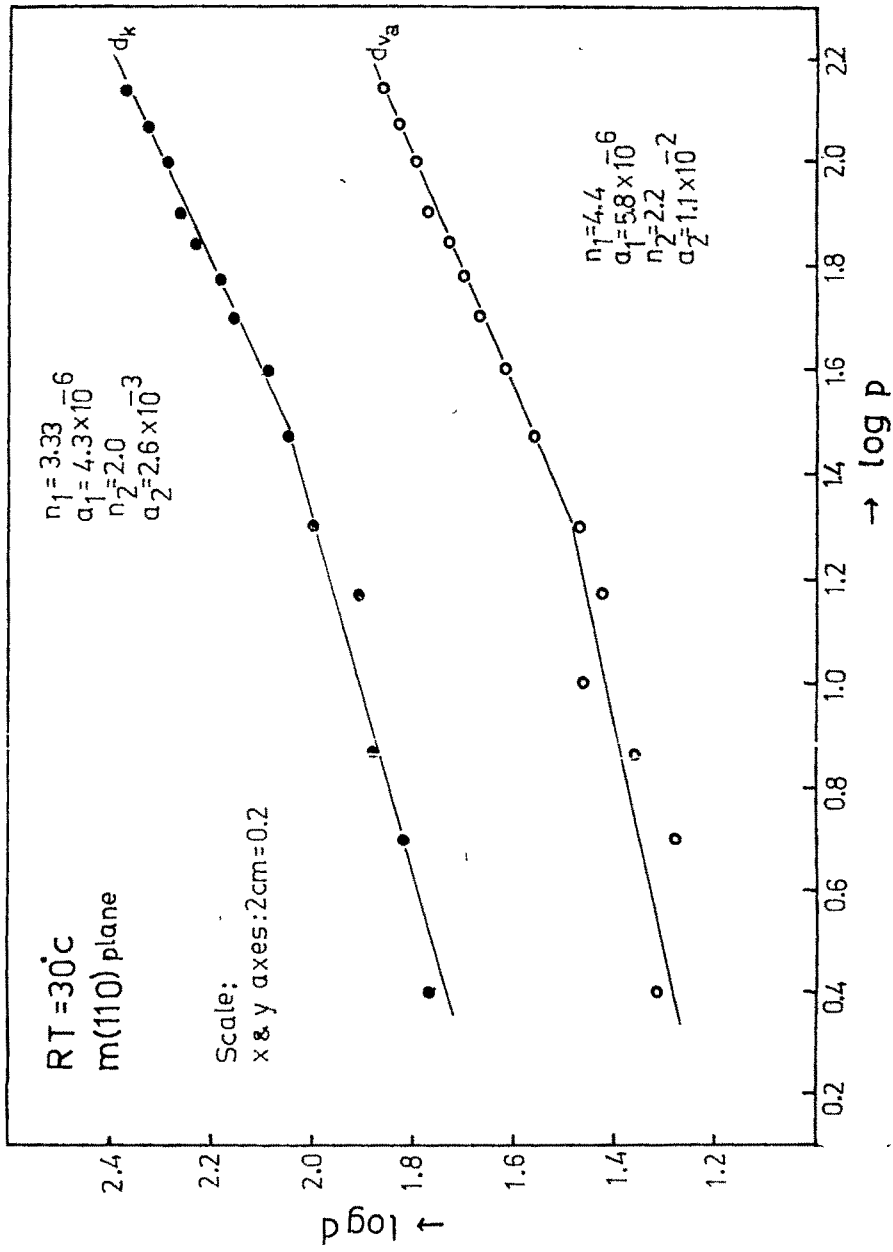


Fig. 10.13

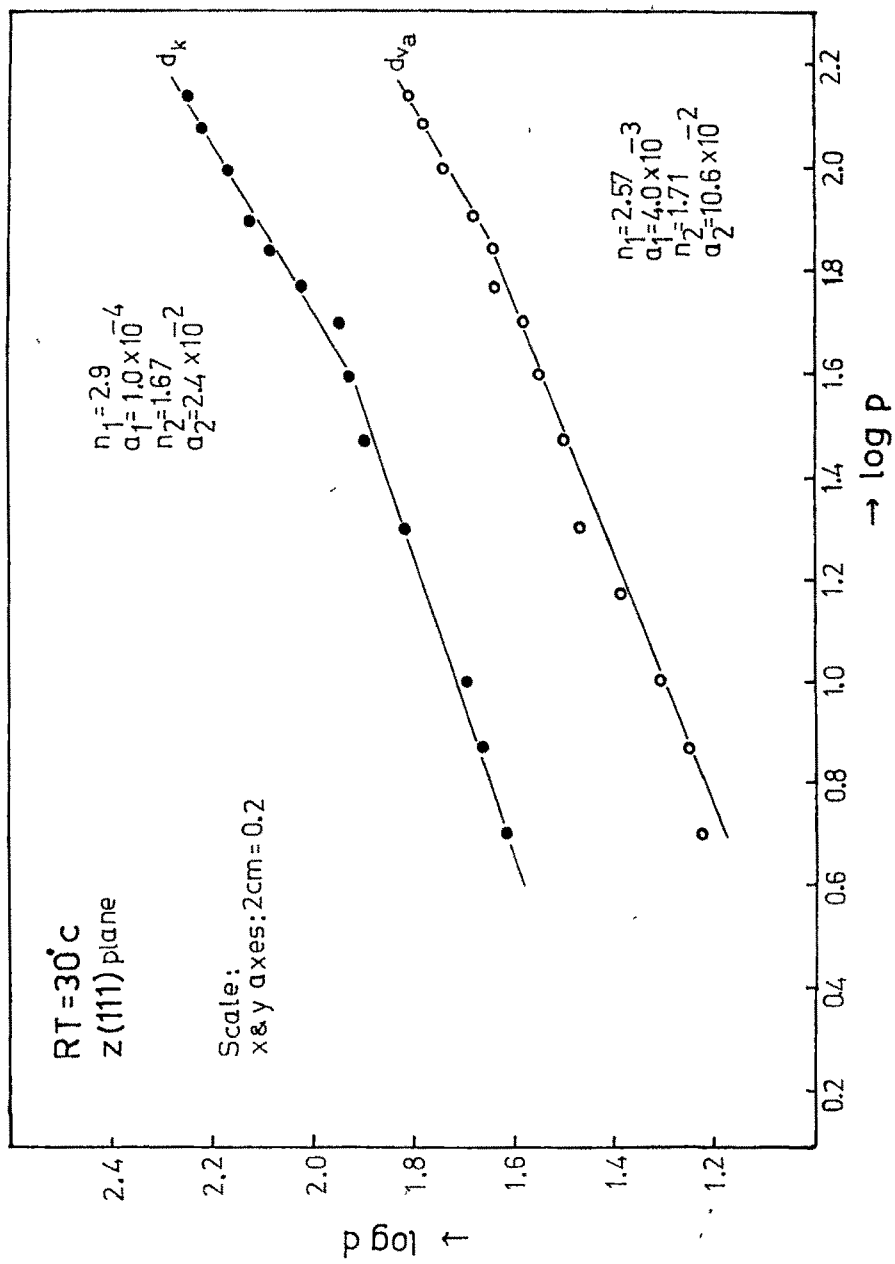


Fig. 10.14

different loads P for two diagonals of vickers indenter for different quenching temperatures. One diagonal of vickers indenter was parallel to C -axis of crystal i.e. along $[001]$ direction, whereas another along $[100]$ direction as mentioned above and represented in the table by V_x and V_y respectively (Fig. 10.1 to 10.5). To compare two hardness numbers (knoop and vickers) in case of vickers, average of two diagonals is taken into account. Table 10.3 and 10.4 present these observations, which are graphically presented in Fig. 10.6 to 10.10. In the same manner in the case of natural faces $m(110)$ and $z(111)$, the observations are tabulated in tables 10.5 and 10.6, respectively, in comparison with cleavage plane (010) at room temperature 30°C and the corresponding plots are given in Fig. 10.11 to 10.14.

The photomicrographs Fig. 10.15, 10.16, 10.17 exhibit indentation marks produced on a freshly cleavage surface and on $z(111)$ faces. Fig. 10.15 is a photomicrograph of a freshly cleaved surface indented under an applied load of 40 g. at 30°C by using vickers indenter. The significant points are the development of wings on one side of the indentation mark and in the direction $[100]$ and crystallographic



Fig. 10.15 (a) Photomicrograph of d-AlH cleavage surface indented by using vickers hardness indenter by for applied load of 40 g, showing the formations of wings, crystallographic cracks and slip lines.

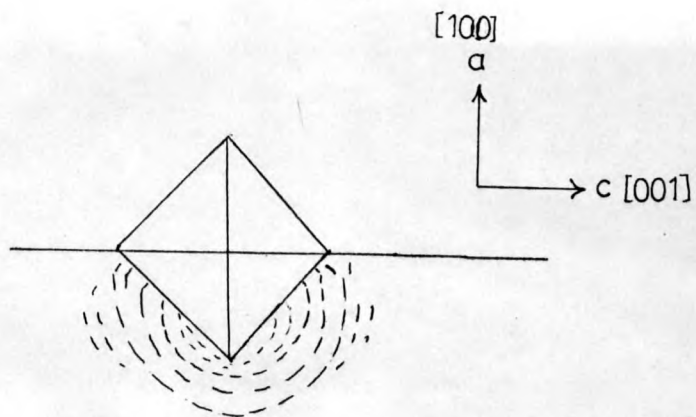
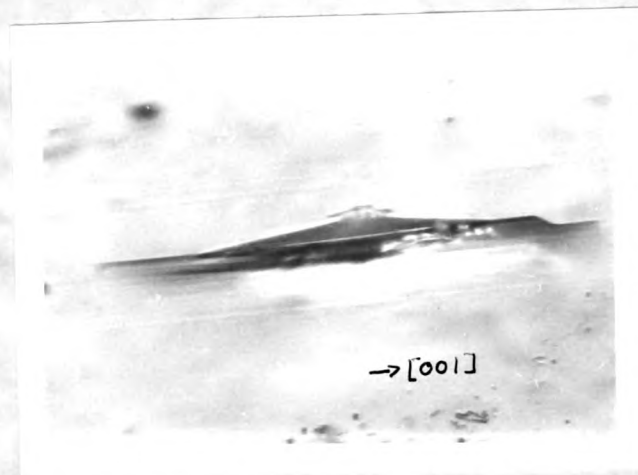
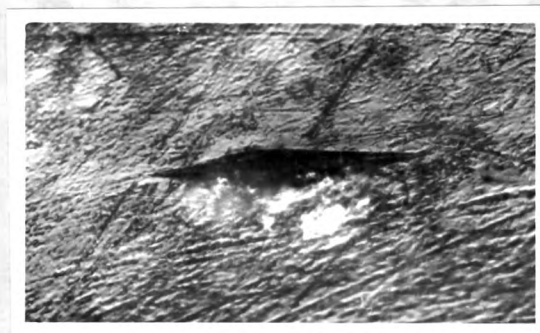


Fig. 10.15 (b) Schematic diagram of the indentation mark on d-AlH cleavage plane (Fig. 10.15a), showing wings, crystallographic cracks and slip lines.



x 250

Fig. 10.16 Photomicrograph of d-AHT cleavage plane surface indented by using knoop hardness indenter for applied load of 40 g. showing slip lines with direction $[001]$.



x 400

Fig. 10.17 Photomicrograph of d-AHT natural sphenoidal face (111) indented by using knoop hardness tester for applied load of 40 gm. along with the growth layers.

cracks and series of faint lines parallel to crack with direction $[001]$. This suggests the propagation of stress wave along definite characteristic direction on the indented d-AHT cleavages. Fig. 10.15b represents, the schematic diagram for the propagation and formation of wings and crystallographic cracks. The formation of cracks and series of faint parallel lines depends on applied load. The development of wings and cracks and faint lines were also observed, when the cleavage surface was indented by knoop indenter (Fig. 10.16), thereby suggesting that they are the basic characteristic of d-AHT cleavages. The faint lines are slip lines. It should be noted that the formation of wings, cracks and faint lines was observed only on d-AHT cleavages and not on natural faces $m(110)$ and $z(111)$ (Fig. 10.17). These indentations were produced on natural faces exhibiting striations and layers. The growth features could not affect the sharp indentation marks.

10.4 RESULTS AND DISCUSSION

There are two ways of studying the relationship between microhardness and applied loads. One way was given by Hanemann (1941) in the form of an empirical

rule that was believed to permit the intercomparison of microhardness values. This rule states that the load P is related to diagonal length of an indentation mark by the expression.

$$P = ad^n \quad \dots\dots (10.1)$$

where 'a' and 'n' are constants of the material under test ; 'a' represents the ' standard hardness ' for an indenter of fixed diameter and 'n' giving the measure of the variation in hardness as a function of 'P' or 'd'. The other way is to study the variation of hardness (Knoop and Vickers hardness numbers) directly with load. In what follows, the detailed study on the variation of load with average diagonal length will be presented.

The equation (10.1) is also known as Kick's law. Taking logarithms of both sides yields

$$\log P = \log a + n \log d \quad \dots\dots (10.2)$$

The values of constants 'a' and 'n' can thus be determined from a graph of $\log P$ versus $\log d$.

Since the relation between $\log P$ and $\log d$ is linear, the graph is a straight line, the slope of this line gives the value of 'n' and the intercept on $\log P$ axis gives the value of $\log a$ and hence 'a'. For all indenters that give geometrically similar shapes (impressions), the above law postulates a constant value of 'n' viz. $n = 2$. This implies a constant hardness value for all loads according to the definition of Knoop and Vickers hardness numbers (KHN and VHN).

A careful study of the graphs ($\log P$ vs $\log d$) shows that there are two clearly recognisable straight lines of different slopes meeting at a kink, which is obtained at a load of 40 gm for knoop diagonals (dk) and about 15 gm for vickers diagonals (dva) at room temperature. As the quenching temperature increases, the load at kink shifts towards higher loads. Further the first part of the straight line corresponding to observations taken at low loads upto 15 gm for vickers diagonals (dv) and 40 gm for knoop diagonals (dk) at room temperature has slope (n_1) of higher value whereas for the second part of straight line for higher loads, the slope (n_2) has values less

than 2. Since n values are different in different regions of the graphs of $\log P$ vs $\log d$, being greater in first region. The 'a' values also vary in two regions being less in first region of low loads and more in second region of high loads. The values of n_1 , n_2 and corresponding intercepts a_1 and a_2 , for knoop and vickers indentations and the load at kink for various quenching temperatures are recorded in Tables 10.7 and 10.8, whereas Tables 10.9 and 10.10 are shown for lengths of diagonals of vickers indentation marks parallel to $[001]$ and normal to it i.e. along $[100]$ directions. In the same way, observations for natural grown faces $m(110)$ and $z(111)$ compared with ^{those of} cleavage plane (010) , are presented in Tables 10.11 and 10.12.

It may be remarked in passing that several workers have reported visible scattering in 'n' values e.g. see Hanemann and Schultz⁶ (1941), Onitsch⁷ (1947) Grodzinski⁸ (1952). However, none has reported the splitting of graphs into two straight lines and their characteristics. The study of variation of load with diagonal lengths of vickers indentation marks on faces of different types (c-, m-, d- and o-faces) of natural

Table 10.7

Constants for Vickers indentation on d-AHF plane (010) (Average of two diagonals of an indentation mark axis taken)

Quenching Temperature T_Q °K	n_1	n_2	$a_1 \times 10^{-4}$	$a_2 \times 10^{-2}$	load at kink (gm)
308	3.7	1.9	1.1	3.6	15
323	3.6	1.9	2.0	3.7	25
343	2.8	1.9	16.5	3.8	40
363	3.6	1.9	1.4	3.8	25
383	3.2	1.9	3.6	4.1	50

Table 10.8

Constants for Knoop indentation d-AIT plane (010) (longer diagonal was
was along [001] direction)

Quenching Temperature T_Q °K	n_1	n_2	$a_1 \times 10^{-8}$	$a_2 \times 10^{-3}$	load at kink (gm)
308	4.2	2.0	8.1	2.5	40
323	3.6	2.0	128	2.6	40
343	3.6	1.8	184	7.0	50
363	4.0	1.8	25.1	9.3	50
383	3.5	1.7	229	11.1	50

Table 10.9

Constants for Vickers indentations on d-AHT plane (010) (measurements of diagonals along $[001]$ direction)

Quenching Temperature T_Q °K	n_1	n_2	$a_1 \times 10^{-5}$	$a_2 \times 10^{-2}$	load at kink (gm)
308	3.8	1.9	9.8	3.5	15
323	3.6	1.9	25.5	4.1	25
343	2.7	1.9	279	4.1	40
363	4.0	1.9	4.8	4.2	40
383	3.2	1.9	5.3	4.3	50

Table 10.10

Constants for Vickers indentations on d-AHT plane (010) (measurement of diagonal length along $[100]$ direction)

Quenching Temperature T_Q °K	n_1	n_2	$a_1 \times 10^{-4}$	$a_2 \times 10^{-2}$	load at kink (gm)
308	3.7	2.0	1.1	2.7	15
323	3.6	2.0	1.2	2.4	25
343	2.8	1.8	1.50	6.2	40
363	4.0	1.8	0.4	4.4	20
383	3.2	1.8	3.4	6.3	50

Table 10.11

Constants for Vickers and Knoop indentations on different faces

For Vickers indentations (average of two diagonals of indentation mark was taken)

Plane	Direction of one of the diagonal of indentation mark	n_1	n_2	$a_1 \times 10^{-6}$	$a_2 \times 10^{-6}$	Load at Kink (gm)
Cleavage plane	[001]	3.7	1.9	112	3.6	15
m-face	[001]	4.4	2.2	5.7	1.1	15
z-face	[101]	2.6	1.7	4010	10.6	20

Plane	Direction of longer diagonal of indentation mark	n_1	n_2	$a_1 \times 10^{-8}$	$a_2 \times 10^{-3}$	Load at Kink (gm)
Cleavage plane	[001]	4.2	2.0	8.0	2.5	40
m-face	[001]	3.3	2.0	433	2.6	40
z-face	[101]	2.9	1.7	10100	24	50

Table 10.12

Constants for Vickers indentations on different faces

Plane	Direction of indentation mark diagonal along	n_1	n_2	$a_1 \times 10^{-6}$	$a_2 \times 10^{-2}$	Load at Kink (gm)
Cleavage plane	[001]	3.8	1.9	98	3.5	15
m-face	[001]	4.7	2.0	4.3	3.0	30
z-face	[101]	2.73	1.9	2630	6.0	70
Plane	Direction of indentation mark diagonal normal to	n_1	n_2	$a_1 \times 10^{-5}$	$a_2 \times 10^{-3}$	Load at Kink (gm)
Cleavage plane	[001]	3.7	2.0	11.0	27	15
m-face	[001]	3.6	2.4	5.2	4.1	50
z-face	[101]	2.9	1.8	187	65	70

and synthetic barite crystals⁹ (Saraf, 1971) has shown very clearly the existence of two clearly recognisable straight lines of the graph of $\log P$ versus $\log d$. Later Shah⁵ (1976), Acharya⁴ (1978), Bhagia² (1982), Shah³ (1984) and Panchal¹⁰ (1981) verified the splitting of graph of $\log P$ versus $\log d$ from their studies of microhardness of calcite, zinc, TGS, KBr, NaNO_3 and InSb crystals. The present investigation is the detailed study of the microhardness of gel-grown d-AHT, single crystals supports the earlier observations of the splitting of the plots with two distinct straight lines.

10.4.1 Characteristics of two straight line regions in the graph :

The separation of straight line graph into two regions with different slopes indicates that in the first region of low loads, the value of hardness is strictly dependent on load and in the second region of high loads this dependence is relatively reduced. It appears that besides this dependence on load, there could also be other factors such as effect of high temperature, work hardening etc. contributing to this behaviour.

In order to determine the effect of deviated temperatures on microhardness and on lengths of indentations the study was carried out on crystal cleavages, quenched from higher temperatures to room temperature. Irrespective of the nature of indenter it is obvious that slopes n_1 (for lower load region) decreases, attains a minimum value at 70°C ($T_Q = 343^\circ\text{K}$) and increasing at 90°C ($T_Q = 363^\circ\text{K}$) again decreases at 110°C ($T_Q = 383^\circ\text{K}$), in all cases (cf. Tables 10.7, 10.8, 10.9 and 10.10). The variation observed in ' n_1 ' values is accompanied by an increase in the ' a_1 ' value. Whereas n_2 values (slopes for higher load region), in case of Vickers indenter are constant for all quenching temperature, (cf. Tables 10.7, 10.9) and a_2 values increase with quenching temperature. In case of knoop indenter and diagonals measured normal to $[001]$ direction for vickers indenter the n_2 value decreases with quenching temperature, whereas converse is the case for a_2 values (Table 10.8 & 10.10).

The constants n_1 , n_2 and a_1 , a_2 for various natural and cleavage faces are represented in Table 10.11 and 10.12. Since n_1 and n_2 are exponents of the average diagonal length of Vickers indentation mark or the length of the longer diagonal of the knoop

indentation mark, their values indicate the relative microhardness of the surface under consideration. The 'a' values determine the microhardness. It is also clear from the 'a' values that irrespective of the nature of the indenter the sphenoidal faces are the hardest among the three faces.

The variations of diagonal lengths of indentation marks with applied load on surface of thermally treated and untreated specimens indicate that 'n' and 'a' values are dependent not only on the crystal anisotropy, but also on the previous history of the specimens. Further the crystal anisotropy is associated with the arrangement of atoms on faces. In case of Vickers indenter, n_1 values show less variation with quenching temperature whereas for Knoop indenter, marked variation is noticeable (Table 10.7 and 10.8). Hence the two regions correspond in general with the structure sensitive and structure insensitive properties of the crystal. They can roughly correspond with extrinsic and intrinsic properties of the crystals. Further, the initial indentation under low loads i.e. initial plastic deformation produces cold working of the crystal. There will also be certain amount of recovery from this

deformation. As a result the degree of hardening of crystal surface should increase. This is more true for low loads near kink. Hence with an increase in applied load the surfaces should offer high resistance to the indentation. The hardness in this region will therefore be ^{higher} ~~lower~~ than that in first region, mostly near kink or at turning point from increasing part to straight portion. In addition to the cold working and recovery of strained crystals, several factors such as surface energy, concentration of different types of imperfections, their interactions, effect of penetration of indenter etc. are also operating in a way unpredictable at present. The experimentally observed deviations from the above remarks are therefore likely to be due to these factors which are not yet clearly understood. It should be mentioned here that although the indentation work was carried out on freshly cleaved surfaces of quenched crystals with the intention of removing the surface hardening, the study of the variation of diagonal length of indentation marks on cleaved surfaces which were once the inner parts or interiors of quenched crystals has shown a noticeable change with quenching temperature ; of course this change is obviously smaller than that of surface hardening of the quenched specimens.

10.5 CONCLUSIONS

The following conclusions are drawn from the above study :

- (i) The graph of $\log P$ versus $\log d$ consists of two clearly recognisable straight lines having different slopes and intercepts on the axes.
- (ii) The indenter load corresponding to kink representing a transition from one straight line to another depends upon quenching temperature.
- (iii) The slope of first part corresponding to low load region of the graph is greater than that of the second part. The intercept made by the first line has less value than that made by second line.
- (iv) The 'a' values obtained by using vickers or knoop indenter clearly indicate that out of the three faces, namely rhombic prism faces on $\{110\}$, sphenoidal faces $\{111\}$ and pinacoidal (cleavage) planes $\{010\}$; the sphenoidal faces are the hardest whereas the pinacoids are the weakest faces of d-AHT.

- (v) The defect structures operate differently in low load and high load regions corresponding to two parts of the plot of $\log P$ vs. $\log d$.

- (vi) Anisotropic character is revealed by different values of diagonal lengths of indentation mark along and normal to direction $[001]$ for the same applied load.

6. HANEMANN, H. and SCHULTZ, F. 1941 Z. Metalkunde, 33, 122
7. ONITSCH, E.M. 1947 Microskopie, 2, 131
8. GRODZINSKI, P. 1952 Schwaiz, arch. angew wiss, 18, 282.
9. SARAF, C.L. 1971 Ph.D. Thesis, M.S. University of Baroda, Baroda.
10. PANCHAL, P.J. 1981 M.Sc. App. Physics dissertation, M.S. University of Baroda, Baroda.

LIST OF TABLES

- 10.1 Logarithms of diagonal of vickers indentation mark measured along $[001]$ direction and of corresponding applied load for different quenching temperatures (T_Q) on cleavage plane (010).
- 10.2 Logarithms of diagonals of vickers indentation mark measured normal to $[001]$ i.e. along $[100]$ direction and of corresponding applied load for different quenching temperatures (T_Q) on cleavage plane (010).
- 10.3 Logarithms of diagonals of knoop indenter mark having longer diagonal along $[001]$ direction and of corresponding applied load for different quenching temperatures (T_Q) on cleavage plane (010).
- 10.4 Logarithm of average of two diagonals of vickers indenter mark and of corresponding applied load for different quenching temperatures (T_Q) on cleavage plane (010).
- 10.5 Logarithm of two diagonals of vickers indenter mark measured along $[001]$ direction in case of cleavage (010) and $m(110)$ plane and along $[101]$ direction in the case of $z(111)$ plane and normal to it in all cases and logarithms of corresponding applied load at room temperature.

- 10.6 Logarithms of diagonals of vickers indentation (average) and knoop indentation mark for different d-AHT planes and of corresponding applied load at room temperature.
- 10.7 Slopes n_1 , n_2 and constants a_1 and a_2 for two regions LLR and HLR of $\log P$ vs. $\log d$ graphs and also peak P_k at kink, for vickers indentation (where average of two diagonal lengths was taken) on d-AHT cleavage plane.
- 10.8 Slopes n_1 , n_2 and constants a_1 and a_2 for two regions LLR and HLR of $\log P$ vs. $\log d$ graphs and also peak P_k at kink, for knoop indenter on d-AHT cleavage plane.
- 10.9 Slopes n_1 , n_2 and constants a_1 and a_2 for two regions LLR and HLR of $\log P$ vs. $\log d$ graphs and also peak P_k at kink, for vickers indentation mark (where diagonal length of indentation mark measured along $[001]$ direction)
- 10.10 Slopes n_1 , n_2 and constants a_1 and a_2 for two regions LLR and HLR of $\log P$ vs. $\log d$ graphs and also peak P_k at kink, for vickers indentation mark (where diagonal length of indentation mark measured normal to $[001]$ direction i.e. along $[100]$ direction).

41

10.11 Slopes n_1 , n_2 and constants a_1 and a_2 for two regions LLR and HLR of $\log P$ vs. $\log d$ graphs and also peak P_k at kink, for vickers (average of two diagonal lengths) and knoop indentation for different d-AHT planes.

10.12 Slopes n_1 , n_2 and constants a_1 and a_2 for two regions LLR and HLR of $\log P$ vs. $\log d$ graphs and also peak P_k at kink, for two diagonal lengths of vickers indentation for different d-AHT planes.

CAPTIONS TO THE FIGURES

- 10.1 Plot of log P versus log d for two normal diagonals of vickers indentation on d-AHT cleavage plane (010) for quenching temperature (T_Q) 308°K.
- 10.2 Plot of log P versus log d for two normal diagonals of vickers indentation on d-AHT cleavage plane (010) for quenching temperature (T_Q) 323°K.
- 10.3 Plot of log P versus log d for two normal diagonals of vickers indentation on d-AHT cleavage plane (010) for quenching temperature (T_Q) 343°K.
- 10.4 Plot of log P versus log d for two normal diagonals of vickers indentation on d-AHT cleavage plane (010) for quenching temperature (T_Q) 363°K.
- 10.5 Plot of log P versus log d for two normal diagonals of vickers indentation on d-AHT cleavage plane (010) for quenching temperature (T_Q) 383°K.
- 10.6 Plot of log P versus log d for vickers indentation (average of diagonals considered) and knoop indentation on d-AHT cleavage plane (010) for quenching temperature (T_Q) 308°K.

- 10.7 Plot of log P versus log d for vickers indentation (average of diagonals considered) and knoop indentation on d-AHT cleavage plane (010) for quenching temperature (T_Q) 323°K.
- 10.8 Plot of log P versus log d for vickers indentation (average of diagonals considered) and knoop indentation on d-AHT cleavage plane (010) for quenching temperature (T_Q) 343°K.
- 10.9 Plot of log P versus log d for vickers indentation (average of diagonals considered) and knoop indentation on d-AHT cleavage plane (010) for quenching temperature (T_Q) 363°K.
- 10.10 Plot of log P versus log d for vickers indentation (average of diagonals considered) and knoop indentation on d-AHT cleavage plane (010) for quenching temperature (T_Q) 383°K.
- 10.11 Plot of log P versus log d for two diagonals for vickers indentation on m(110) face of d-AHT at room temperature (30°C).
- 10.12 Plot of log P versus log d for two diagonals for vickers indentation on z(111) face of d-AHT at room temperature (30°C).

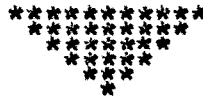
- 10.13 Plot of log P versus log d for vickers indentation (average of diagonals taken) and knoop indentation on m(110) face of d-AHT at room temperature (30°C).
- 10.14 Plot of log P versus log d for vickers indentation (average of diagonals taken) and knoop indentation on z(111) face of d-AHT at room temperature (30°C).
- 10.15 (a) Photomicrograph of d-AHT cleavage surface indented by using vickers hardness indenter for applied load of 40 g, showing the formations of wings, crystallographic cracks and slip lines.
- (b) Schematic diagram of the indentation mark on d-AHT cleavage plane (Fig. 10.15a), showing wings, crystallographic cracks and slip lines.
- 10.16 Photomicrograph of d-AHT cleavage plane surface indented by using knoop hardness indenter for applied load of 40 g. showing slip lines with direction 001 .
- 10.17 Photomicrograph of d-AHT natural sphenoidal face (111) indented by using knoop hardness tester for applied load of 40 gm alongwith the growth layers.

CHAPTER - 11

VARIATION OF HARDNESS WITH LOAD

	<u>PAGE</u>
11.1 Introduction 	220
11.2 Observations 	225
11.3 Results and discussion 	227
11.3.1 Relation between hardness and quenching temperature, for vickers and knoop hardness numbers in HLR 	229
11.3.2 Relation between vickers hardness number and quenching temperature along mutually normal crystallographic directions 	232
11.4 Conclusions 	233

References



11.1 INTRODUCTION

It is clear from the discussion of the previous chapter that 'standard hardness', 'a' is a function of quenching temperature, 'a₁' and 'a₂' in general vary with quenching temperature (T_Q). However, the variation of a₁ with quenching temperature is more noticeable than that of a₂. It is now interesting and useful to study in detail how hardness changes with quenching temperature.

The Knoop and Vickers hardness numbers (H_K and H_V) are defined by equations, (Mott, 1956).

$$\text{KHN, } H_K = \frac{14230 P}{d^2} \quad \dots\dots (11.1)$$

$$\text{VHN, } H_V = \frac{1854.4 P}{d^2} \quad \dots\dots (11.2)$$

where load P is measured in grams and the diagonal length d, of the indentation mark in microns. The hardness number is not an ordinary number, but a constant having dimensions and a depth, but less understood, physical meaning. The combination of these equations with

$$P = ad^n \quad \dots (11.3)$$

yields,

$$H = ad^{n-2} \quad \dots (11.4)$$

or,

$$H = aP^{\frac{n-2}{n}} \quad \dots (11.5)$$

In case of Vickers microhardness, the value of exponent 'n' equals 2 (Kick's law 1885) for all indenters that give impressions geometrically similar to one another. Thus, $n = 2$ implies that hardness for a given shape of pyramidal indenter is constant and independent of load. In order to appreciate the detailed physical meaning of the above equations it will be instructive to consider the example of a solid subjected to a uniaxial compression. For such a simple case, the modulus of elasticity (Young's ^{modulus} ~~modulus~~) is given by

$$E = \frac{\sigma}{\epsilon} \quad \dots (11.6)$$

where σ is the compressive stress defined as load per unit area

$$\sigma = \frac{P}{A} \quad \dots (11.7)$$

and the compressive strain ϵ is defined as the decrease in length per unit length. Now the area of cross-section, A , increases with compression. Hence for a constant volume of a solid, length is inversely proportional to the area of cross-section. If A_0 represents initial area of cross-section with a normal length l_0 and A the final area with normal length l after small compression, one obtains,

$$lA = l_0A_0 = \text{volume constant}$$

$$\text{or } \frac{l}{l_0} = \frac{A_0}{A} \quad \dots\dots (11.8)$$

Therefore

$$\epsilon = \frac{l - l_0}{l} = \frac{A_0 - A}{A} \quad \dots\dots (11.9)$$

substitution of σ and ϵ from equations (11.7) and (11.9) gives

$$E = \frac{\sigma}{\epsilon} = \frac{P}{A_0 - A} \quad \dots\dots (11.10)$$

Hence for a simple uniaxial compressive stress when the area is a geometrical function of the deformation,

determined hereby constant volume, the resistance to permanent deformation can be expressed simply in terms of load and corresponding area. In indentation hardness work the volume change is very very small. Hence the indentation hardness can be measured by using above formula (eqn. 11.10). Indenters are made in various geometrical shapes such as spheres, pyramids etc. The area over which the force due to load on indenter acts, increases with the depth of penetration. The resistance to permanent deformation or hardness can be expressed in terms of force or load and area alone (and/or depth of penetration). These remarks are true for solids which are amorphous or highly homogeneous and isotropic.

The above analysis presents a highly simplified picture of the process involved because there is a great difference between deforming a solid in a simple uniaxial compression and deforming a surface of a solid by pressing a small indenter into it. Around the indentation mark, the stress distribution is exceedingly complex and the stressed material is under the influence of multi-axial stresses. The sharp corners of a pyramidal indenter produces a sizable amount of plastic deformation

which may reach 30% or more at the top of the indenter. Further the surface of contact is inclined by varying amounts to the directions of applied force. In view of these complications a simple expression corresponding to that for the modulus of elasticity cannot be derived for hardness. In the absence of any formula based on sound theory, an arbitrary² expression is used which includes both known variables, load and area in the present case. Hence the hardness number, H , is defined as the ratio of the load to the area of impression,

$$H = \frac{P}{A} \quad \dots\dots (11.11)$$

For pyramidal indenters the load (P) varies as the square of the diagonal, d . Thus for a given shape of pyramid,

$$P = bd^2 \quad \dots\dots (11.12)$$

where b is constant which depends on the material and shape of pyramid. The area of the impression, A , is also proportional to the square of the diagonal,

$$A = cd^2 \quad \dots\dots (11.13)$$

Table 11.1

Vickers Hardness numbers (average) on d-AHT cleavage plane (010) for different quenching temperatures

Load P in gm	T_Q	H_{va} (kg mm^{-2})				
		308°K	323°K	343°K	363°K	383°K
2.5		24.27	22.10	28.08	18.79	21.19
3.75		26.77	25.58	28.93	23.31	22.49
5.0		29.27	32.09	33.95	24.52	25.21
7.5		32.12	36.52	36.52	34.69	36.77
10.0		45.01	41.04	37.49	34.29	37.33
15		57.32	51.86	42.16	53.48	41.77
20		50.89	55.25	52.12	52.73	47.07
25		49.52	60.23	52.03	55.25	50.41
30		50.11	50.62	55.43	48.71	51.79
40		52.58	50.97	58.91	52.08	56.70
50		50.50	46.88	55.41	50.64	58.80
60		53.13	49.25	57.15	51.28	56.69
70		48.16	51.96	52.72	51.13	54.61
80		54.71	54.39	49.45	51.80	57.96
100		52.80	56.02	51.03	45.68	52.94
120		48.27	63.96	53.89	50.01	57.29
140		50.06	55.82	53.68	49.70	56.15

Table 11.2

Knoop Hardness numbers along $[001]$ on d-AHT cleavage plane (010) for different quenching temperatures

Load P in gm	T_Q	H_k (kg mm ⁻²)				
		308°K	323°K	343°K	363°K	383°K
2.5		10.16	11.28	10.98	10.36	12.65
3.75		14.25	12.42	13.52	12.52	14.99
5.0		15.93	16.70	18.50	15.33	16.69
7.5		19.20	17.70	21.39	17.57	18.73
10.0		24.98	19.16	27.44	23.19	23.93
15		29.08	24.67	29.64	26.61	25.33
20		32.32	27.75	32.75	28.80	28.72
25		35.03	36.61	37.23	30.78	33.00
30		35.44	36.38	34.09	34.00	36.52
40		38.21	38.76	42.11	38.68	42.39
50		37.33	38.31	42.71	43.35	45.06
60		36.42	34.52	39.82	42.11	43.34
70		37.59	34.58	37.03	41.88	42.55
80		35.32	35.22	36.87	39.33	39.68
100		35.57	35.60	39.65	39.11	34.61
120		35.18	36.45	35.49	38.45	38.98
140		35.58	37.10	37.32	38.07	39.56

Table 11.3

Vickers Hardness numbers along [001] direction
on d-AHT cleavage plane (010) for different
quenching temperature

Load P in gm	T_Q	H_{VX} (kg/mm ²)				
		308°K	323°K	343°K	363°K	383°K
2.5		22.42	25.57	30.95	20.34	23.40
3.75		24.47	29.98	32.24	25.29	24.61
5.0		30.14	37.92	36.62	28.35	25.22
7.5		33.42	43.16	40.06	40.08	40.66
10.0		48.35	47.94	41.20	44.56	39.29
15		55.24	55.24	45.03	57.30	46.42
20		52.73	66.23	54.82	54.40	49.63
25		53.72	70.17	55.25	65.92	54.24
30		52.22	61.03	57.86	63.31	54.01
40		52.65	60.25	61.67	73.24	60.25
50		52.46	61.73	59.20	64.75	60.87
60		54.91	59.49	59.15	67.75	59.29
70		51.13	62.17	54.84	70.06	61.07
80		56.81	65.10	53.97	68.18	64.00
100		52.26	59.35	56.84	57.38	65.80
120		46.90	72.28	59.41	63.58	68.20
140		46.90 49.22	72.28 61.46	59.41 52.84	63.58 61.69	68.20 66.34

Table 11.4

Vickers Hardness numbers normal to [001] direction
on d-AHT cleavage plane (010) for different
quenching temperature

Load P in gm	T_Q	H_{vy} (in kg mm^{-2})				
		308 $^{\circ}$ K	323 $^{\circ}$ K	343 $^{\circ}$ K	363 $^{\circ}$ K	383 $^{\circ}$ K
2.5		26.37	19.29	25.57	17.41	19.29
3.75		26.11	22.08	26.11	21.58	20.63
5.0		29.44	27.51	31.58	21.42	25.23
7.5		30.90	31.31	33.42	30.31	33.42
10		42.00	35.52	34.29	27.20	35.52
15		59.49	41.54	39.55	49.67	37.79
20		49.15	46.80	49.63	51.15	44.70
25		45.78	52.26	49.11	46.97	46.97
30		48.13	42.67	53.14	38.64	49.70
40		51.97	43.68	56.34	38.92	53.46
50		48.65	36.90	52.00	40.69	56.83
60		51.43	41.44	55.24	40.17	54.25
70		45.44	44.08	50.72	42.79	49.12
80		52.73	46.13	45.47	38.07	52.73
100		53.35	52.98	46.07	37.22	43.52
120		49.70	55.64	49.10	40.36	48.81
140		50.93	50.93	50.68	40.89	48.14

Table 11.5

Hardness numbers (Vickers and Knoop) on (010), (110) and (111) planes of α -AlH

Load P in gm	Cleavage plane		prism-face(110)		sphenoid-face (111)	
	H_{va} kg. mm^{-2}	H_k kg. mm^{-2}	H_{va} kg. mm^{-2}	H_k kg. mm^{-2}	H_{va} kg. mm^{-2}	H_k kg. mm^{-2}
2.5	24.270	10.160	10.919	10.306	14.385	22.410
5.0	29.777	15.930	25.105	16.387	33.135	41.900
7.5	32.122	19.198	25.716	18.733	43.156	49.769
10.0	45.010	24.977	21.914	30.288	43.682	57.124
15	57.320	29.076	40.160	32.543	46.032	77.861
20	50.892	32.319	41.209	28.796	42.387	65.550
30	50.110	35.442	41.397	33.303	54.014	65.197
40	52.583	38.213	41.356	36.878	59.693	77.293
50	50.500	37.325	42.298	33.853	63.271	90.490
60	53.127	36.416	43.468	36.538	58.747	74.719
70	48.162	37.587	43.367	34.248	69.625	65.610
80	54.714	35.324	41.222	34.303	62.933	63.956
100	52.800	35.567	46.972	36.948	61.125	64.165
120	48.272	35.179	49.176	37.216	61.340	62.386
140	50.064	35.575	49.757	35.699	60.539	62.669

Table 11.6

Hardness numbers (Vickers in two normal directions) on (010), (110) and (111) planes of d-AHT

Load P in gm	Cleavage plane		m-face		z-face	
	H_{Vx} kg. mm ⁻² along [001]	H_{Vy} kg. mm ⁻² along [100]	H_{Vx} kg. mm ⁻² along [001]	H_{Vy} kg. mm ⁻² along 010	H_{Vx} kg. mm ⁻² along [101]	H_{Vy} kg. mm ⁻² normal to [101]
2.5	22.419	26.367	13.632	8.944	16.567	12.607
5.0	30.137	29.440	31.576	20.442	36.620	30.124
7.5	33.419	30.898	31.501	21.389	45.186	41.259
10.0	48.350	42.002	27.540	17.850	46.397	41.198
15	55.239	59.487	51.431	32.234	49.673	42.777
20	52.733	49.147	57.220	31.085	45.469	39.609
30	52.218	48.130	63.581	29.081	56.367	51.790
40	52.646	51.971	55.257	32.111	63.152	56.509
50	52.462	48.652	49.573	36.519	70.319	57.223
60	54.909	51.432	53.047	36.271	60.246	57.304
70	51.127	45.440	52.564	36.283	72.097	67.278
80	56.809	52.731	53.224	32.870	66.230	59.876
100	52.261	53.350	56.837	39.470	62.040	60.229
120	46.903	49.702	60.416	40.804	62.713	60.011
140	49.223	50.934	61.112	41.298	61.304	59.795

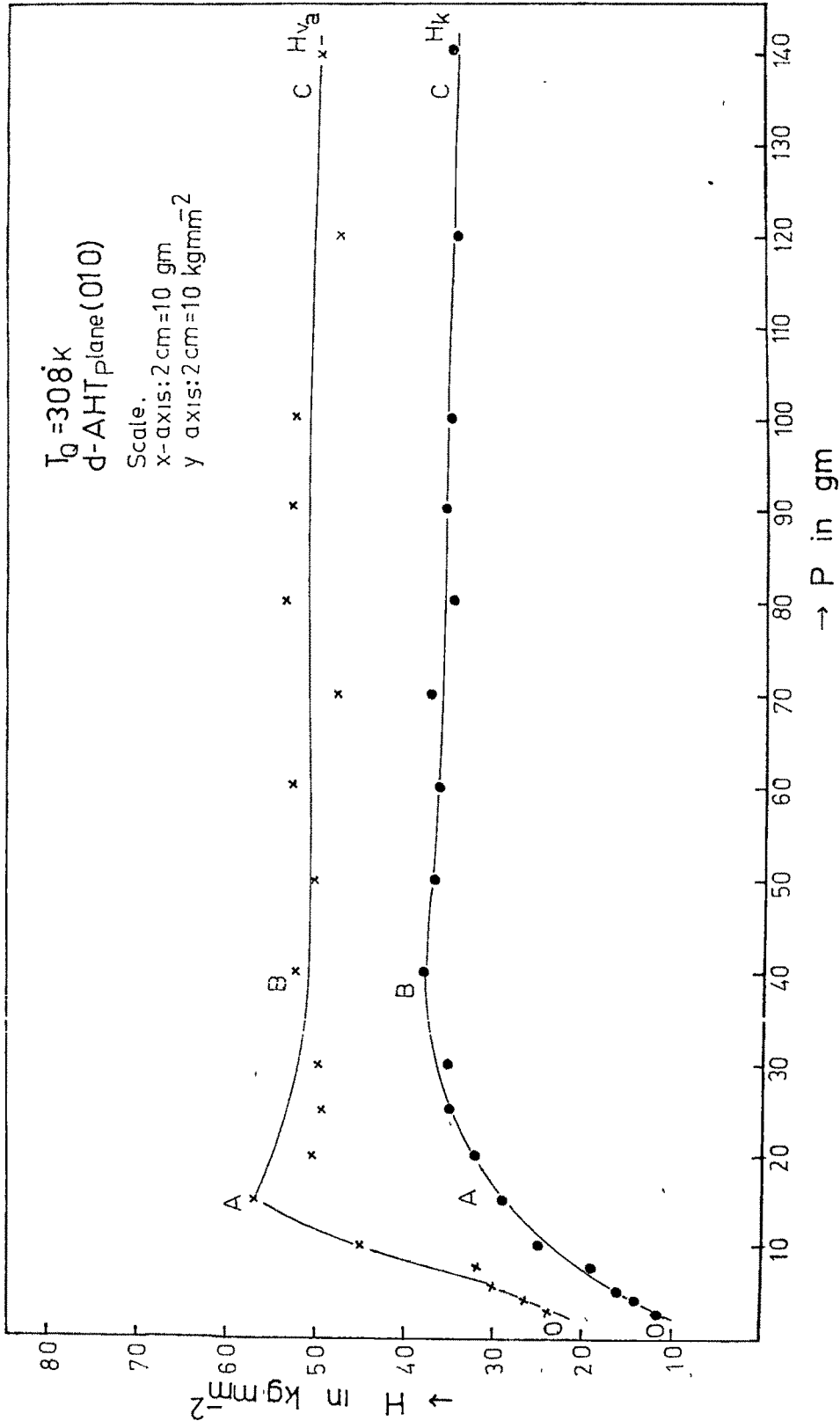


Fig. 11.1

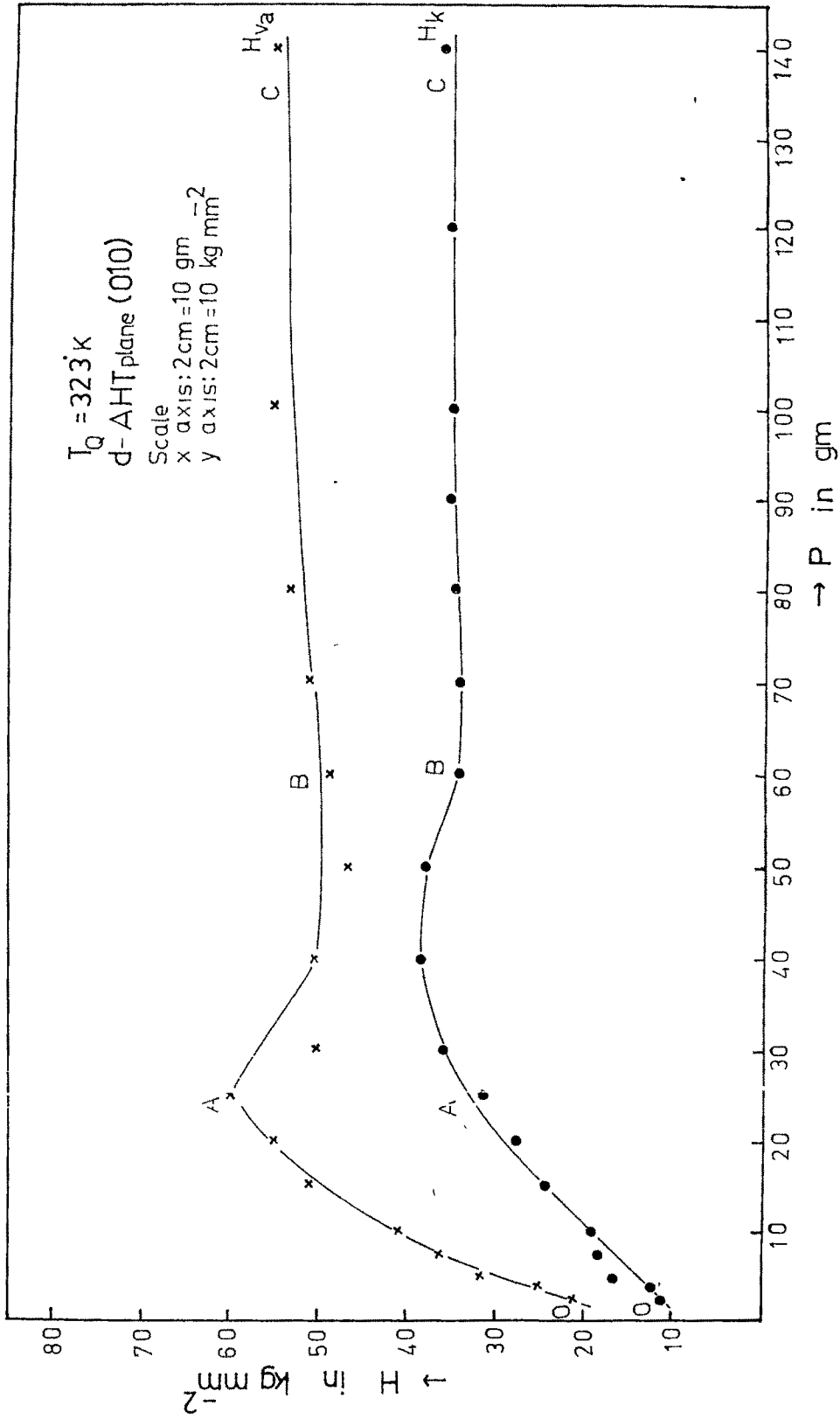
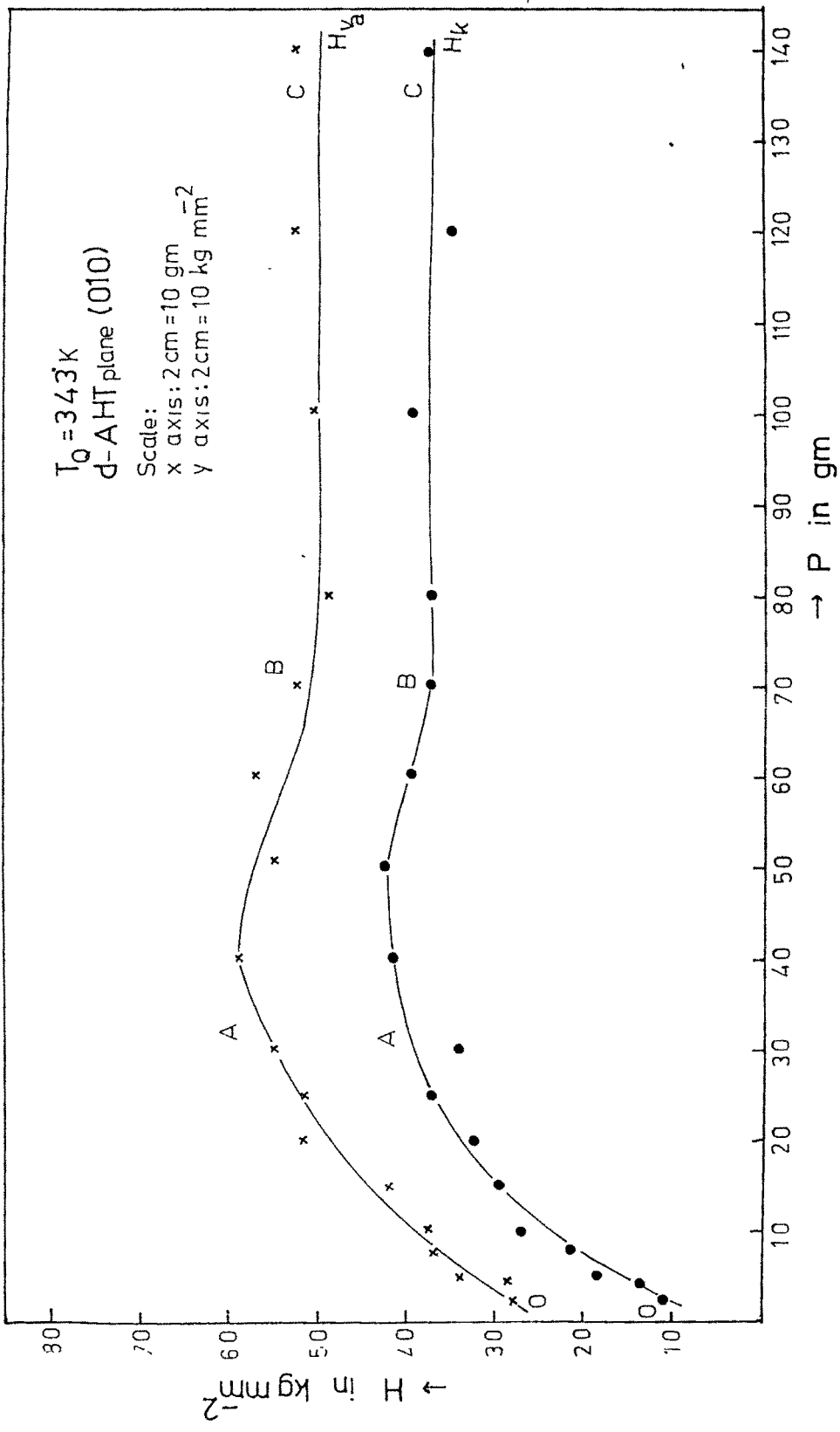


Fig. 11.2



GAIFFAY

Fig. 11.3

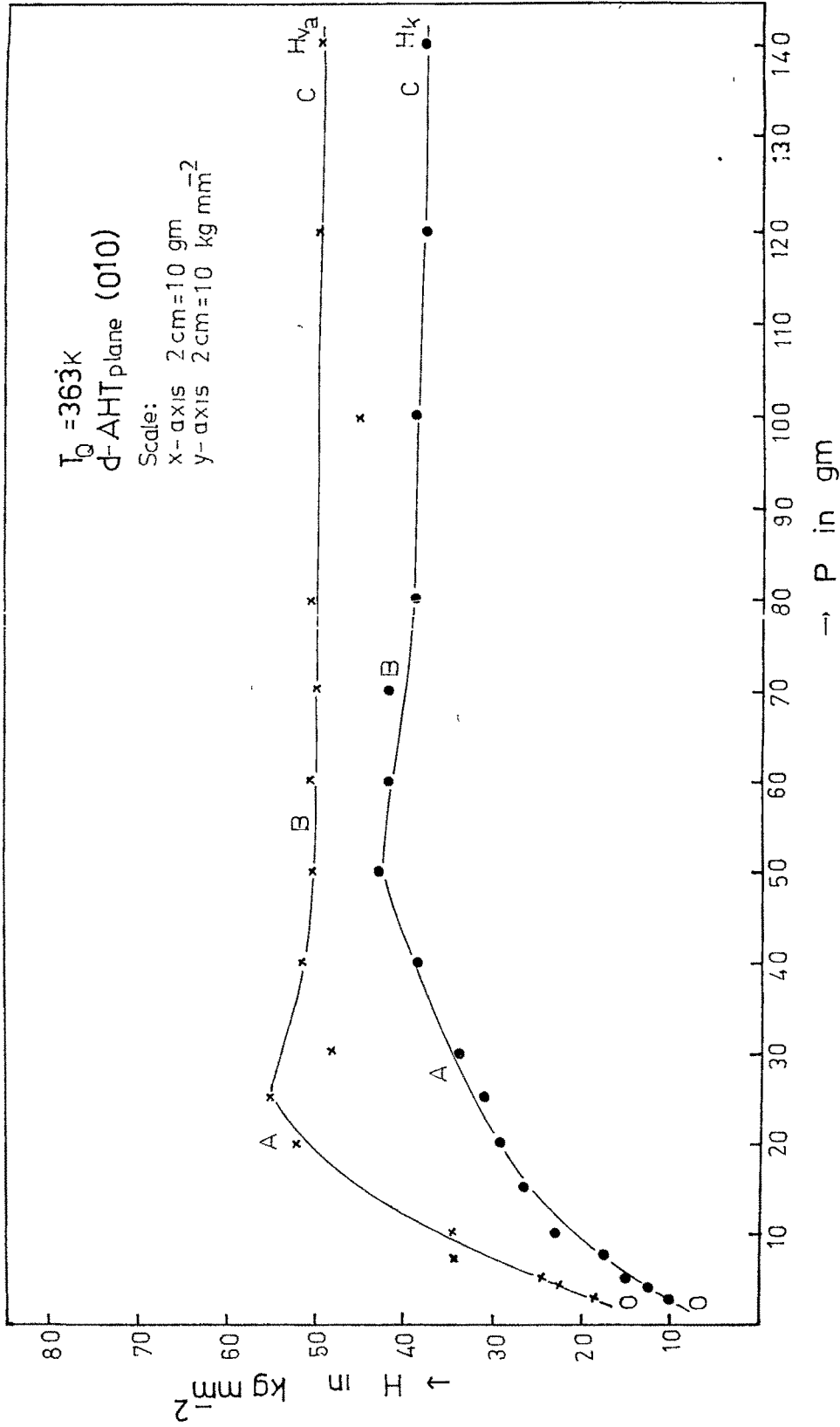


Fig. 11.4

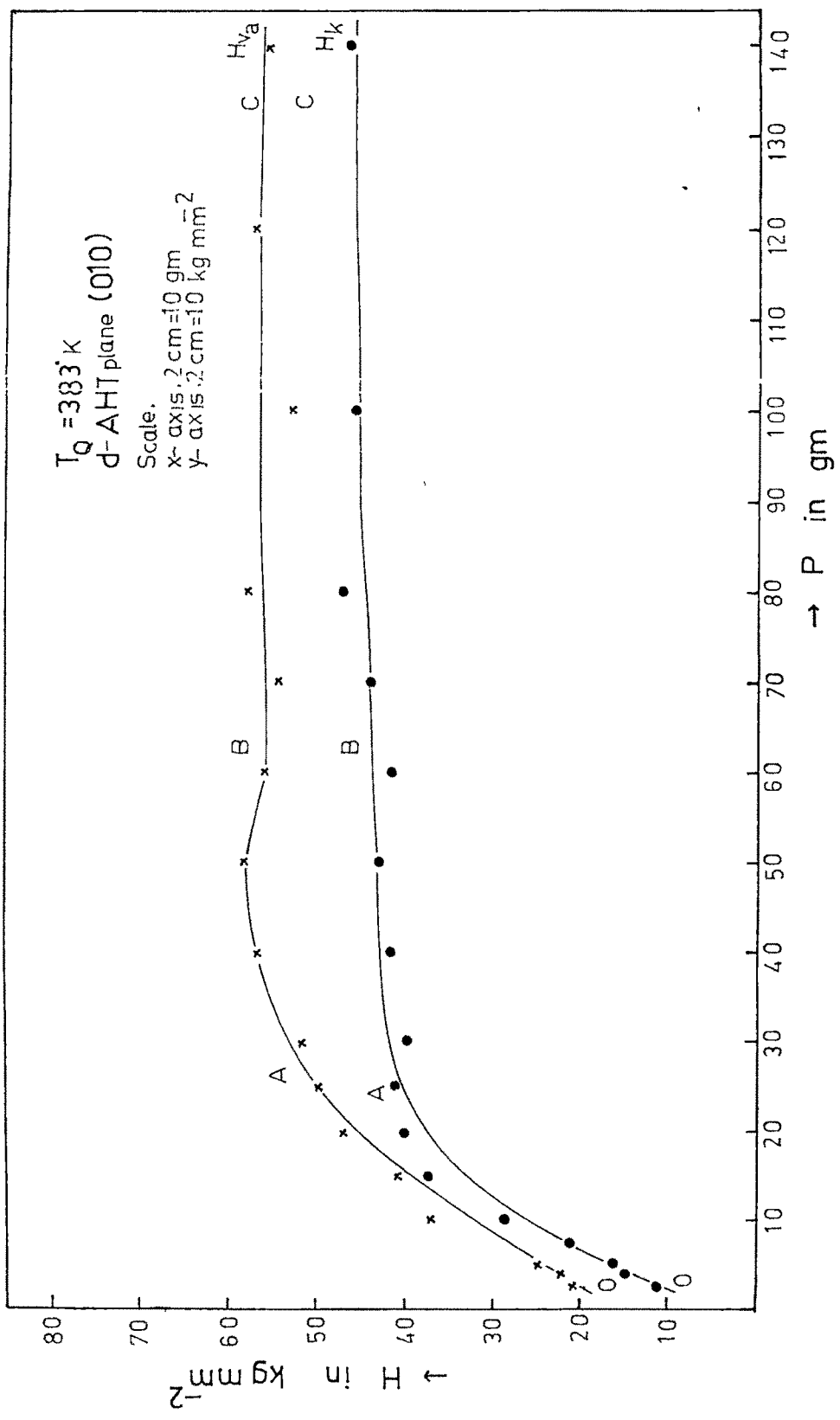


Fig. 11.5

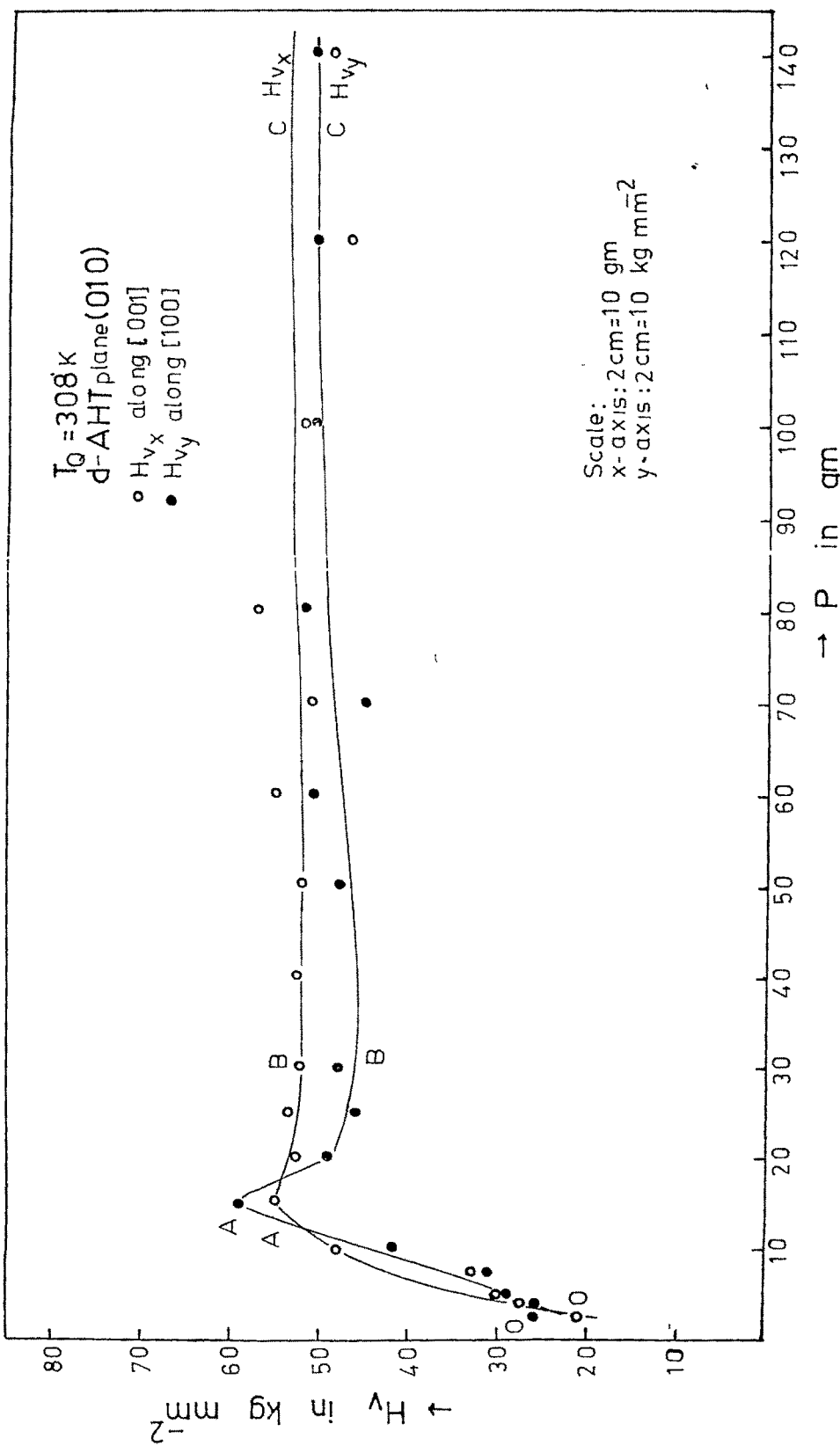


Fig. 11.6

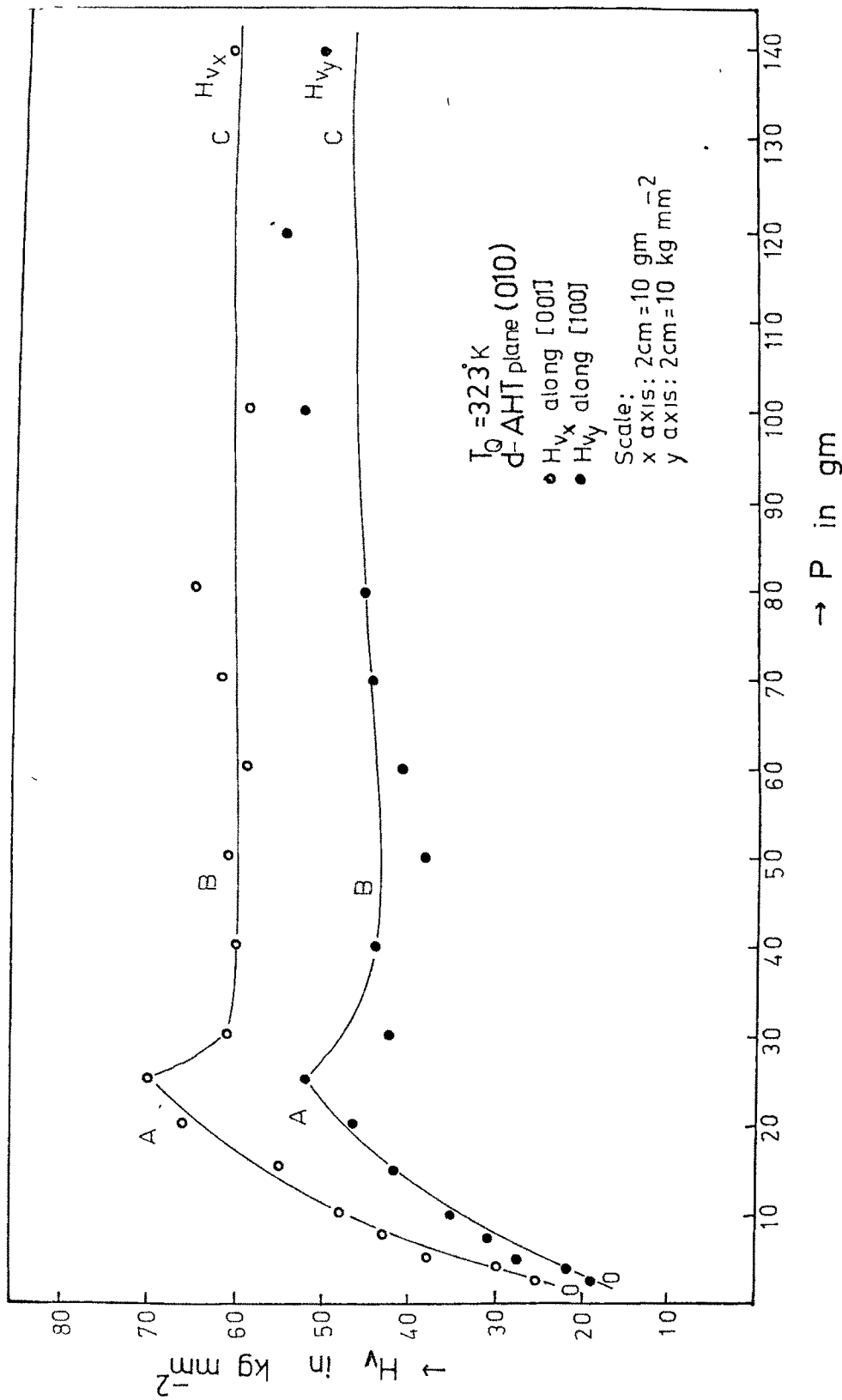


Fig. 11.7

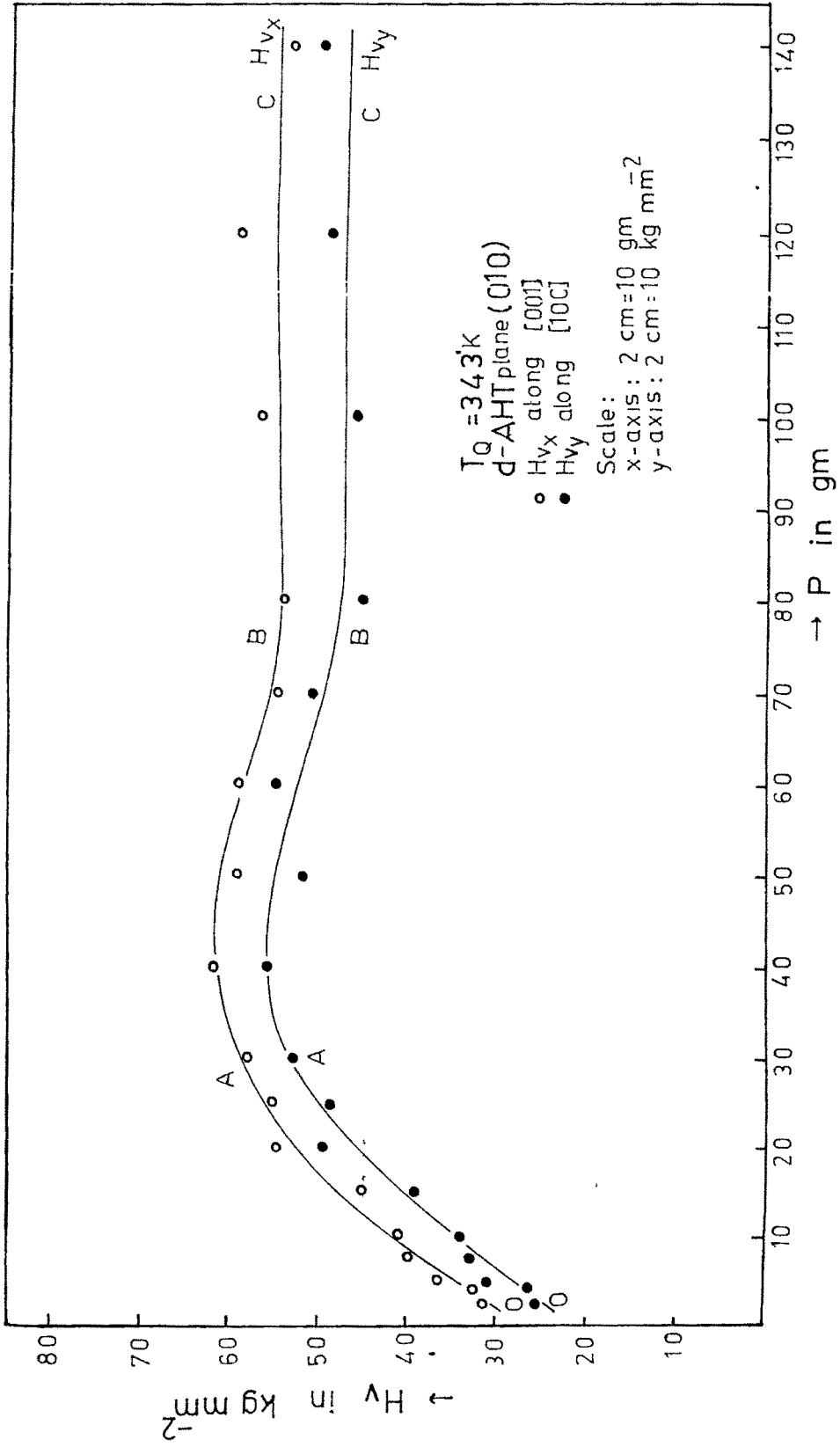
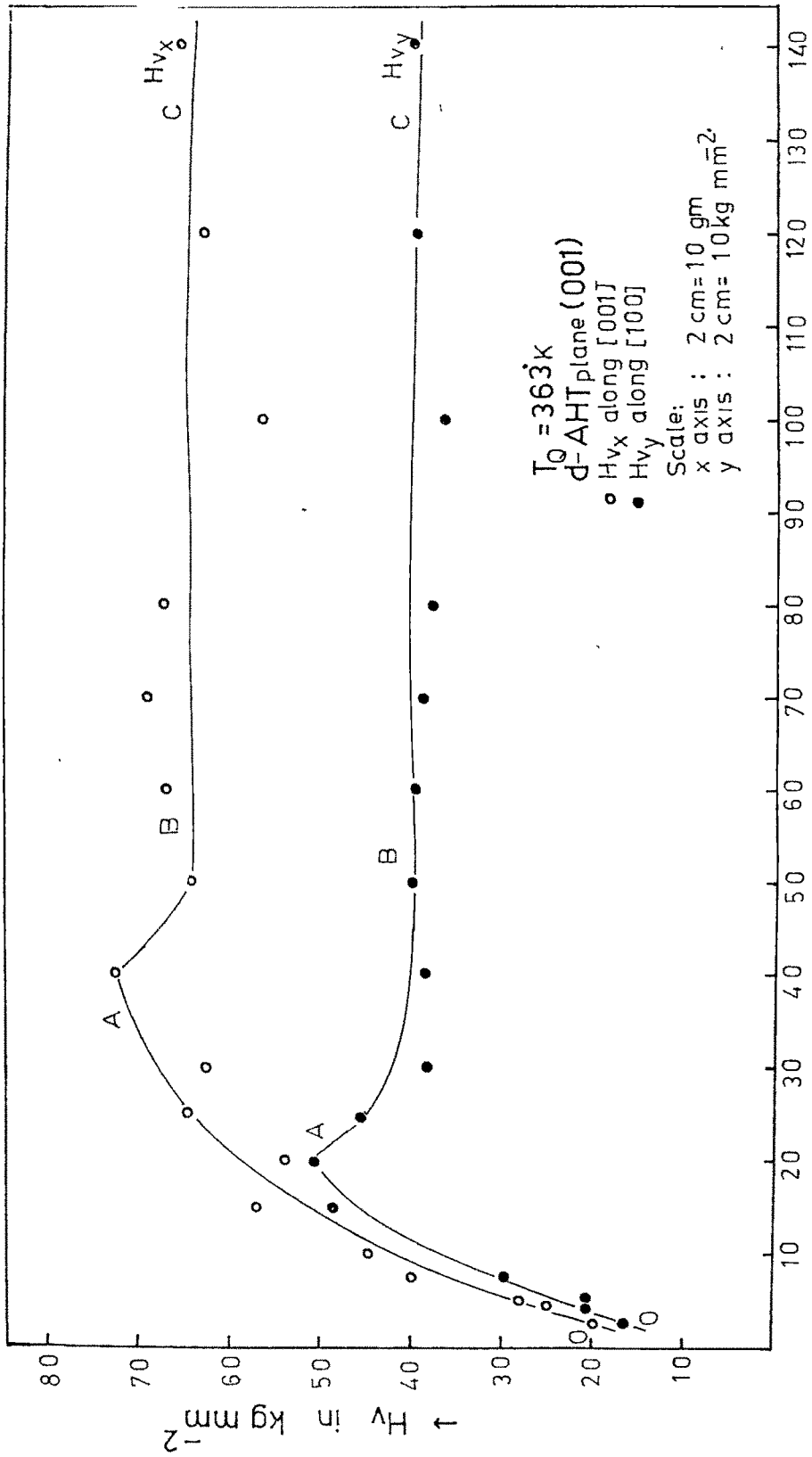


Fig. 11.8



→ P in gm

Fig. 11.9

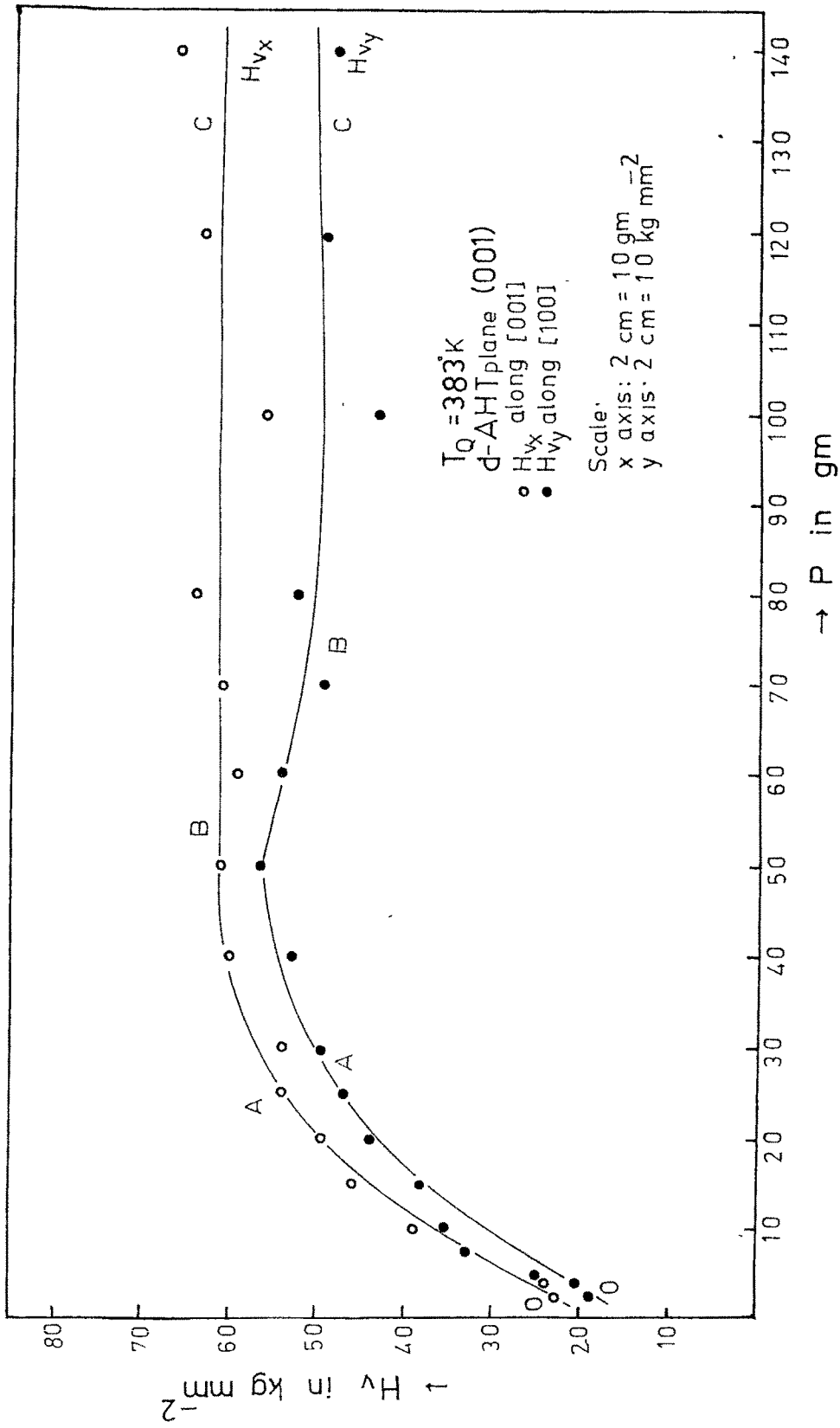


Fig. 11.10

along and normal to $[101]$. It should be noted that direction $[101]$ is normal to C-axis. Using data of Table 10.6, hardness numbers were calculated (cf tables 11.5 and 11.6) and plots of hardness number versus applied load ^{are} were shown in Figures 11.11 to 11.14.

11.3 RESULTS AND DISCUSSION

It is clear from the graphs of hardness number (H) versus load (P) that contrary to theoretical expectations, the hardness varies with load. The hardness at first increases with load, reaches a maximum value then gradually decreases and attains constant value for all loads. This behaviour is found more prominent in Vickers hardness number (H_V) than in Knoop hardness number (H_K). Further, Knoop hardness number (H_K) has less values than Vickers hardness number (H_V) for all loads and for all samples irrespective of heat treatment. The theoretical conclusion that hardness is independent of load thus appears to be true only at higher loads. The maximum value of hardness or starting point of constant hardness region corresponds with a load which is nearer the value of the load at which kink in the graph of

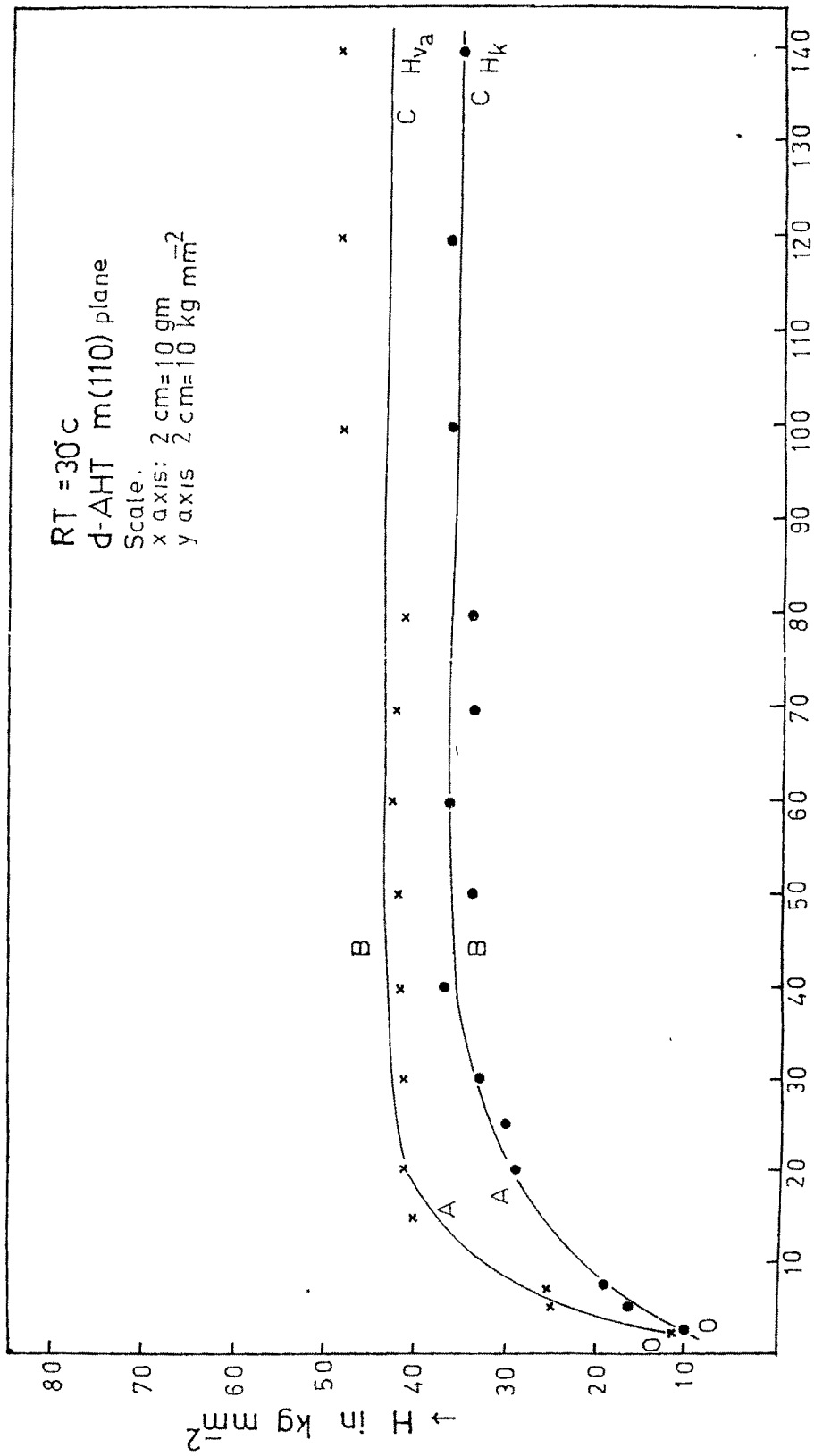


Fig. 11.11

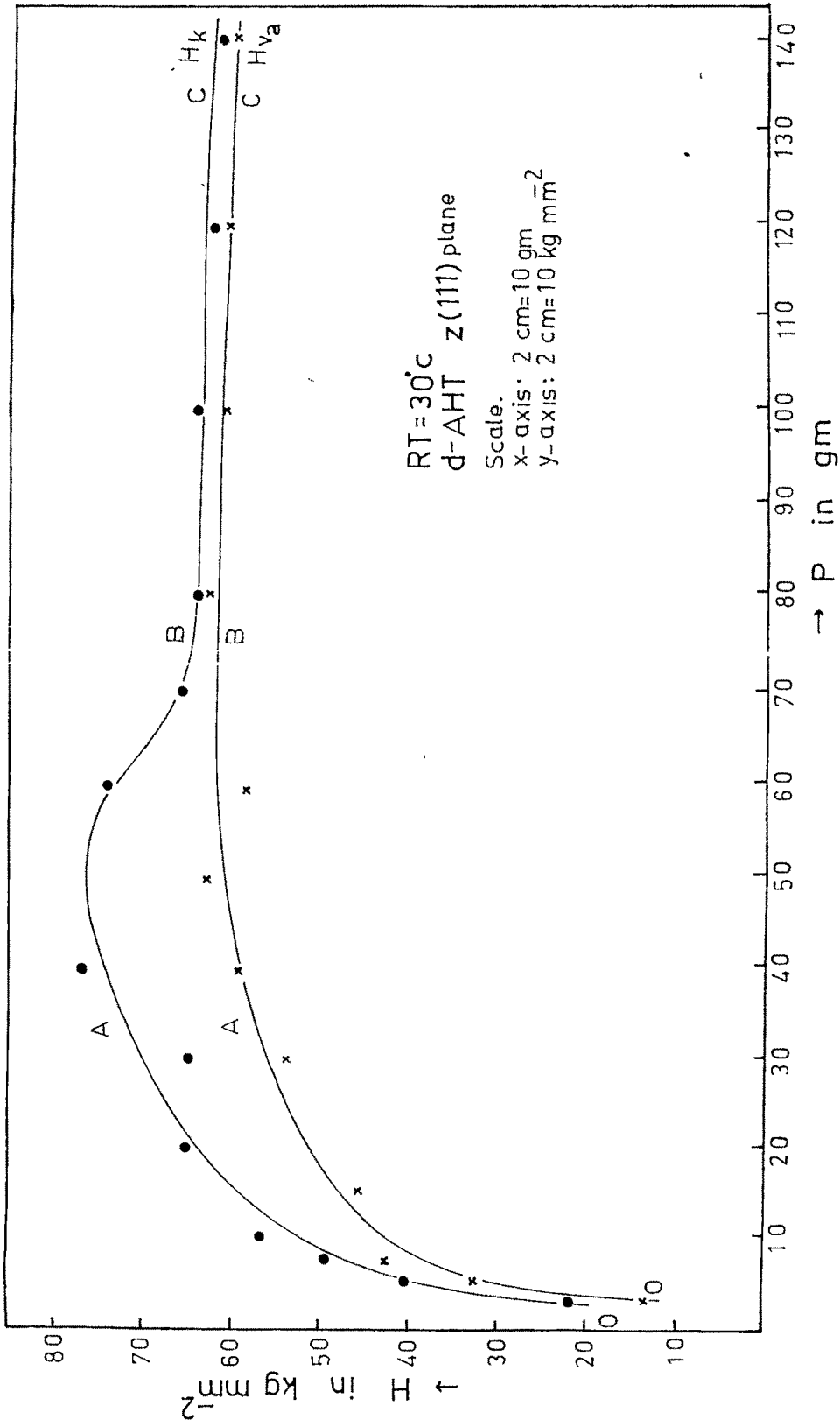


Fig. 11.12

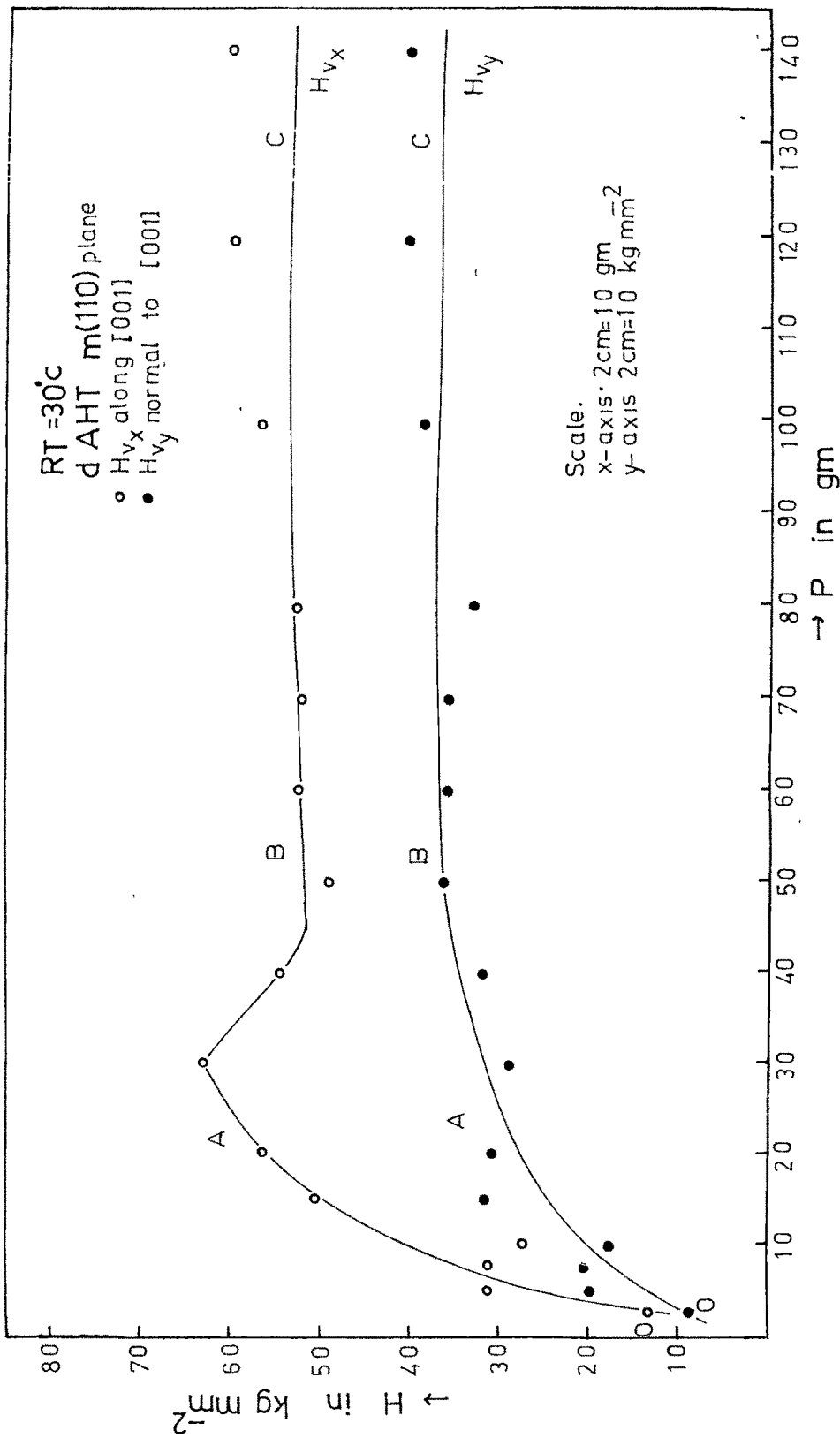


Fig. 11.13

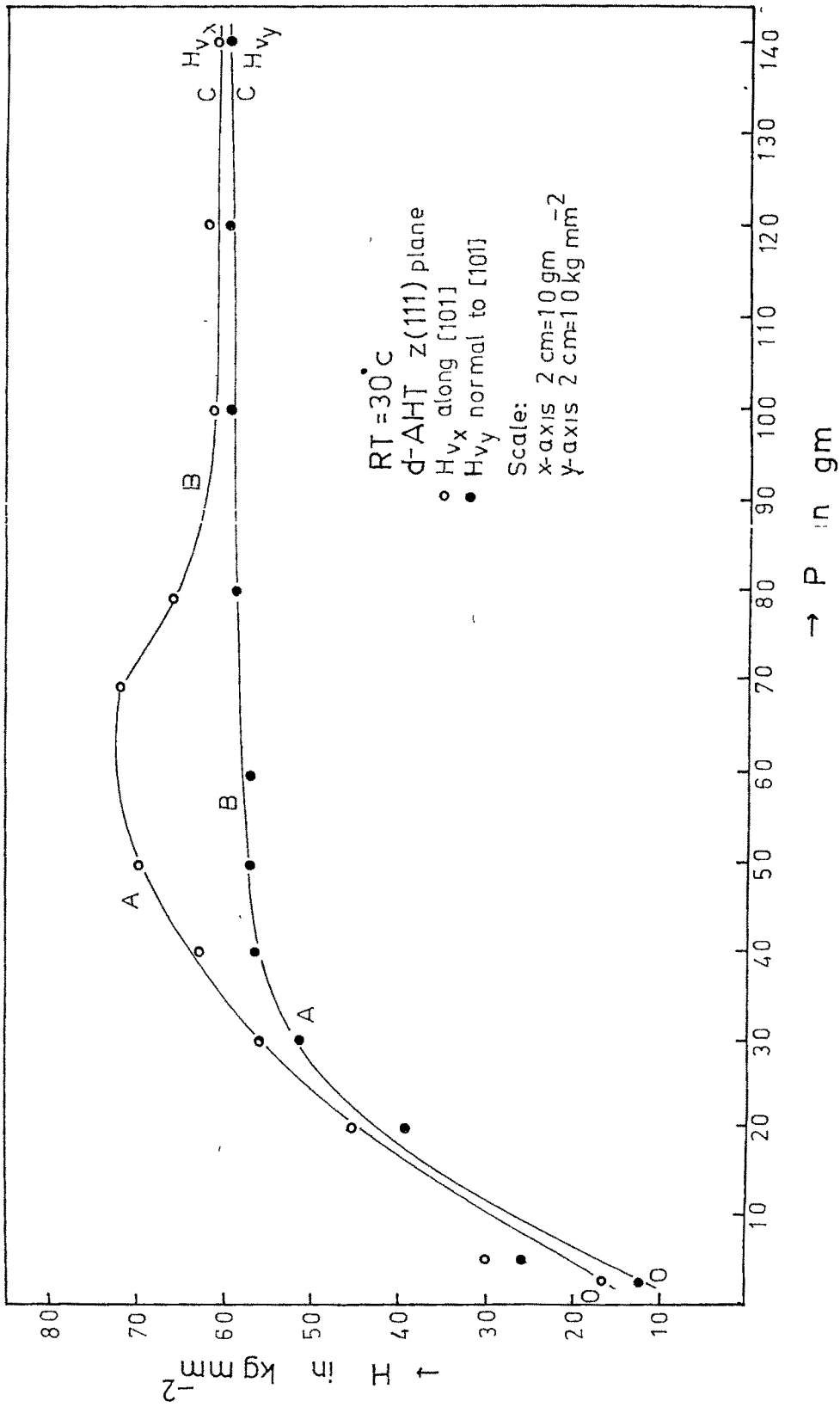


Fig. 11.14

log P versus log d is observed (cf. Chapter 10). The graph of H (H_k or H_{vk}) versus P can be conveniently divided into three parts OA, AB and BC where the first part represents linear relation between hardness and load, the second part, the non-linear relation and the third part the linear one. This reflects varied reactions of the cleavage surface and natural faces to loads belonging to different regions. Besides, it supports, to a certain extent, the earlier view about the splitting of the graph of log P versus log d into two recognizable lines (cf Chapter 10). These three regions will henceforth be referred to as low load region (LLR), intermediate load region (TLR) and high load region (HLR) corresponding OA, AB and BC respectively.

The qualitatively complex behaviour of microhardness with load can be explained on the basis of the depth of penetration of the indenter. At small loads the indenter penetrates only surface layers, hence the effect is shown more sharply at these loads. However, as the depth of the impression increases, the effect of surface layers becomes less dominant and after a certain depth of penetration, the effect of inner layers becomes more and more

prominent than those of surface layers and ultimately there is practically no change in value of hardness with load. It is also clear from the graph that the Vickers hardness number at lower loads increases rapidly with load as compared with the change in Knoop hardness number with load in identical load region. Since the Knoop hardness number, H_k , in general measures the hardness of surface layers, the above explanation based on the depth of penetration is quite logical.

11.3.1 Relation between hardness and quenching temperature for Vickers and Knoop Hardness numbers in HLR :

It is clear from the observations of hardness of quenched and unquenched samples (Tables 11.1 and 11.2) that hardness depends upon the quenching temperature (T_Q). Hardness in high load region (HLR) is independent of load. Hence average values of hardness (\bar{H}) in HLR are computed and are recorded in Table 11.7. Fig. 11.15 shows the plot of $\log(\bar{H}T_Q)$ versus $\log T_Q$. The plot is a straight line for Knoop as well as Vickers hardness numbers. Further, both the straight lines are parallel to each other

Table 11.7

Variation of hardness number (average) in HIR on a d-AHT cleavage plane with quenching temperature

Quenching Temperature T_Q °K	$\log T_Q$	\bar{H}_{VQ}^{-2} kg.mm ⁻²	\bar{H}_K kg.mm ⁻²	$\log \bar{H}_{VQ} T_Q$	$\log \bar{H}_K T_Q$	$\frac{\bar{H}_{VQ}}{\bar{H}_K}$	Mean $\frac{\bar{H}_{VQ}}{\bar{H}_K}$
308 [±]	2.4886	51.19	35.41	4.1977	4.0377	1.45	
323	2.5092	52.50	35.58	4.2294	4.0604	1.48	
343	2.5353	52.99	37.70	4.2595	4.1116	1.41	1.42
363	2.5599	51.56	39.83	4.2693	4.1601	1.33	
383	2.5832	55.94	38.74	4.3356	4.1714	1.44	

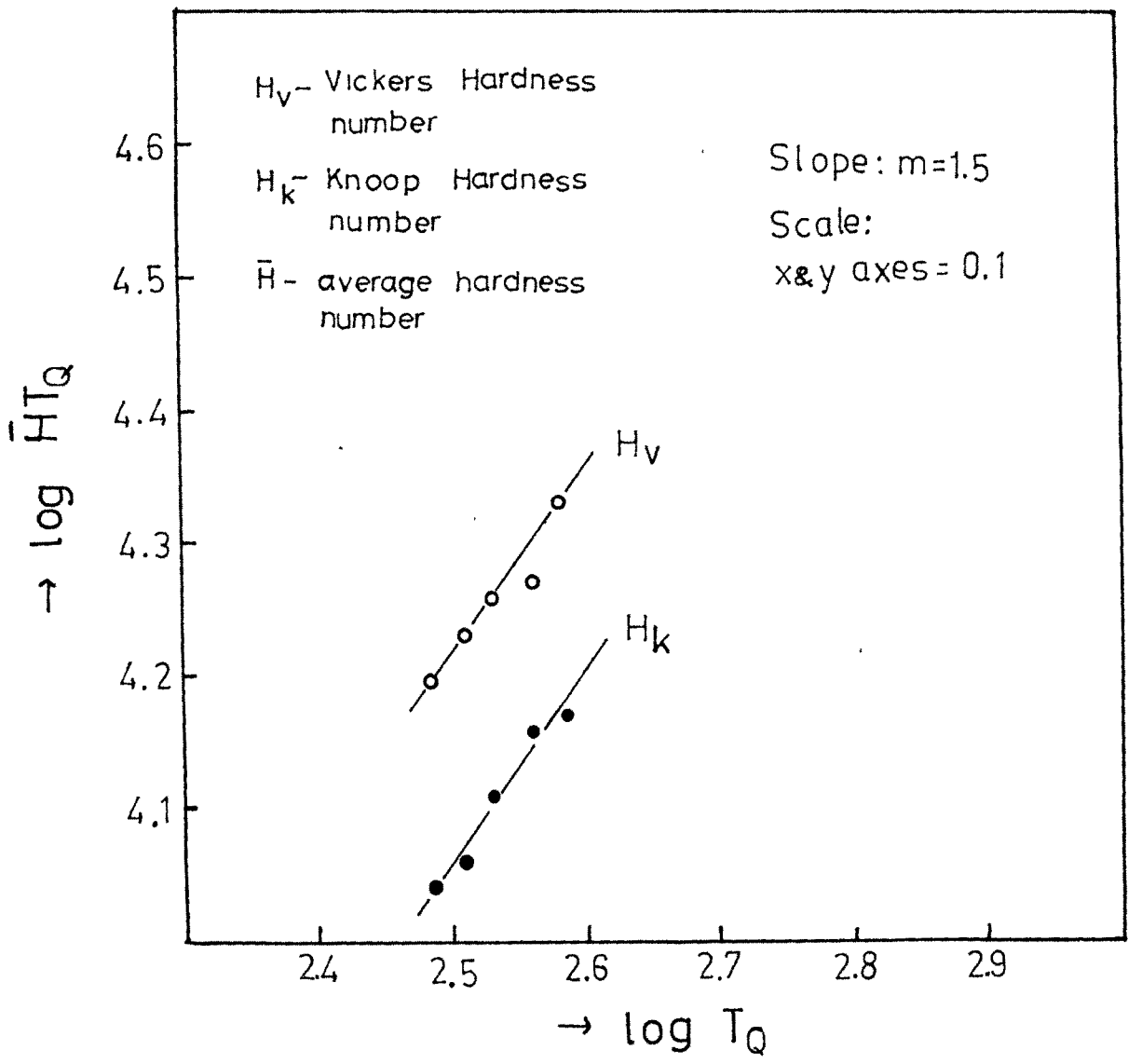


Fig. 11.15

having a constant slope and different intercepts on $\log (\overline{HT}_Q)$ axis. The straight line graph follows the equation,

$$\log \overline{HT}_Q = m \log T_Q + \log C \quad \dots (11.15)$$

where m is the slope and C is a constant.

Therefore,

$$\overline{HT}_Q^{1-m} = C \quad \dots (11.16)$$

or,

$$\overline{HT}_Q^k = C \quad \dots (11.17)$$

where $k = 1 - m$. The value of k is -0.5 for d-AHT.

It is clear from Table 11.7 that quantitatively Vickers hardness number is 1.42 times the Knoop hardness number of d-AHT cleavage faces in the HLR region. Further for both indenters, the hardness number increases with quenching temperature. However the percentage increase in hardness with respect to hardness at room temperature (308°K) is quite small.

Table 11.8

Percentage deviations of the constant $(C = HT_Q^k)$ from its mean value for different quenching temperature

Quenching Temperature T_Q °K	C_v (By calc)	C_k (By calc)	% deviation of C_v from mean C_v	% deviation C_v from value of C_v (graph)	% deviation of C_k from mean value of C_k	% deviation of C_k from value of C_k (graph)
308	2.9168	2.0177	2.03	0.56	0.13	3.43
323	2.9212	1.9786	2.17	0.71	2.07	5.20
343	2.8612	2.0356	0.08	1.36	0.75	2.57
363	2.7062	2.0905	5.34	6.71	3.47	0.06
383	2.8891	1.9795	1.06	0.40	2.02	5.26
Mean	2.8589	2.0204				
Value from graph	2.9007	2.0893				

11.3.2 Relation between Vickers hardness number and quenching temperature along mutually normal crystallographic directions :

Tables 11.3 and 11.4 show hardness for vicker indenter mark along $[001]$ direction i.e. H_{VX} and normal to it along $[100]$ direction i.e. H_{VY} , for all quenching temperatures on cleavage plane (010). Hardness numbers in HLR for both directions are independent of load. Average values of hardness (\bar{H}) in HLR are computed and represented in Table 11.9. For all quenching temperatures and also at room temperature \bar{H}_{VX} along $[001]$ direction is higher. Further ratio of $\bar{H}_{VX}/\bar{H}_{VY}$ for various quenching temperatures is different from unity showing that hardness numbers are different along different directions on a cleavage plane. Anisotropy was also exhibited by other faces (m- and z- faces) of d-AHT. \bar{H}_{VX} and \bar{H}_{VY} were also determined for m-face along and normal to direction $[001]$ and for z-face along and normal to $[101]$ which is normal to growth direction $[001]$ and the ratio of $\bar{H}_{VX}/\bar{H}_{VY}$ were computed. This work was carried out at room temperature by employing both indenters and results were incorporated in Table 11.10. showing the values of \bar{H}_{Va} , \bar{H}_k and ratio \bar{H}_{Va}/\bar{H}_k for the three faces at room temperature. It is clear from this table that z-face is the hardest amongst all faces. This conclusion is supported by the earlier studies of variation of applied load with diagonal^{of} indentation mark (cf Chapter 10).

Table 11.9

Variation of vickers hardness number (H_V) along different directions on a d-AHT cleavage plane with quenching temperatures (T_Q)

Quenching Temp. T_Q °K	\bar{H}_{Vx} kg.mm ⁻²	\bar{H}_{Vy} kg.mm ⁻²	$\frac{\bar{H}_{Vx}}{\bar{H}_{Vy}}$	\bar{H}_{Vx}	\bar{H}_{Vy}
308	51.87	50.60	1.03	1.27	
323	61.51	48.53	1.27	12.98	
343	56.17	49.55	1.13	6.62	
363	64.77	39.91	1.63	24.86	
383	64.11	49.41	1.3	14.70	

Table 11.10

Comparison of values of Vickers and Knoop hardness numbers on different d-AHT planes at room temperature

	\bar{H}_{Va} kg. mm ⁻²	\bar{H}_k kg. mm ⁻²	% variation of \bar{H}_k to \bar{H}_{Va}	$\frac{\bar{H}_{Va}}{\bar{H}_k}$	\bar{H}_{Vx} kg. mm ⁻²	\bar{H}_{Vy} kg. mm ⁻²	$\frac{\bar{H}_{Vx}}{\bar{H}_{Vy}}$
Cleavage plane	51.19	35.41	30.8	1.45	51.87	50.60	1.03
m-face	45.66	35.82	21.55	1.27	56.2	37.83	1.49
z-face	60.94	63.76	- 4.6	0.96	62.51	60.75	1.03

14.4 CONCLUSIONS

- (i) The comparative study of hardness of the cleaved specimens at different quenching temperatures indicate that the plot between hardness and load can be qualitatively divided into three parts for both indenters. They are respectively low load region corresponding to linear part, intermediate load region corresponding to non-linear part and high load region corresponding to linear portion of the graph.
- (ii) Relation between hardness number and quenching temperature is derived $\bar{H}_Q^k = \text{constant}$ where $k = -0.5$ for d-AHT.
- (iii) Vickers hardness number has higher value than knoop hardness number at any given temperature.
- (iv) Of all the faces studied for hardness, z-face is the hardest.

REFERENCES

1. BHAGIA, L.J. 1982 Ph.D. Thesis,
M.S. University of
Baroda, Baroda.

LIST OF TABLES

- 11.1 Vickers Hardness numbers (average) on d-AHT cleavage plane (010) for different quenching temperatures.
- 11.2 Knoop Hardness numbers along [001] on d-AHT cleavage plane (010) for different quenching temperatures.
- 11.3 Vickers Hardness numbers along [001] direction on d-AHT cleavage plane (010) for different quenching temperatures.
- 11.4 Vickers Hardness numbers normal to [001] direction on d-AHT cleavage plane (010) for different quenching temperatures.
- 11.5 Hardness numbers (Vickers and Knoop) on (010), (110) and (111) planes of d-AHT.
- 11.6 Hardness numbers (Vickers in two normal directions) on (010), (110) and (111) planes of d-AHT.
- 11.7 Variation of hardness number (average) in HLR on a d-AHT cleavage plane with quenching temperature.

11.8 Percentage deviations of the constant C
($C = \bar{H}_Q^k$) from its mean value for different
quenching temperatures

11.9 Variation of vickers hardness number (\bar{H}_V) along
different directions on a d-AHT cleavage plane
with quenching temperatures (T_Q).

11.10 Comparison of values of vickers and knoop
hardness numbers on different d-AHT planes at
room temperature.

CAPTIONS TO THE FIGURES

- 11.1 Plot of hardness numbers (H) for Vickers (average) and Knoop versus applied load (P) on a d-AHT cleavage plane (010) for quenching temperature (T_Q) 308^oK.

- 11.2 Plot of hardness numbers (H) for Vickers (average) and Knoop versus applied load (P) on a d-AHT cleavage plane (010) for quenching temperature (T_Q) 323^oK.

- 11.3 Plot of hardness numbers (H) for Vickers (average) and Knoop versus applied load (P) on a d-AHT cleavage plane (010) for quenching temperature (T_Q) 343^oK.

- 11.4 Plot of hardness numbers (H) for Vickers (average) and Knoop versus applied load (P) on a d-AHT cleavage plane (010) for quenching temperature (T_Q) 363^oK.

- 11.5 Plot of hardness numbers (H) for Vickers (average) and Knoop versus applied load (P) on a d-AHT cleavage plane (010) for quenching temperature (T_Q) 383^oK.

- 11.6 Plot of Vickers hardness number along H_{VX} and normal (H_{VY}) to [001] direction versus applied load (P) on a d-AHT cleavage plane (010) for quenching temperature (T_Q) 308^oK.

- 11.7 Plot of Vickers hardness number along (H_{VX}) and normal (H_{VY}) to $[001]$ direction versus applied load (P) on a d-AHT cleavage plane (010) for quenching temperature (T_Q) 323°K .
- 11.8 Plot of Vickers hardness number along (H_{VX}) and normal (H_{VY}) to $[001]$ direction versus applied load (P) on a d-AHT cleavage plane (010) for quenching temperature (T_Q) 343°K .
- 11.9 Plot of Vickers hardness number along (H_{VX}) and normal (H_{VY}) to $[001]$ direction versus applied load (P) on a d-AHT cleavage plane (010) for quenching temperature (T_Q) 363°K .
- 11.10 Plot of Vickers hardness number along (H_{VX}) and normal (H_{VY}) to $[001]$ direction versus applied load (P) on a d-AHT cleavage plane (010) for quenching temperature (T_Q) 383°K .
- 11.11 Plot of hardness number (H) for Vickers (average) and Knoop versus applied load (P) on a d-AHT m(110) face at Room Temperature.
- 11.12 Plot of hardness number (H) for Vickers (average) and Knoop versus applied load (P) on a d-AHT z(111) face at Room Temperature.

- 11.13 Plot of Vickers hardness number along (H_V) and normal (H_{vy}) to $[001]$ direction versus applied load (P) on a d-AHT $m(110)$ face, at room temperature.
- 11.14 Plot of Vickers hardness number along (H_{yx}) and normal (H_{vy}) to $[101]$ direction versus applied load (P) on a d-AHT $z(111)$ face, at room temperature.
- 11.15 Plot of $\log \bar{H}_{TQ}$ versus $\log T_Q$, in HIR of Vickers and Knoop hardness numbers.

12.1 INTRODUCTION

It is well-known that physical measurement is always associated with an error. While carrying out the indentation work several precautions were taken. Some of them were as under :

- (i) Surface to be indented was normal to the axis of the indenter and the microscope.
- (ii) Specimen was firmly fixed on a glass slide.
- (iii) The centre of gravity of the applied load, vertical axis of the indenter and microscope were colinear.
- (iv) Vibrations of any form affecting the indentation mark were avoided.
- (v) The micrometer eyepiece division was set on one end of a diagonal of indentation mark. It was moved only in one direction so that error due to backlash was avoided.
- (vi) The region to be indented was free from cleavage lines, cracks, twins etc.
- (vii) The speed of fine motion of indenter was

required direction and a gentle blow was given by a soft hammer so that a cleavage surface of crystallographically low indices (010), and not a concluded fracture with high indices, was produced.

- (xiii) For indentation mark on sphenoidal faces, special type of triangular jig was prepared to accommodate the crystal in such a way, that z-face remained flat and normal to direction of applied load and also to vertical direction of microscope and the indenter.
- (xiv) Humid atmosphere during indentation work was avoided.
- (xv) Personal errors were minimized.

The author had taken adequate precautions to avoid/minimize the errors resulting from the non-compliance of the above points.

The best way to study the relation between any two physical quantities is by graphical plot. The present chapter is concerned with the estimation of the best straight line through the plotted observations on the growth and microhardness of d-AHT, viz.,

straight line plots of (i) setting time for gel versus quantity of TA in SMS (cf Chapter - 6) (ii) optical rotation versus concentration of aqueous solution of d-AMP (cf Chapter - 7) (iii) $\log p$ versus $\log d$ (cf Chapter - 10) and $\log \bar{H}T_{D_{out}}$ versus $\log T_D$ (cf Chapter - 11). But of these plots, since actual relation between gelation time and amount of TA in SMS is unknown, the concerned plot (fig. 6.1, cf Chapter - 6) was not discussed in the present chapter. In the case of optical rotation work, the aim was to determine its dextro - or levo - rotatory character. The plot (fig. 7.4 cf Chapter - 7) was not considered here. In view of the limitations imposed by various methods for estimating best line, two methods namely, Zero sum method and statistical method, were employed to determine the best fit for the straight line plot. The procedural details were given in the chapter on error analysis (cf Chapter - 3).

12.2 ANALYSIS OF PLOT OF LOG p VS. LOG d AT ROOM TEMPERATURE

(1) Zero-sum method

It was shown in the Chapter - 10, on variation of load with diagonal of indentation mark

that the straight line plot of $\log p$ vs. $\log d$ was split up into two recognizable distinct lines with different slopes and intercepts. Since due to anisotropic nature, Vickers indentation mark was not a perfect square, measurements were carried out for both diagonals and slopes n_{v1} and n_{v2} calculated separately for both the diagonals and also for the average value of these diagonals as mentioned in the concerned chapter. Subscript V indicates vickers indenter. Theoretically, it was shown that for $n = 2$, hardness was independent of applied load. However, this is not the case in actual practice. Hence, attention was focussed on the values of n_{v1} and n_{v2} , n_{k1} and n_{k2} , calculated by utilizing the above method and by using the graphical plots. Subscripts V and k indicate vickers and knoop indenters respectively. They are mentioned in Tables 12.1 and 12.2 alongwith the percentage changes in the values of n_{v1} and n_{v2} , n_{k1} and n_{k2} from their calculated values. Ignoring the sign and considering absolute values of deviations, it is clear that deviations in n_k are more, than those in n_v from their calculated values for cleavage faces of d-AHT. Knoop indenter is normally used for determining surface effects. Since n_k was more

T A D L E : 12.1

ZERO - SUM METHOD : PLOT OF LOG P VS LOG d FOR ROOM TEMPERATURE FOR

VICKERS INDENTATION

REGION - I

Measurement of diagonal length along [001] direction
 for cleavage p and m - face and along [101] for
 z - face
 Measurement of diagonal length normal to [001]
 for cleavage plane and m - face and [101] for
 z - face

	Calculated value of n ₁	Value from graph n ₁	% change in n $\left\{ \left \frac{a-b}{a} \right \times 100 \right\}$	Calculated value of n ₁	Value from graph n ₁	% change in n ₁ $\left\{ \left \frac{a-b}{a} \right \times 100 \right\}$
	(a)	(b)		(a)	(b)	
Cleavage Plane	3.96	3.80	4.0	3.45	3.75	8.7
Z - face	2.9	2.73	5.9	2.89	2.78	3.8
m - face	4.71	4.66	1.1	3.56	3.63	2.0

REGION - II

	Calculated value of n ₂	Value from graph n ₂	% change $\left\{ \left \frac{a-b}{a} \right \times 100 \right\}$	Calculated value of n ₂	Value from graph n ₂	% change in n ₂ $\left\{ \left \frac{a-b}{a} \right \times 100 \right\}$
	(a)	(b)		(a)	(b)	
Cleavage Plane	1.98	1.93	2.5	2.06	2.0	2.9
Z - face	1.87	1.86	0.5	1.92	1.83	4.7
m - face	2.09	2.0	4.3	2.35	2.4	2.1

T A B L E : 12.2

ZERO - SURF METHOD : PLOT OF LOG p VS LOG d FOR ROOM

***** TEMPERATURE *****

REGION - I

FOR VICKERS INDENTATION
 (average length of two diagonals were taken)

FOR KNOOP INDENTATION

	Calculated value of n_{V1}	Value from graph n_{V1}	% change in n_{V1} $\left\{ \left \frac{a-b}{a} \right \times 100 \right\}$	Calculated value of n_{K1}	Value from graph n_{K1}	% change in n_{K1} $\left\{ \left \frac{a-b}{a} \right \times 100 \right\}$
	(a)	(b)		(a)	(b)	

Cleavage Plane	3.69	3.71	0.5	4.13	4.25	2.9
z - face	2.97	2.57	13.5	3.23	2.91	9.9
m - face	3.77	4.4	16.7	3.44	3.33	3.2

REGION - II

	Calculated value of n_{V2}	Value from graph n_{V2}	% change in n_{V2} $\left\{ \left \frac{a-b}{a} \right \times 100 \right\}$	Calculated value of n_{K2}	value from graph n_{K2}	% change in n_{K2} $\left\{ \left \frac{a-b}{a} \right \times 100 \right\}$
	(a)	(b)		(a)	(b)	

Cleavage Plane	1.98	1.93	2.5	1.96	2.0	2.0
z - face	1.74	1.71	1.7	1.57	1.67	6.4
m - face	2.19	2.2	0.5	2.06	2.0	2.9

than n_v , it could be conjectured that the process of cleaving could have created more strain than necessary and/or could be little imperfect.

(2) Statistical method

There are two ways of statistically estimating the best straightlines by considering regression of abscissae on ordinates and regression of ordinates on abscissae. Values of slopes based on the above two ways, were mentioned in Tables 12.3 and 12.4 alongwith the percentage changes in their values from their calculated values. It can be seen from the tables that calculated slope values (regression coefficients) differ from each other by a wide margin. This is due to the built-in assumption of the method, namely one variable (abscissa or ordinate) is assumed to be free from error. The slope values (n_{v1}) are different along two mutually normal directions as can be seen from the Table 12.3. This indicates the anisotropic nature of a surface of d-AHT crystal. Table 12.4 presents slopes n_{v1} and n_{v2} and n_{k1} and n_{k2} calculated by using statistical method. In this case, also the percentage deviations from calculated values of slopes are more for knoop indenter than those for vickers indenter. Hence the conclusions, which were

T A B L E : 12.3

STATISTICAL ESTIMATION

Plot of log p Vs log d for room temperature

FOR VICIERS INDENTATION

REGION - I

Measurement of diagonal length along (101) for cleavage plane and m-face and (101) for z-face.

Measurement of diagonal length normal to (001) for cleavage plane and m-face and (101) for z-face

Regression coefficients

ml	1/m ²	Average coefficient	Value of slope (n _{v1}) from graph	% change in n _{v1} { $\frac{a-b}{a} \times 100$ }	Calculated slopes (n _{v1})	Value of slope (n _{v1})	% change in n _{v1} { $\frac{a-b}{a} \times 100$ }			
			(a)	(b)						
Cleavage Plane	3.87	4.08	3.93	3.8	4.4	3.18	3.66	3.42	3.75	9.5
z - face	2.9	3.3	3.1	2.73	11.9	2.92	3.24	3.08	2.78	9.7
m - face	3.85	4.9	4.38	4.66	6.4	3.36	4.53	3.99	3.63	9.1

Regression co-efficients

ml	1/m ²	Average coefficient	Value of slope (n _{v2}) from graph	% change in n _{v2} { $\frac{a-b}{a} \times 100$ }	Calculated slopes (n _{v2})	Value of slope (n _{v2}) from graph	% change in n _{v2} { $\frac{a-b}{a} \times 100$ }			
			(a)	(b)						
Cleavage plane	1.92	1.93	1.925	1.93	0.3	1.96	1.98	1.97	2.0	1.5
z - face	1.87	1.90	1.89	1.86	1.3	1.91	1.96	1.94	1.83	5.4
m - face	1.99	2.05	2.02	2.0	1.0	2.4	2.4	2.4	2.4	0.0

REGION - II

Regression co-efficients

ml	1/m ²	Average coefficient	Value of slope (n _{v2}) from graph	% change in n _{v2} { $\frac{a-b}{a} \times 100$ }	Calculated slopes (n _{v2})	Value of slope (n _{v2}) from graph	% change in n _{v2} { $\frac{a-b}{a} \times 100$ }			
			(a)	(b)						
Cleavage plane	1.92	1.93	1.925	1.93	0.3	1.96	1.98	1.97	2.0	1.5
z - face	1.87	1.90	1.89	1.86	1.3	1.91	1.96	1.94	1.83	5.4
m - face	1.99	2.05	2.02	2.0	1.0	2.4	2.4	2.4	2.4	0.0

Regression co-efficients

ml	1/m ²	Average coefficient	Value of slope (n _{v2}) from graph	% change in n _{v2} { $\frac{a-b}{a} \times 100$ }	Calculated slopes (n _{v2})	Value of slope (n _{v2}) from graph	% change in n _{v2} { $\frac{a-b}{a} \times 100$ }			
			(a)	(b)						
Cleavage plane	1.92	1.93	1.925	1.93	0.3	1.96	1.98	1.97	2.0	1.5
z - face	1.87	1.90	1.89	1.86	1.3	1.91	1.96	1.94	1.83	5.4
m - face	1.99	2.05	2.02	2.0	1.0	2.4	2.4	2.4	2.4	0.0

T A B L E 1 11.4

STATISTICAL ESTIMATION

Plot of Log P Vs. Log d for at room temperature

REGION - I

FOR VICKERS INDENTATION
(Average length of diagonal were taken)

Regression Co-efficients		Regression Co-efficients								
FOR VICKERS INDENTATION		FOR KNOOP INDENTATION								
Calculated slopes (n_{v1})	Value of slope (n_{k1}) from graph	Calculated slopes (n_{k1})	Value of slope (n_{k1}) from graph							
$\left\{ \frac{a-b}{a} \times 100 \right\}$										
m1	1/m2	m1	1/m2							
Average Co-efficient (a)		Average Co-efficient (b)								
Cleavage Plane	3.57	3.84	3.71	3.71	0.1	4.16	4.11	4.19	4.25	116
z - face	2.9	3.11	3.01	2.57	14.5	3.06	3.27	3.17	2.91	8.1
m - face	3.15	5.14	4.15	4.4	6.1	3.31	3.59	3.45	3.33	3.5

REGION - II

Regression Co-efficients		Regression Co-efficients								
FOR VICKERS INDENTATION		FOR KNOOP INDENTATION								
Calculated slopes (n_{v2})	Value of slope (n_{k2}) from graph	Calculated slopes (n_{k2})	Value of slope (n_{k2}) from graph							
$\left\{ \frac{a-b}{a} \times 100 \right\}$										
m1	1/m2	m1	1/m2							
Average Co-efficient (a)		Average Co-efficient (b)								
Cleavage Plane	1.94	1.95	1.945	1.93	0.8	1.97	1.98	1.975	2.0	1.3
z - face	1.70	1.71	1.705	1.71	0.3	1.60	1.19	1.595	1.67	4.7
m - face	2.18	2.25	2.215	2.2	0.7	2.02	2.04	2.03	2.0	1.5

drawn, while calculating deviations by zero-sum method get added support.

12.3 ANALYSIS OF (i) $\log p$ vs. $\log d$ for different quenching temperature and (ii) $\log \bar{H}T_Q$ vs. $\log T_Q$ plots in HLR

All possible precautions were taken by the author to minimize/avoid the errors mentioned above while carrying out indentation work on cleavage planes of d-AHT (cf. Chapters 10 & 11). Further, two methods, namely, zero-sum method and statistical estimation, were used to determine the best fit of the above straight line plots.

Tables 12.5, 12.6, 12.7, 12.8 and 12.9 present the calculated and observed values of slopes of the straight lines plots of (i) $\log p$ vs. $\log d$ in the low-load and high-load regions of applied loads (cf Chapter 10, figs. 10.1 to 10.14) and (ii) $\log \bar{H}T_Q$ vs. $\log T_Q$ for different quenching temperatures in the high load region of the graph of hardness number versus applied load (cf Chapter 11, figs. 11.1 to 11.5) The column of percentage change in slopes in the two regions of the graphs of $\log p$ vs. $\log d$ indicates very clearly that for most quenching temperatures, the

T A B L E : 12.5

ZERO SUM. METHOD

Plot of Log p Vs. Log d for different quenching temperature

FOR VICKERS INDENTATION

REGION - I

Quenching Temperature T_0 K	Measurement of diagonal length along [001] - $\{d_{vx}\}$	Measurement of diagonal length along [100] - dy
308	3.96	3.8
323	3.5	3.6
343	2.67	3.7
363	4.1	4.0
383	3.2	3.2

Quenching Temperature T_0 K	Calculated value of n_c	% change in n $\left\{ \left \frac{a-b}{a} \right \times 100 \right\}$	Value from graph n_g	Calculated value of n_c	Value from graph n_g	% change in n $\left\{ \left \frac{a-b}{a} \right \times 100 \right\}$
308	3.96	4.0	3.8	3.45	3.8	3.7
323	3.5	2.0	3.6	3.49	3.6	3.2
343	2.67	1.5	3.7	2.89	2.8	2.1
363	4.1	2.4	4.0	4.1	4.0	2.4
383	3.2	0.0	3.2	3.2	3.3	1.6

(a) (b)

REGION - II

Quenching Temperature T_0 K	Calculated value of n_c	% change in n $\left\{ \left \frac{a-b}{a} \right \times 100 \right\}$	Value from graph n_g	Calculated value of n_c	Value from graph n_g	% change in n $\left\{ \left \frac{a-b}{a} \right \times 100 \right\}$
308	1.96	1.5	1.9	2.06	2.0	2.9
323	1.96	1.5	1.9	2.41	2.0	17.0
343	1.92	0.5	1.9	1.76	1.8	3.4
363	1.91	1.0	1.9	1.87	1.8	2.7
383	2.3	16.1	1.9	1.74	1.80	3.4

T A B L E : 12.6
 STATISTICAL ESTIMATION

Plot of log p Vs. log d for different quenching temperature
 FOR VICKERS INDENTATION

REGION - I

Measurement of diagonal length
 along (001) - (dv_x)

Measurement of diagonal length
 along (100) - (dv_y)

Regression Co-efficients

Quenching temperature T ₀ K	Calculated slopes n _c		Value of slope from graph - n _g	Δ change in n { $\frac{a-b}{a}$ } X 100 }	Calculated slopes n _c		Value from graph - n _g	Δ change in n { $\frac{a-b}{a}$ } X 100 }
	m1	1/m2			m1	1/m2		
303	3.37	4.08	3.98	4.4	3.18	3.66	3.42	3.8
323	3.57	3.59	3.58	0.3	3.5	3.51	3.55	3.6
343	3.69	2.71	2.7	0.4	2.86	2.88	2.87	2.8
363	3.97	4.09	4.03	0.7	3.79	4.29	4.04	4.0
383	3.15	3.23	3.19	0.3	3.27	3.31	3.29	3.3

REGION - II

Regression Co-efficients

308	1.92	1.93	1.925	0.3	1.96	1.98	1.97	2.0
323	1.90	1.92	1.91	1.0	2.12	2.23	2.18	2.0
343	1.98	1.99	1.985	2.8	1.82	1.84	1.83	1.8
363	1.89	1.91	1.9	1.6	1.82	1.84	1.83	1.8
383	2.29	2.30	2.295	15.9	1.82	1.85	1.84	1.8

T A B L E : 12.7

 ZERO - SUM METHOD

Plots of log p Vs. Log d for different quenching temperature

REGION - I

FOR VICKERS INDENTATION
 (average of length of two diagonals were taken)

Quenching Temperature T_q , K	FOR VICKERS INDENTATION		FOR KNOOP INDENTATION	
	Calculated Slope n_c	Value from graph - n_q	Calculated slope n_c	Value from graph - n_q
308	3.69	3.7	4.13	4.2
323	3.58	3.6	3.65	3.6
343	2.8	2.8	3.59	3.6
363	3.76	3.6	3.76	4.00
383	3.09	3.2	3.43	3.5

	%		%	
	change in n $\left\{ \frac{a-b}{a} \times 100 \right\}$			
	0.3	0.3	4.2	1.7
	0.5	0.5	3.6	1.4
	0.0	0.0	3.6	0.3
	4.3	4.3	4.00	6.4
	3.6	3.6	3.5	2.0

REGION - II

308	1.98	1.9	1.96	2.0	2.0
323	2.23	1.9	2.05	2.0	2.4
343	1.82	1.9	1.80	1.8	0.0
363	1.93	1.9	1.76	1.8	2.3
383	1.94	1.9	1.69	1.7	0.6

T A B L E 1 12.9

STATISTICAL ESTIMATION

Plots of $\log R$ vs. $\log d$ for different quenching temperature

REGION - I

FOR VICKERS INDENTATION
 (Average length of two diagonals were taken)

Quenching Temperature T_Q K	Regression Co-efficient			Regression Co-efficient		
	Calculated slope n_c	1/m ²	Average value	Calculated slope n_c	1/m ²	Average value
309	3.57	3.84	3.71	4.16	4.21	4.19
323	3.57	3.59	3.58	3.54	3.58	3.56
343	2.73	2.80	2.79	3.62	3.75	3.69
363	3.46	3.65	3.56	3.81	3.87	3.84
383	3.10	3.14	3.12	3.47	3.49	3.48

(a)

(b)

Quenching Temperature T_Q K	Value from graph - nq		Value from graph - nq		Change in n $\left\{ \frac{a-b}{a} \times 100 \right\}$
	Calculated slope n_c	1/m ²	Calculated slope n_c	1/m ²	
309	0.1	3.7	4.16	4.21	0.4
323	0.6	3.6	3.54	3.58	1.1
343	0.4	2.8	3.62	3.75	2.3
363	1.3	3.6	3.81	3.87	3.3
383	2.6	3.2	3.47	3.49	0.6

REGION - II

Quenching Temperature T_Q K	Value from graph - nq		Value from graph - nq		Change in n $\left\{ \frac{a-b}{a} \times 100 \right\}$
	Calculated slope n_c	1/m ²	Calculated slope n_c	1/m ²	
308	2.3	1.9	1.97	1.98	1.3
323	9.3	1.9	2.0	2.02	0.5
343	1.1	1.9	1.77	1.79	1.1
363	2.3	1.9	1.77	1.77	1.7
383	1.6	0.9	1.74	1.77	3.1

Table 12.9

CALCULATED AND OBSERVED SLOPES OF STRAIGHT LINE

plots $\log \bar{H}_T Q$ vs. $\log T Q$

(1) ZERO-SUM METHOD

	Calculated slope n_c	Value from graph n_g	% change in n
	(a)	(b)	$\left \frac{a-b}{a} \right \times 100$

Vickers hardness	1.39	1.5	7.9
Knoop hardness	1.61	1.5	6.8

(2) STATISTICAL ESTIMATION :

(i) Regression of y on x :

Vickers hardness	1.43	1.5	4.9
Knoop hardness	1.49	1.5	0.7

(ii) Regression of x only :

Vickers hardness	1.45	1.5	3.4
Knoop hardness	1.52	1.5	1.3

deviations are not quite significant except for the observations at room temperature (308°K) in region-I (low-load) and quenching temperatures 323°K and 383°K . There is no thermal treatment of the specimen at room temperature (308°K). However, this temperature is the one at which the hardness numbers of specimens quenched from high temperature were determined. Due to anisotropic nature, the formation of wings has seriously affected the measurement of vickers diagonal in a direction normal to $[001]$. However, it is interesting to observe that the measurements of diagonals made at other quenching temperatures were not affected by this formation. The quenching temperature 383°K is nearer the dissociation temperature 393°K of d-AHT crystals. As a result there is a distinct possibility that anisotropic character and wing formation became more noticeable along prominent crystallographic direction $[001]$ growth axis of d-AHT crystals, giving rise to a large deviation of observed slope from the calculated one. A glance at the columns of the above tables showing percentage deviations of observed slopes from calculated ones suggests that experimental conditions producing quenching are imperfect. This is obviously inherent in the basic experimental work, where the attempt was made to have

quenching rate as high as possible. However, this has not remained consistently constant for all quenching temperatures, as can be seen from the deviations. It should be noted that this point had remained unnoticed for the deviations of observed slopes from calculated ones for plots of $\log \bar{HT}_Q$ vs. $\log T_Q$ (cf Table 12.9). This appears to be due to the fact that changes in quench-hardness numbers with quenching temperatures are comparatively less. However, it is difficult to arrive at definite reason(s) for these noticeable deviations of observed slopes from calculated ones.

LIST OF TABLES

- 12.1 Zero-sum method : Plots of log p vs. log d for room temperature for vickers indentation.

- 12.2 Zero-sum method : Plots of log p vs. log d for room temperature for vickers (average length of diagonals) and knoop indentation.

- 12.3 Statistical estimation : Plots of log p vs. log d for room temperature for vickers indentations.

- 12.4 Statistical estimation : Plots of log p vs. log d for room temperature for vickers (average length of diagonals) and knoop indentations.

- 12.5 Zero-sum method : Plots of log p vs. log d for different quenching temperatures for vickers indentation.

- 12.6 Statistical estimation : Plots of log p vs. log d for different quenching temperatures for vickers indentation.

- 12.7 Zero-sum method : Plots of $\log p$ vs. $\log d$ for different quenching temperatures for vickers (average length of two diagonals) and knoop indentations.
- 12.8 Statistical estimation : Plots of $\log p$ vs. $\log d$ for different quenching temperatures for vickers (average length of two diagonals) and knoop indentations.
- 12.9 Calculated and observed slopes of straight line plots $\log \overline{HT}_Q$ vs. $\log T_Q$.